NASA Contractor Report 3258

Argon/UF_6 Plasma Experiments: UF_6 Regeneration and Product Analysis

Ward C. Roman

CONTRACT NAS1-14329
MARCH 1980

NASA

NASA Contractor Report 3258

Argon/UF_6 Plasma Experiments: UF_6 Regeneration and Product Analysis

Ward C. Roman
United Technologies Research Center
East Hartford, Connecticut

Prepared for
Langley Research Center
under Contract NAS1-14329

National Aeronautics
and Space Administration

**Scientific and Technical
Information Office**

1980

TABLE OF CONTENTS

TABLE OF CONTENTS (Concluded)

SUMMARY

An experimental and analytical investigation was conducted to aid in developing some of the technology necessary for designing a self-critical fissioning uranium plasma core reactor (PCR). This technology is also applicable to gaseous uranium hexafluoride (UF_6) nuclear pumped laser systems.

The principal equipment used included the United Technologies Research Center (UTRC) 1.2 MW rf induction heater, a dc plasma torch, uranium tetrafluoride (UF_4) feeder system, and batch-type fluorine/UF_6 regeneration systems.

This follow-on research included the following overall objectives: (1) continue to develop and test materials and handling techniques suitable for use with high-temperature, high-pressure, gaseous UF_6; (2) continue development of complementary diagnostic instrumentation and measurement techniques to characterize the effluent exhaust gases and residue deposited on the test chamber and exhaust system components. Specific objectives included: (1) development of a batch-type UF_6 regeneration system employing pure, high-temperature fluorine; (2) development of a ruggedized time-of-flight (T.O.F.) mass spectrometer and associated data acquisition system capable of making on-line concentration measurements of the volatile effluent exhaust gas species in a high rf environment and corrosive environment of UF_6 and related halide compounds.

The overall test results have demonstrated that batch-type UF_6 regeneration experiments utilizing UF_4 and other uranium compounds can provide up to 100 percent conversion efficiencies. At operating temperatures up to 650 K, typical 250 mg samples of laboratory-grade UF_4 were converted to pure gaseous UF_6 after one minute exposures to a 1 atm pressure of pure fluoride. Similar results were also obtained using solid test samples of residue removed, after a hot flow test, from the exhaust system of the UF_6 rf plasma test facility. Included in these experiments was the development of a system for the safe handling, flow metering, and collection of fluorine gas. These

results are considered significant because they demonstrate the feasibility of chemically converting on a batch-type basis all the nonvolatile test chamber and exhaust products to pure UF_6 using a single reactant.

A ruggedized T.O.F. mass spectrometer system was designed, fabricated, and successfully tested on-line with the rf UF_6 plasma experiments. This on-line system was demonstrated to be capable of measuring UF_6 and other volatile contaminant concentrations down to 50 ppm. The use of a high-speed data system permitted obtaining the results within minutes. This system will prove useful in future UF_6 reprocessing tests and related composition measurements necessary in the study of UF_6 reactors and nuclear pumped laser systems.

Supporting studies included:

(a) Tests employing a flowing UF_4/fluorine system to investigate the effect of configuration and operating conditions on the conversion process. A demonstration of the feasibility of continuously injecting pure fluorine through the walls of a porous duct (5 μm nominal pore size) without wall degradation was conducted. This has direct application in future UF_6 plasma experiments;

(b) Evaluation of available thermodynamic property data for UF_6, UF_5, and UF_4;

(c) Adaptation of a photoacoustic spectrometer diagnostic technique for providing quantitative information on the amorphous uranium compound residue found in the exhaust system after UF_6 rf plasma hot flow tests; and

(d) Exploratory tests to investigate the effect of hot UF_6 on different candidate materials being considered for use in future rf uranium plasma exhaust reprocessing experiments and nuclear pumped laser windows.

Encouraging experimental results obtained using a flowing UF_4/fluorine to UF_6 regeneration system indicate this technique appears viable and warrants further investigation. This will aid in demonstrating the feasibility of a continuous (non batch-type) UF_6 reconstitution process using flowing high temperature fluorine.

RESULTS AND CONCLUSIONS

As part of the overall objective of continued development of a UF_6 injection, confinement, handling, and exhaust gas reprocessing/diagnostic system for the rf-heated uranium plasma experiments, the following results were obtained:

1. A batch-type fluorine/UF_6 regeneration system was developed. This included the fluorine supply and transfer system, reaction vessel, exhaust trap system, and remote control console including a fluorine leak detection/alarm system. Using this system, a test matrix for converting solid UF_4 and other nonvolatile uranium compounds to pure UF_6 was established. The reactor temperature was determined to be the dominant variable in achieving high conversion efficiencies. Complete conversion (100 percent) of UF_4 to UF_6 was achieved using a reactor temperature of approximately 660 K, fluorine pressure of 1 atm, and residence time of one minute. No conversion was measured at temperatures below about 520 K. Supporting tests revealed the importance of minimizing contamination and prepassivating the system to ensure reproducible test results. Other regeneration tests included the use of laboratory pure mixtures of UF_4, UO_2F_2, and UO_3. These are representative of the type of uranium compounds deposited into the exhaust system of the UF_6 rf plasma test facility. At comparable test conditions as above, conversion efficiencies ranging from 65 to 98 percent were achieved.

Residue material removed from the exhaust of the 1.2 MW rf UF_6 plasma test facility was also tested using the batch-type regeneration system. At approximately 660 K, 100 percent conversion efficiency was achieved. Reducing the residence times to as short as twelve seconds, still provided conversion efficiencies up to about 95 percent. The overall results obtained using the batch-type conversion technique indicate it to be a viable scheme for converting all the uranium compound residue collected in the exhaust system back to pure UF_6.

2. A test facility was established for conducting controlled flowing-type UF_4/UF_6 regeneration experiments. As in the prior batch-type tests, a separate system for safe handling and injection of pure fluorine was developed. Use of different test configurations and test conditions permitted achieving conversion efficiencies up to 60 percent at a reaction gas temperature of 880 K. The corresponding fluorine pressure and flow rate were 1 atm and 0.2 g/s, respectively. Future tests at higher reaction gas temperatures should permit still greater on-line conversion efficiencies. Initial tests were completed using a porous Monel duct for injecting pure fluorine into the reaction chamber containing the flowing UF_4; post-test inspection revealed no measurable uranium compound coating on the inside wall surface. These results are considered

significant and demonstrate the feasibility of continuously injecting pure fluorine through a porous (5 μm nominal pore size) duct without wall degradation and/or coating. This technique has potential for application in future uranium plasma exhaust gas/UF_6 regeneration systems.

3. A ruggedized T.O.F. mass spectrometer, data acquisition, and data processing system was designed and developed for use in on-line UF_6 and other volatile contaminant concentration measurements. The system was tested and proved to be operational under both a high rf environment and after long time exposure to corrosive UF_6 and other uranium halides. A specially developed cold-finger type cryopumping technique was required to minimize instrument contamination. Analysis of the calibration data showed agreement with the limited published data; the UTRC spectrometer sensitivity was determined to be a factor of three greater than that of commercial T.O.F. devices.

A series of initial tests completed with the entire T.O.F. system adapted to the exhaust of the 1.2 MW rf UF_6 plasma test facility yielded the following results: (a) negligible UF_6 was detected downstream of the cold trap system, thus indicating the effectiveness of the trap system in minimizing downstream UF_6 losses; (b) very low concentrations of UF_6 (less than or equal to 50 ppm) were measured in the axial bypass exhaust line (this result confirms the effectiveness of the radial inflow argon buffer vortex scheme employed in the rf plasma test chamber to affect good uranium vapor confinement); (c) the UF_6 concentration at the upstream centerline of the UF_6 cryogenic trap system was measured to be about 465 ppm. Considerably more experimental measurements over a wide range of test conditions and locations, including off-axis, are required before a complete exhaust gas species concentration analysis can be determined. The results to date confirm the acceptability of the T.O.F. mass spectrometer system to acquire this information.

4. Additional rf plasma tests were followed by a complete disassembly of all major components to permit an estimation of the type and quantity of uranium compound residue remaining on the walls. After a test of 4.8 minutes with a total mass of UF_6 injected into the test chamber of 8.93 gms, less than 1 percent of the total UF_6 injected was deposited out within the rf plasma test chamber. Approximately 90 percent of the total injected UF_6 was collected in the cryogenic trap/downstream exhaust duct system where efficient post-test batch-type UF_6 regeneration techniques could be applied. Approximately 1 percent of the total UF_6 injected was deposited uniformly on the walls of the axial bypass exhaust duct. The primary constituents of the residue were UF_4 (dominant), UO_2F_2, and occasionally a trace of a uranium oxide (UO_2 or UO_3).

5. Supporting exploratory tests conducted using the batch-type regeneration system indicated the acceptability of several candidate materials (both solid and porous) being considered for use in future uranium plasma/exhaust

regeneration system test components. Monel, copper, nickel, and materials with a high nickel content were most resistant to hot UF_6 ($\leq$ 673 K) after exposure for times up to seventeen hours. Relative to possible candidate nuclear pumped laser window material, aluminum oxide (sapphire) withstood UF_6 pressures of 1 atm, and temperatures of 700 K for up to seventeen hours with excellent resistance to UF_6. High quality fused-silica and calcium fluoride exhibited some attack under corresponding test conditions.

6. An evaluation of the limited available thermodynamic property data for UF_6, UF_5, and UF_4 revealed the following. There is generally good comparison except for the enthalpy of UF_5. Calculated thermal decomposition products of UF_6, based on data from Hildenbrand, Kistemaker, and Hassan indicate some variation in the start of UF_6 decomposition. The temperature at the start of decomposition was found to range from 1250 K to 1700 K.

7. A new technique using photoacoustic spectrometry was adapted for use in nondestructive post-test analysis of uranium compound exhaust residue. In addition to positive, quantitative identification of stable amorphous uranium compounds, the technique also has application in aiding to study the effects of contaminants within the U-O-F system. For example, by monitoring the ratio of UO_2F_2 to UF_4 in the deposits, thermodynamic equilibrium analysis is applicable to determine the effect of common contaminants such as water vapor and oxygen. This new technique can now be used to supplement other techniques already in use (e.g., ISS/SIMS; a considerably more expensive and time consuming scheme that requires extensive calibration).

INTRODUCTION

Uranium nuclear reactors which employ gaseous fissile fuel can be operated at high temperatures. This leads conceptually to power conversion systems for space and terrestrial applications with performance characteristics and thermodynamic cycle efficiencies significantly improved over conventional solid fuel element nuclear reactors. In addition to aerospace propulsion applications, new options may use the direct coupling of energy in the form of electromagnetic radiation. These include laser pumping, photochemical or thermochemical processes, MHD, and advanced closed-cycle gas turbine driven electrical generator systems (Refs. 1 through 4).

The continuous reprocessing of gaseous nuclear fuel also leads to a low steady-state fission product inventory in the reactor and limits the buildup of long half-life transuranium elements. This, together with the low critical mass, could result in increased safety and higher nuclear fuel resource utilization. References 1 through 4 summarize various reactor concepts, designs, principles of operation, applications, and associated performance estimates.

Several principal technologies are required to establish the feasibility of fissioning uranium plasma core reactors: (1) the fluid mechanical confinement of the hot fissioning uranium plasma with sufficient containment to both sustain nuclear criticality and minimize deposition of uranium or uranium compounds on the confinement chamber peripheral walls; (2) a reliable argon/UF_6 handling, injection, reconstitution and recirculation system applicable to closed-fuel-cycle gas-core nuclear reactor systems.

A long-range program plan to establish the feasibility of fissioning uranium gaseous UF_6 and uranium plasma reactors has been formulated by the National Aeronautics and Space Administration (NASA). Reference 5 summarizes the plan which comprises a series of experiments with reflector-moderator cavity reactors. Los Alamos Scientific Laboratory (LASL) is currently performing these experiments in cooperation with UTRC. Integrated into this plan is the demonstration of an argon/UF_6 injection, separation, and recirculation system to efficiently separate UF_6 from argon in a form adaptable to subsequent recycling in the uranium plasma experiment. A review of the past work is contained in Ref. 6. Performance of static UF_6 critical experiments has been accomplished (Ref. 7). Flowing UF_6 reactor experiments are in progress.

Plasma core reactor technology studies at UTRC consist of several experiments and theoretical investigations directed toward evaluating the feasibility of the PCR concept. Reference 8 summarizes some of the past fluid mechanics (nonplasma) experiments. Reference 9 includes test results on

confinement of argon rf plasmas. Reference 10 summarizes the results of initial laboratory-scale experiments in which pure UF_6 was injected into an argon-confined, steady-state, rf-heated plasma to investigate some of the characteristics of PCRs. Reference 11 summarizes experimental results on developing a primary exhaust system capable of transporting the UF_6 effluent exhaust gas to a downstream trap system with minimum uranium compound wall deposition. The different exhaust systems employed included provision for varying the temperature of the individual endwalls and primary exhaust duct sections, in addition to the use of an exploratory porous exhaust duct assembly (sintered Monel material) incorporating a diluent-bleed radial flow injection of argon. These techniques were effective in aiding to reduce the wall coatings due to uranium compound deposition. The preliminary development of complementary diagnostic measurements included both off- and on-line IR spectrometric absorption and T.O.F. mass spectrometer techniques. In selected cases, post-test residue analysis was conducted on the material deposited on the various key components of the test chamber and exhaust system. The overall results demonstrated that operating the test components at a high temperature and using appropriate traps and getters on the inlet gas systems (i.e., eliminate sources of contamination) together with auxiliary diluent gas injection significantly reduced the uranium compound coatings on the wall (to levels of about 0.04-0.4 mg/cm^2, greater than an order of magnitude reduction compared to earlier test results) and thereby allow a large fraction of the total UF_6 injected into the test chamber available for recovery/regeneration back to pure UF_6.

This research report presents results of the continuing UF_6 plasma tests, together with the associated diagnostics and exhaust gas/UF_6 regeneration systems applicable to plasma core reactors and UF_6 nuclear pumped laser systems. Emphasis was placed on investigating a batch-type fluorine/UF_6 regeneration system; included in these experiments was the initial development of a system for the safe handling, flow metering, and collection of high pressure fluorine and the design and development of a dedicated on-line T.O.F. mass spectrometer system. Exploratory experiments were then conducted using a dc arc plasma heater/preheated UF_4/fluorine system to investigate the effect of several key variables on the UF_6 regeneration process. Some tests included direct injection of fluorine into the reaction chamber using a porous Monel duct technique.

These results will aid in establishing the reliability of a pressurized UF_6 handling and fluorine/UF_6 regeneration system that is applicable to future closed-cycle UF_6 plasma core reactor and nuclear pumped laser experiments.

Identification of commercial products in this report is to adequately describe the materials and does not constitute official endorsement, expressed or implied, of such products or manufacturers by the National Aeronautics and Space Administration.

DESCRIPTION OF PRINCIPAL EQUIPMENT

Fluorine Test Facility for UF_4/F_2 Batch UF_6 Regeneration Tests

A previously existing chemical laser components test stand was modified to permit conducting the UF_6 regeneration tests using the pure fluorine in a manner acceptable to safety standards for hazardous gas applications. Figure 1 is a schematic of the components used in the UF_4/F_2 batch UF_6 regeneration tests. The main components were the fluorine supply with vent and nitrogen purge system, the fluorine transfer vessel, the nickel reaction vessel, the cryogenic trap, and the fluorine trap. Safety considerations associated with handling high temperature, high pressure fluorine required the use of remote control valves and a fluorine leak detection/alarm system.

Figure 2 is a photograph of the overall test facility as used in the UF_4/F_2 batch UF_6 regeneration tests. The large removable tank dome (1.5-m-dia) permitted rapid access to the test components after each test. The entire tank was maintained under vacuum (approximately 10 Torr) during the tests and was vented to a large spherical vacuum chamber located outside the laboratory; this allowed rapid scavenging of the test gas in the event of a component failure.

Figure 3 is a photograph of the remote master control console located in an adjacent room, including a portion of the fluorine detection system. Instrumentation for monitoring the pressures (pressure transducers), temperatures, valve positions, and safety interlocks were connected to the readout of the remote master control console.

Figure 4 is a photograph of the main test components located within the test tank shown with the front dome removed. The main fluorine inlet line can be seen entering at the lower center of the photograph. Located immediately downstream of the inlet was a sodium-fluoride (NaF) pellet trap used for removing any trace quantities of hydrogen fluorine (HF) from the fluorine. Nickel screens were used to contain the NaF within the trap. Several large Nupro bellows valves (remote solenoid operation) can be seen on either side of the 500 mℓ fluorine transfer vessel. The 984 mℓ electrolytic nickel-200 reaction vessel surrounded by the clamshell-type electrical resistance heater can be seen in the center of Fig. 4. Small orifices were located at the inlet and exit ends of the vessel to reduce entrainment of any portion of the solid UF_4 out of the vessel during the fill and/or purge portion of the tests. A remotely located variac was used to control the clamshell heater assembly and permitted heating the reaction vessel up to uniform temperatures of approximately 1000 K. A chromel-alumel thermocouple (nickel sheath) was used for temperature measurement. Small nickel boats (15 cm x 0.7 cm x 0.3 cm)

fabricated from high purity electrolytic nickel sheet (0.013-cm-thick) were used to contain the UF_4. These weighed approximately 2 g and permitted an accurate tare measurement to be made of the amount of UF_4 converted to UF_6.

As shown in Fig. 1, located downstream of the reaction vessel was a liquid argon (87 K) cold trap, with independent valving which was used to trap the regenerated UF_6. Downstream of the cold trap was a fluorine trap containing NaCl pellets. This trap collected the excess fluorine not used in the regeneration reaction. A post-test wet-chemistry analysis was used to determine the quantity of fluorine. Chlorine liberated from the NaCl material in the fluorine trap was collected in the NaOH pellet trap located immediately downstream of the fluorine trap (see Fig. 1). A large capacity vacuum system connected into the exit of these trap systems permitted pretest outgassing and bakeout of all critical components.

Contamination of the test components and trace impurities in the reactant materials (UF_4,F_2) may result in inconsistent or erroneous data; secondary reactions may also occur which could mask desired effects. Because of this, considerable emphasis was placed on reducing sources of impurities. All materials used in the test apparatus were selected based on their chemical resistance to F_2/UF_6 attack (see APPENDIX A of Ref. 11). A time-consuming passivation procedure was used which involved thorough chemical cleaning, leak checking, outgassing, and bakeout, followed by long time residence (>1 hr) under a pure fluorine atmosphere at elevated pressure (7.5 atm). The high purity nickel used for the reaction vessel and associated components was chemically assayed for verification of minimum impurity level and identification.

Fluorine Test Facility for UF_4/F_2 Flowing UF_6 Regeneration Tests

The results of the static fluorine UF_6 regeneration tests using the facility described in the prior section indicated that high conversion efficiency is possible under conditions of chemical equilibrium. However, information from static-batch-type tests is insufficient for design of a high conversion efficiency flowing system. Therefore some of the test equipment previously described was modified to permit conducting experiments with flowing UF_4/F_2 mixtures under simulated test conditions.

Figure 5 is a schematic of the components used in the UF_4/F_2 flowing UF_6 regeneration tests. Figures 6 and 7 are photographs showing the overall test facility and details of the test components as located within the large test tank (front cover removed). As shown in Fig. 5, the main components were the fluorine supply and flow metering system, the UF4 powder feeder system,

the dc arc plasma torch system, the fluorine injection manifold and reaction chamber, the uranium compound cryogenic trap system, and the post-test UF_6 regeneration/conversion trap system. The main fluorine supply was similar to that used in the prior batch-type experiments. A flow metering venturi was designed, fabricated, and calibrated to measure the fluorine injection flow rate. An in-line NaF trap was used to remove HF impurities from the fluorine supply. To provide a uniform and controlled feed of UF_4 powder, a powder feeder system developed under a previous NASA program (Ref. 9) was modified and adapted to the UF_4 system. The basic feeder system was a modified commercially available Roto-Feed hopper system (Model 1000A) manufactured by Geotel, Inc. The feeder operated on a volumetric feed/entrained flow principle. The feeder was adapted to the plasma torch system (see Fig. 6) to provide a positive feed at repeatable rates for UF_4 powder ranging in size from about 10-100-μm-dia. In operation the UF_4 powder ($\approx$0.5 kg) was loaded into the 2500 cc cylindrical canister. A variable-speed motor was used to drive a perforated wheel located at the base of the canister. The UF_4 particles entered the perforations and were carried by the wheel to an azimuthal exit port where they were discharged and entrained into the flowing stream of argon. A deagglomerator, incorporating a tangential inlet and a conical annulus, was located downstream of the canister to prevent the seed material leaving the canister from reagglomerating; it also acted as a pulsation damper. Inclusion of the deagglomerator significantly improved the steadiness of the flow.

For seed mass flow calibration purposes, a ball valve was located downstream of the deagglomerator to allow the seeded stream to be directed into either the plasma torch chamber or a seed collection system (for determination of time-averaged feed flow rate). This system was used to determine the steadiness and controllability of the seeded stream; the seed collector consisted of a foam collector and balance system. In all tests, prepurified argon was used as the carrier gas for entraining the UF_4 particles and transporting them to the plasma torch chamber.

The basic components of the plasma heater system consisted of a dc arc argon plasma torch, high-frequency starter, dc power supply, control console, and gas and water cooling systems. This system was assembled to supply argon at temperatures up to approximately 1000 K within the reaction chamber. The torch was a 50 kW modified commercial plasma torch (Thermal Dynamics H-50). The torch employed a water-cooled thoriated tungsten pin cathode and a hollow water-cooled cylindrical anode. Prepurified argon gas was fed axially through the annulus between the two electrodes. The use of argon gas resulted in essentially sputter-free operation. Ignition of the torch was accomplished with a high-frequency (15 kHz), high-voltage (18 kv peak-to-peak) starter system. Upon ignition, the starter was deactivated and the argon flow and arc current level were adjusted to provide the desired test conditions. The current to

the torch electrode was adjusted by varying a power-control rheostat. The torch control console (see right side of Fig. 6) contained all the necessary operating components, electrical meters, and flow metering system.

The components comprising the inlet mixing plenum, reaction chamber, and exhaust/trap/regeneration system are shown in Fig. 5. In the initial tests, a fused-silica test section was used to permit viewing the reaction via a closed-circuit television camera/monitor system. The thermally annealed fused-silica tubes were 17-mm-ID x 19-mm-OD x 15-cm-long (see Figs. 5 and 7). For tests conducted at higher reaction chamber temperatures, the upstream fused-silica tube was replaced with a similarly sized nickel tube, as indicated in Fig. 5. A shielded viton O-ring seal was used at the junctions. A fluorine injection ring manifold assembly was located, as shown in Fig. 5, between the fused-silica tubes and permitted injection of controlled amounts of fluorine ranging from approximately 0.09-0.3 g/s. Provision was also made for inclusion of a porous wall fluorine injector assembly in place of the standard fluorine injector manifold ring. This porous duct assembly was constructed similar to the unit previously tested and described in Ref. 11. A thermocouple was located downstream of the reaction chamber on the centerline location. A pressure transducer was used to monitor the pressure in the reaction chamber.

As shown in Fig. 6, the cryogenic trap system was located downstream of the reaction chamber, but outside of the test tank. Two trap systems were employed, as shown in Fig. 5; one used liquid argon and the other used liquid nitrogen. The liquid nitrogen trap system was used to convert the UF_6 that was generated in the reaction chamber and trapped in the upstream liquid argon trap to sodium metauranate (Na_2UO_4) for post-test analysis. The following equation describes the reaction:

$$UF_6 + 8NaOH \rightarrow Na_2UO_4 + 6NaF + 4H_2O$$

For this net reaction, the following two subreactions are also involved:

$$UF_6 + 4NaOH \rightarrow Na_2UO_4 + 4HF + 2NaF, \text{ and}$$

$$4HF + 4NaOH \rightarrow 4NaF + 4H_2O$$

The traps were isolated from one another by appropriate valves, as shown in Fig. 5, in order to measure separately the amount of uranium compounds collected. The effluent exhaust trap system was sized to permit quantitative determination of the amount of UF_4 converted to UF_6. To reclaim the UF_6 from the UF_6/argon cold trap, its temperature was raised slightly above 373 K (heat gun). The complete recovery and post-test procedure was conducted slowly since the reaction of the desorbed UF_6 with the sodium hydroxide solution (1.9 molar)

produced a brilliant-yellow precipitate and some HF vapor. The yellow precipitate (Na_2UO_4) formed upon reaction of the UF_6 with the sodium hydroxide solution was highly insoluble and was readily filtered, washed, dried, and weighed. The thoroughly washed precipitate was oven dried at 350 K and accurately weighted on an electronic balance prior to any post-test chemical analysis to determine uranium content. From the post-test chemical analysis, the equivalent mass of UF_6 could be readily calculated.

Fluorine Test Equipment and 1.2 MW RF UF_6 Plasma Facility for Selected Uranium-Oxygen-Fluorine Post-Plasma-Test Uranium Compound Batch UF_6 Regeneration Tests and Material Effects Tests

Figure 8 is a schematic of the fluorine supply and control system that was designed, fabricated, and installed at the 1.2 MW rf UF_6 plasma test facility. The major components included (1) the fluorine supply, enclosure system, and charcoal trap system located outside the uranium plasma laboratory, (2) the jacketed trough to safely route the main fluorine supply line to a location adjacent to the exhaust section of the rf plasma test configuration, (3) a calibrated venturi and associated pressure monitoring equipment located within a secondary sealed aluminum enclosure, (4) a portable remote control console including switches, interlocks, and activation/warning lights, and (5) a fluorine leak detection/alarm system (not shown in Fig. 8). The same type of nickel reaction vessel and nickel test boat assembly employed in the batch tests and described in the prior section was again used in these experiments.

Figure 9 is a photograph of the fluorine supply and exhaust trap system that was located for safety reasons outside the laboratory. Figure 10 is a photograph of the secondary sealed aluminum enclosure (front cover removed) which contained the fluorine flow metering equipment and nickel reaction vessel. The top half of the electrical resistance heater assembly is shown removed to better illustrate the reaction vessel assembly. The portable remote control console is shown at the top right of Fig. 10. Figure 11 is a photograph of the single channel fluorine leak detector/alarm system. This system was designed to provide an instantaneous indication should a hazardous condition develop; it was calibrated to detect ≥ 0.5 ppm of fluorine.

Refer to Ref. 10 for a detailed description of the rf induction heater system. The rf operating frequency normally used in all the experiments was approximately 5.4 MHz. All components of the rf induction heater were water-cooled; measurements were made of all quantities necessary for performing a component and overall system power balance on the rf equipment.

Figure 12 is a sketch showing a simplified cross section of the basic test chamber configuration employed in the tests using the 1.2 MW rf induction heater system with pure UF_6 injection. The selection of this configuration was based on the test results reported in Ref. 10, several desirable features are incorporated including the ability to independently vary the distribution of exhaust gas flow (axial bypass) and cooling water to the peripheral wall annulus and each endwall assembly. The peripheral wall was comprised of a concentric set of water-cooled fused-silica tubes. The argon vortex was driven from the right endwall only by a set of vortex injectors located tangent to the periphery of the endwall. The axial distance between endwalls was 10 cm. The rotationally symmetric rf argon plasma was initiated using a vacuum start technique to eliminate possible contamination. The rf power was coupled into the plasma via a pair of (9-cm-dia) single turn, water-cooled silver-plated work coils. (Refer to Ref. 11 for additional details of the rf system.)

To inject the pure UF_6 into the rf plasma, a UF_6 injector assembly was located on-axis and concentrically within the right endwall. It was fabricated from a 50-cm-long three concentric copper tube assembly; the injector tip protruded 2 cm into the test chamber from the face of the endwall. High pressure water heated via a steam heat exchanger system was used to control the temperature of the injector, thus eliminating solidification of UF_6 in the injector transfer line.

Figure 13 is a photograph of the UF_6/transfer system used in the tests. The 2ℓ Monel boiler assembly, surrounded by an electrical resistance heater, is shown located within a plexiglass enclosure which in turn was connected via a flexible metal duct to an exhaust gas scrubber system. Monel or other high nickel content materials were used throughout the majority of the system because of the high resistance to chemical attack by the hot, pressurized UF_6. (Refer to Ref. 11 for additional details on the corrosion aspects.) Details of the design and operation of the system are described in Ref. 10. This UF_6 handling and feeder system was developed to provide a controlled and steady flow of heated UF_6 at temperatures up to about 450 K. In conducting tests using UF_6 and other uranium-oxygen-fluorine compounds, it is extremely important to eliminate as much moisture and oxygen in the test system as possible. To aid in reducing these contaminants, several different trap systems were employed (see Ref. 11). In addition, the UF_6 was filtered through an elevated temperature NaF trap to remove the majority of HF.

DIAGNOSTIC EQUIPMENT

Figure 14 is a photograph of the overall 1.2 MW rf uranium plasma test facility and associated diagnostic equipment. The rf uranium plasma test tank was centrally located with the UF_6 feeder system located adjacent on the right side (not shown in Fig. 14) and the T.O.F. mass spectrometer system located adjacent on the left side. As shown in Fig. 14, the fluorine/UF_6 regeneration test tank was located between the mass spectrometer equipment and the master control console for the 1.2 MW rf system; the remote control console for the fluorine/UF_6 system was located adjacent to the mass spectrometer instrumentation rack and the large isolation table containing the mass balance and dye laser system. Details of the dye laser uranium line absorption monitoring technique are described in Ref. 10.

Figure 15 is a photograph of the portable custom-built ruggedized T.O.F. mass spectrometer vacuum station/spectrometer head assembly used in the argon/UF_6 rf plasma exhaust gas tests. Visible is the vacuum system comprised of a Varian 10-cm-dia M-4 diffusion pump with high speed valves and baffles to provide a net flow rate of 400 ℓ/s. On the top is shown a portion of the electronic subsystem, ion source, and inlet system (with cover plates removed), including the flight tube and instrumentation for the detectors and focusing grids. Two ion source cryopumping methods were devised and fabricated for evaluation to determine the one most effective in reducing drift tube and detector contamination by UF_6 and related halogenates (including UO_2F_2).

Figure 16 is a photograph showing the T.O.F. master control console which allowed the spectrometer to be remotely operated. Remote cables permitted operation up to a distance of about 6.75 m. Figure 17 is a photograph of the data system developed for use with the T.O.F. mass spectrometer system in the exhaust gas analysis tests. The main components were a Northern Scientific NS575A signal averager and a seven-track magnetic tape system.

Figure 18 is a schematic of the exhaust gas sampling, data acquisition, and data processing system as used in the T.O.F. mass spectrometer exhaust gas analysis experiments. A 0.5ℓ Monel canister containing filtered UF_6 was used to calibrate the instrument. The UF_6 data obtained with the signal averager and recorded on the seven-track magnetic tape were, in turn, transferred and processed on a PDP-6 computer system using a previously developed UTRC spectral data reduction program. Figure 18 also shows locations of the 1-mm-ID nickel sampling probes used to extract a sample of the effluent exhaust gas during a hot flow test with the rf UF_6 plasma. The sampling probe was positioned on the centerline of the exhaust duct at the following locations: in the thru-flow exhaust duct relatively close to the rf plasma test chamber;

downstream of the liquid argon cold trap; and, in the axial bypass duct relatively close to the rf plasma test chamber. The sampling line lengths were made as short as possible to enhance the response time of the system; electrical resistance heater tape was wrapped around all the nickel transfer lines and maintained at ≈ 450 K to eliminate possible condensation of the gaseous uranium compounds on the walls. All the nickel tubing transfer lines were prepassivated with pure fluorine (7.5 atm for one hour) at room temperature prior to introduction of UF_6.

Figure 19 is a photograph showing the complete T.O.F. mass spectrometer and exhaust gas sampling system located adjacent to the exit of the UF_6 rf plasma test chamber. The liquid nitrogen cold-finger cryopump scheme selected to reduce detector (and drift tube) contamination by UF_6 is shown in the upper left portion of the photograph. The exhaust gas sampling lines wrapped with heater tapes and in turn connected to the inlet of the mass spectrometer system can be seen at the top portion of the photograph. To the right of the mass spectrometer diffusion/fore pump vacuum system is the liquid argon exhaust trap used to collect the UF_6 from the effluent exhaust gas. (Refer to APPENDIX A for additional information on the UTRC custom-built, ruggedized T.O.F. mass spectrometer system.)

Diagnostic Instrumentation Used for Determining Form and Composition of Post-Test Uranium Compound Residue

Several different, complementary diagnostic methods were used in the post-test residue analysis: (1) x-ray diffraction; (2) emission spectroscopy; (3) wet chemistry; (4) scanning electron microprobe; (5) ion mass spectrometry/secondary ion mass spectrometry (ISS/SIMS); (6) IR spectrophotometry; and (7) photoacoustic spectrometry. The first six techniques were reported and discussed in detail in Ref. 10. The IR spectrophotometric technique was previously used for IR absorption measurements in the 2.5-20 μm wavelength range. A catalog of reference laboratory prepared uranium material standard compounds and samples of residue actually removed from different test configuration components was previously tabulated (Ref.11). A recently developed and improved IR spectrophotometer (Perkin-Elmer Model 599) was acquired under Corporate sponsorship during this test program, permitting an updating of the existing uranium compound reference catalog, particularly at the longer wavelengths (i.e., 10-40 μm regime). Figure 20 is a photograph of the IR spectrophotometer as used in the residue analysis. The source unit and sample location are shown at the right of the instrument; a typical output trace of absorbance as a function of wavelength is shown at the left side of Fig. 20.

Some of the residue obtained in several of the tests was amorphous in nature. This precluded obtaining quantitative information using the x-ray or electron diffraction techniques. The relatively expensive and time consuming ISS/SIMS procedures have been used with some success to provide insight into the chemical composition of the various residues formed on the different surfaces of the test apparatus. However, a considerable amount of reference and calibration standards have been required to allow a direct quantitative "fingerprinting" of the different compounds. The photoacoustic spectrometric (PAS) technique, on the other hand, can provide useful information of the characteristics of the amorphous uranium compound residues. Figure 21 is a schematic diagram of the PAS system and detection cell used in the post-test residue analysis. The basis of this technique is the radiationless conversion of resonant, periodic incident radiation into heat within the sample surface resulting in a periodic increase of the kinetic energy of the gas molecule in contact with the sample to produce pressure changes detectable as sound (refer to APPENDIX C for a detailed description of the development and application of this technique). The UTRC Analytical Chemistry Laboratory assisted in developing this technique and, in particular, tailoring it to nondestructive testing of the various uranium compounds found in the exhaust system after the rf uranium plasma tests.

DISCUSSION OF RESULTS

The overall objective of this research effort was continued development of a UF_6 injection, confinement, handling, and reprocessing system for the open-cycle rf-heated uranium plasma experiments. Successful design and operation of such a system will provide a basis for the design of UF_6 handling and recirculation systems applicable to future cavity reactor experiments directed toward establishing the feasibility of closed-cycle gaseous-fueled nuclear reactors. Some of this technology is also applicable to UF_6 nuclear pumped laser systems. Particular emphasis has been placed on the exhaust gas chemical reprocessing aspects and development of associated on-line exhaust gas sampling diagnostic techniques.

UF_4/F_2 Batch-Type UF_6 Regeneration Tests

A series of tests were conducted using the fluorine batch-type test facility described in the DESCRIPTION OF PRINCIPAL EQUIPMENT section and illustrated in Figs. 1 through 4. These tests were directed toward investigating the potential for converting solid UF_4 and other nonvolatile uranium compounds (representative of those formed in the actual rf uranium plasma exhaust system) to gaseous UF_6 in a static fluorine environment. This permitted establishing a test matrix for the effect of temperature, pressure, and residence time of pure fluorine on the overall conversion efficiency of the UF_4 to UF_6. The majority of tests were conducted using a fixed sample amount of laboratory-pure UF_4 which was loaded into the nickel test boat (see Fig. 22) and inserted into the nickel reaction vessel shown in Figs. 1 and 4. In the majority of tests, the reaction vessel and the boat were prepassivated with pure fluorine. A single fluorine gas fill and purge cycle procedure was used in each test. From the results of an initial series of tests, it was determined that the use of a NaF filter for removal of HF and prepassivation of the nickel boat with fluorine was required to achieve reproducible and consistent results. In these initial tests, the boat was examined for evidence of chemical attack after exposure to the fluorine. The UTRC ISS/SIMS instrumentation was used to examine the post-test coating/corrosion on the boats. After thorough prepassivation, this diagnostic analysis was no longer required.

An example of the results obtained from these batch-type regeneration tests is shown in Fig. 23. (See Fig. 22 for an example photograph of the pre- and post-test UF_6 regeneration test boat.) The conversion efficiency, η_c, defined as the percent of the initial mass of pure UF_4 powder converted to gaseous UF_6 (determined by post-test chemical analysis) is shown as a function of the nickel reaction vessel temperature. Based on separate calibration

measurements, the fluorine gas temperature was approximately equal to the measured reaction vessel temperature. The range of the fluorine pressure and residence time for these tests is shown at the top of Fig. 23. In all cases, the initial UF_4 sample weight was 250 mg. This amount was sufficient to uniformly cover the bottom of the boat. The results indicate that temperature is the dominant variable for obtaining a high conversion efficiency. As an example, for the tests at 1 atm fluorine pressure and a residence time of one minute (shown by the square symbols in Fig. 23), a temperature increase of 100 K, from 560 K to 660 K, resulted in an increase in the conversion efficiency from approximately 30 to 100 percent. Tests conducted at temperatures between 300 K and approximately 500 K (not shown in Fig. 23) consistently yielded conversion efficiencies less than 10 percent irrespective of the residence time used (up to and including one hour). Operation at fluorine pressures above 3 atm was not possible due to facility safety considerations. The results shown in Fig. 23 also indicate approximately the same increase in conversion efficiency was obtained by increasing the fluorine pressure from 1 atm to 3 atm at constant residence time (one minute) as was obtained by increasing the residence time from one minute to five minutes at a constant fluorine pressure of 1 atm. The error bar shown in the lower square symbol in Fig. 23 denotes the estimated experimental error associated with these tests.

Tests were also performed to investigate the conversion efficiencies of other solid uranium oxide and oxygen/fluoride compounds. In general, the results indicated relatively high batch-type conversion efficiencies could also be achieved under proper test conditions. For example, at a temperature of 630 K, a fluorine pressure of 3 atm, and a residence time of five minutes (250 mg sample weight), conversion efficiencies for several different laboratory-pure uranium compounds tested were as follows: UF_4-100%, U_3O_8-68%, UO_3-61%, UO_2F_2-50%, and UF_4/UO_2F_2 (50:50 mixture)-80%. Thus UF_4 is easier to convert than UO_2F_2 by a factor of about 2X. Also note that the combination, 50:50 mixture of UF_4/UO_2F_2 appears to convert approximately proportional to the compound composition ratio.

Batch-Type UF_6/Materials Compatibility Tests at Elevated Temperatures

Several exploratory tests were performed to investigate the effect of hot UF_6 on different candidate materials being considered for use in future rf uranium plasma exhaust gas reprocessing experiments. A total of fifteen different metal samples were simultaneously subjected to controlled exposure to hot UF_6. Both solid and porous metal samples were used. Figure 24 is a photograph showing the nickel boat and typical array of samples used in these tests. The results served to provide an indication of the types of fluoride coating and corrosion effects which might be expected in rf uranium plasma tests. Of all the materials tested, porous 316 stainless steel exhibited

extremely poor resistance to hot UF_6. The sample was found to have disintegrated after exposure to UF_6 at 673 K for seventeen hours. The overall results indicated Monel, copper, nickel, and the materials with high nickel content appeared to be most resistant to the hot UF_6. Refer to APPENDIX A of Ref. 11 for additional information on the corrosion/contamination aspects of UF_6 and associated reactant species.

The severity of UF_6 attack on possible candidate nuclear pumped laser window materials is also of interest and therefore several exploratory tests directed at this aspect were also included in this test series. Window material for use in a self-critical, direct nuclear pumped laser reactor must be compatible with UF_6 at temperatures up to approximately 600 K. Small samples ($\approx$200 mg) of high quality fused-silica, calcium fluoride, and aluminum oxide (sapphire) were simultaneously tested in the prepassivated nickel boat assembly. The test results indicated aluminum oxide to be the best candidate window material at the expected pressure and temperature operating conditions of future nuclear pumped laser systems. For example, at a UF_6 pressure of approximately 1 atm, a temperature of 700 K and a residence time of seventeen hours, the sapphire showed excellent resistance to the UF_6, while both the fused-silica and calcium fluoride experienced some attack. Other tests under similar test conditions but with the operating temperature increased to approximately 975 K revealed the aluminum oxide to also show signs of degradation.

Flowing UF_4/Fluorine Tests

The purpose of these tests was to obtain initial data necessary to determine the conditions under which solid UF_4 may be efficiently converted to gaseous UF_6 in a flowing argon/fluorine system. The results of the batch-type tests, described previously, have shown that high conversion efficiencies are possible under equilibrium conditions. However, the information from the static batch-type fluorine/UF_6 regeneration tests is insufficient for design of a high conversion efficiency flowing system where only relatively short residence times are available.

Figures 5, 6, and 7 illustrate the components used in these tests. The argon carrier and UF_6 flow rates and gas stream temperatures were selected to be comparable to those anticipated in future rf uranium plasma tests. For reference, the typical test procedure consisted of: pretest calibration of the UF_4 powder feeder system; activation of the plasma torch and argon feed systems (without UF_4/fluorine and argon discharging through the bypass system); initiation of gaseous fluorine flow; initiation of UF_4 powder flow; and test operation for preset times of 10 s or 20 s. Shutdown procedure was accomplished in the reverse order of the above.

Figure 25 is an example of measured UF_4 conversion data obtained from the flowing UF_6 regeneration tests. The conversion efficiency, η_c, was defined as the percent of the total mass of UF_4 powder injected into the test section for a specified test time that was converted to gaseous UF_6. The quantity of UF_6 generated was determined from post-test chemical analysis of the mass of Na_2UO_4 formed via the reaction of NaOH with the UF_6 transferred into the cryogenic collection trap. The corresponding net reaction was: $UF_6 + 8NaOH \rightarrow Na_2UO_4 + 6NaF + 4H_2O$. The gas temperatures shown in Fig. 25 were measured at the centerline of the reaction chamber at the exit location (see Fig. 5). Results are shown for three test configurations: a standard reference geometry; a geometry with a modified nickel inlet assembly which allowed a higher UF_4 flow rate; and a geometry with a porous Monel wall fluorine injector assembly. Refer to Fig. 5 for a schematic of the standard reference configuration. In this configuration the UF_4 powder feeder system was operated at a mass flow rate of 0.15 g/s. The plasma torch argon mass flow rate was maintained constant at 1.82 g/s throughout all tests in this series. The reaction test chamber pressure was typically 1.2 atm. The fluorine flow was held constant at 0.2 g/s.

The data shown in Fig. 25 shows the effect of increasing gas temperature on the conversion efficiency for a fixed chamber pressure and argon carrier gas flow rate. As found in prior batch-type UF_6 regeneration tests, the gas temperature has a pronounced effect on the conversion efficiency. For this test series the maximum conversion efficiency reached was approximately 60 percent and occurred at a gas temperature of about 880 K. Additional tests were attempted in an effort to investigate the effect of higher temperatures but minute water leaks in the plasma torch system during high power operation prevented reproducible results from being obtained. This re-emphasized the fact that even a minute trace of H_2O in the system can strongly influence the test results.

For operation at higher UF_4 flow rates and to better simulate the type and size of exhaust geometry employed in the 1.2 MW rf uranium plasma tests, the relatively large UF_4 mixing plenum (see Fig. 7) attached to the exit of the plasma torch was removed and replaced with a 1.7-cm-ID nickel tube. The triangular data points shown in Fig. 25 correspond to test results obtained with this modified system; the mass flow rate of the UF_4 powder was increased and maintained constant at 0.22 g/s. A similar variation in conversion efficiency with temperature was obtained; at 680 K essentially none of the UF_4 was converted to UF_6.

The square data points shown in Fig. 25 correspond to test results obtained with a configuration wherein a porous Monel duct, of the same type as used previously in the primary exhaust of the 1.2 MW rf uranium plasma system (see Ref. 11), was substituted for the fluorine injection manifold and test

section that are shown in Fig. 5. During these tests, the gaseous fluorine flow rate through the porous duct assembly was limited to 0.322 g/s due to pressure limitations imposed by the fluorine supply. This relatively low fluorine flow was approximately one order of magnitude (10X) less than the amount of argon bleed flow employed in prior 1.2 MW rf uranium plasma tests (Ref. 11). The argon thru-flow exhaust flow rate of approximately 1.89 g/s used in prior rf tests compares closely with the 1.82 g/s of argon flow used in these plasma torch flowing UF_4/fluorine tests. The shallow slope of the curve connecting the square data points in Fig. 25 may be due to several factors. A considerable fraction of the UF_4 may be concentrated in the central region of the exhaust duct, beyond the influence of the radial injection of the relatively low fluorine mass flow (see APPENDIX B of Ref. 11 for a detailed analysis of the heat and mass transfer aspects of flow within a porous duct with bleed flow augmentation)) and the radial temperature profile within the duct may be such that several hundred degrees Kelvin temperature difference exists between the centerline and the region near the wall. The data point shown at approximately 700 K corresponds to a pure fluorine mass flow rate of 0.101 g/s; the remaining three data points were all obtained under identical fluorine flow rate test conditions of 0.322 g/s. The two data points shown at approximately 870 K indicate the reproducibility obtained in these tests.

Post-test chemical analysis of the porous duct assembly revealed no measurable uranium compound coating. As a reference comparison, the weight of the uranium compound residue deposited on the porous duct in prior rf plasma tests using argon bleed flow (Ref. 11) was typically 0.1-0.3 mg for UF_6 injection mass flow rates of approximately 0.023 g/s.

These results are considered significant and demonstrate, for the first time, the feasibility of continuously injecting pure fluorine through the walls of a porous (5 μm nominal pore size) Monel exhaust duct without wall degradation and/or coating. Thus, this technique has potential application in future uranium plasma exhaust gas and UF_6 regeneration syetems.

Batch-Type Fluorine Tests Conducted At 1.2 MW RF Uranium Plasma Test Facility Using Actual Exhaust Residue

The purpose of these tests was to determine the conversion efficiencies obtainable using a batch-type fluorine/UF_6 regeneration system with actual residue material, as obtained from the exhaust after rf uranium plasma hot flow tests. Figure 10 is a photograph of the fluorine/UF_6 batch regeneration test apparatus used in these rf uranium plasma tests; Fig. 8 is a schematic of

the fluorine supply and control system. The test apparatus shown in Fig. 10 was located adjacent to the rf uranium plasma test tank (see Fig. 14).

Figure 26 is an example of the uranium compound conversion data acquired using actual samples of residue obtained from the rf uranium plasma exhaust trap system after hot flow tests. As in prior batch tests, the conversion efficiency, η_c, was defined as the percent of the initial mass of uranium compound material converted to pure gaseous UF_6. For reference, a laboratory-pure UF_4 standard sample was also tested; this result appears as the open symbol in Fig. 26. Complete (i.e., 100 percent) conversion from UF_4 to UF_6 occurred at a temperature of 650 K with a fluorine pressure of 1 atm and a residence time of 5 minutes. A 50 mg sample of UF_4 was used in this test. The remaining open symbols shown in Fig. 26 correspond to regeneration tests conducted using actual post-test exhaust trap residue obtained from the rf uranium plasma tests. This residue was removed from the liquid argon cold trap after the trapped UF_6 was cryopumped into the $NaOH/Na_2UO_4$ conversion system. The curve drawn through the open circle symbols illustrates the significant effect of increasing the reactor vessel temperature on conversion efficiency for the exhaust trap residue samples. At a temperature of about 660 K, a 100 percent conversion efficiency was obtained. Data from two additional tests are also included in Fig. 26. The open triangle and open diamond symbols correspond to shorter residence times of 1 and 0.2 minutes, respectively. Thus, residence times as short as 12 s can provide conversion efficiencies of about 95 percent.

Several different complementary diagnostic methods (see DESCRIPTION OF PRINCIPAL EQUIPMENT section and APPENDIX C) were used to determine the form and composition of the residue collected in the test chamber exhaust trap. Based on an analysis of the samples, the residue was determined to be a combination of UF_4 and UO_2F_2; the UF_4 being the dominant species. In some specimens, minor amounts of the oxide of uranium were also detected (UO_3 or UO_2). For comparison, the conversion efficiencies obtained with different mass ratios of laboratory-pure samples of these compounds correspond to the three solid symbols shown in Fig. 26. These results indicate that UO_2F_2 is relatively difficult to convert when compared to pure UF_4. The 50:50 ratio (mass basis) of UF_4 and UO_2F_2 yielded a conversion efficiency of approximately 66 percent.

The results shown in Fig. 26 indicate that a batch-type UF_6 regeneration scheme using static fluorine and temperatures of approximately 700 K is a viable technique for complete conversion of the uranium compound post-test residue collected in the exhaust trap/separator system.

To provide additional information on the effect of sample mass on conversion efficiency, a series of tests was also completed wherein the mass of test sample was increased (in ≈ 500 mg increments) from 50 mg to 2500 mg. The results indicated that for pure UF_4, sample quantities up to about 600 mg could be used at the test conditions shown in Fig. 26 (i.e., P_{F_2} = 1 atm, T = 660 K, t = 5 m) before a decrease in conversion efficiency was noted. For sample quantities of 2500 mg, the conversion efficiency was reduced to about 30 percent. At the higher sample quantities the amount of UF_4 could not be uniformly spread over the boat surface area and, therefore, a multiple layer shielding effect was present and not accounted for.

Time-of-Flight Mass Spectrometer, On-Line Exhaust Gas Sampling Tests, and Exhaust Trap Analysis

The rf uranium plasma tests using the time-of-flight (T.O.F.) mass spectrometer and on-line exhaust gas sampling system were conducted using the equipment shown in Figs. 15 through 19. A schematic of the rf uranium plasma exhaust gas sampling, exhaust gas trap, and post-test UF_6 regeneration, data acquisition, and effluent processing systems is shown in Fig. 18. The concentration of UF_6 and other volatile constituents present within the exhaust system at three distinct locations was determined from measurements using the nickel sampling probes. A sampling probe was positioned on the centerline of the exhaust duct at the three locations shown in Fig. 18. Prior to calibration tests with the canister of filtered UF_6 shown in Fig. 18, the entire system was prepassivated with pure fluorine at 7.5 atm pressure for a one hour time duration. Samples of UF_6 from the calibration canister source were transferred into the mass spectrometer system; the data system, as shown in Fig. 18, was employed to process the data. The UF_6 fragmentation pattern obtained with the signal averager was recorded on seven-track magnetic tape. These data were in turn transferred and processed on the PDP-6 computer system using a UTRC spectral data reduction program.

Figures 27 and 28 are examples of the pure UF_6 mass spectrum, over two mass ranges, obtained directly from the computer printout visual display using the entire data processing system shown in Figs. 17 and 18. The data point number given on the abcissa is equivalent to the corresponding address number in the multichannel scaler. The UF_5^+ peak, which is the dominant ion, was used to estimate the UF_6 concentration. The precision of this peak is typically one percent.

Example data from actual mass spectrometer system hot flow tests are shown in Figs. 29 and 30. The data shown in Fig. 29 were obtained with the system set on a low sensitivity. The number of counts indicated on the abscissa of the plot is proportional to the concentration of a given mass

number species in the mixture. In comparison, the data shown in Fig. 30 were obtained with the system set on a high sensitivity. This high sensitivity permitted detecting low concentrations of impurities such as trichloroethylene (C_2Cl_3H) as shown in Fig. 30.

Refer to APPENDIX A for supporting information on the calibration data, fragmentation patterns, and sensitivity scale factors. In the majority of tests, the scan time for the entire mass range from 20-400 atomic mass units was 6 s and, generally, thirty-two spectra were averaged per data file.

Following the comprehensive calibration test series, and after completion of several hours of shakedown testing using the exhaust gas sampling instrumentation with the rf uranium plasma system, the CuO-BeO detector gain characteristics were diminished to below an acceptable minimum and, hence, the detector was replaced. The instrument was inspected, serviced by the UTRC Instrumentation Laboratory, and restored to operation in less than one day. It was estimated that the detector was exposed to various concentrations of UF_6, ranging up to 100 percent, for approximately six hours. The total instrument time for the detector was in excess of 500 hours. The majority of this time included instrumentation checkout and cold flow calibration. Through SIMS analysis, UF_4 coating of the CuO-BeO surface was confirmed. In addition, detailed inspection of the ion-source pump cryofinger confirmed that the major fraction of the ingested UF_6 and related halogenates were deposited as UF_4. A complete inspection of the ion source, flight tube, and vacuum station indicated negligible UF_4 deposition. Background impurity levels in the mass spectrometer were sufficiently small that any impurities observed in the mass spectra were definitely attributed to the feed gases and/or the sampling system (e.g., trace of trichloroethylene as shown in Fig. 30); this solvent was used as part of the final chemical cleaning procedure.

Refer to TABLE I for an example of the UF_6 concentrations measured at the different exhaust locations of the 1.2 MW rf UF_6 plasma facility using the on-line T.O.F. system, as shown in Figs. 18 and 19. The highest concentration of UF_6 determined was about 500 ppm and was measured on the centerline of the thru-flow duct upstream of the trap system. Concentrations less than 50 ppm were present in the axial bypass exhaust duct. This was approximately the noise equivalent concentration of UF_6, as measured by the UF_5^+ ion after averaging the spectra in the background rf environment. In comparison, the sensitivity of commercially available T.O.F. units is typically 500 ppm.

The liquid argon exhaust trap and liquid nitrogen conversion trap system (see Fig. 18) were developed to affect high UF_6 recovery efficiencies. The test results indicated that almost all the UF_6 transferred through the primary exhaust system can be collected in the liquid argon exhaust trap system. UF_6 concentration measurements conducted using the mass spectrometer

system operating in the highest sensitivity mode and with the sampling probe located downstream of the liquid argon exhaust trap (location No. 3 in Fig. 18) indicated no trace of UF_6 was detected downstream of the trap system. To confirm these results, in selected tests a small Lithium Hydroxide (LiOH) pellet was positioned (contained within a nickel screen) inside the exhaust line downstream of the trap; no color change to bright yellow normally associated with the presence of UF_6 was observed.

Post-Test Residue Sample Diagnostic Analysis

TABLE II is an example of a complete post-test analysis conducted using the various complementary diagnostic equipment described in DESCRIPTION OF PRINCIPAL EQUIPMENT section. In this example the total operating time was 4.8 m corresponding to a total UF_6 injected mass of 8.93 gms. The corresponding test conditions shown in TABLE I are representative of those obtained using the 1.2 MW rf UF_6 plasma test facility. Based on the post-test residue analysis, less than one percent of the total UF_6 injected was deposited out within the rf plasma test chamber. Approximately one percent of the total injected UF_6 was deposited uniformly on the walls of the axial bypass exhaust duct. Approximately 90 percent of the total injected UF_6 was collected in the cryogenic trap/downstream exhaust duct system where efficient post-test batch-type UF_6 regeneration techniques could be applied. The approximately 6 percent of the total that was unaccounted for was believed to be located in the fittings, valves, and associated hardware where complete disassembly and removal for post-test analysis was difficult. As shown in TABLE II, the primary constituents of the residue were UF_4, UO_2F_2, and occasionally a trace of uranium oxide (either UO_2 or UO_3).

Of the total mass of residue collected in the cryogenic trap system, 317.4 mg was UF_6 which was transferred to the conversion trap system, as shown in Fig. 18. To reclaim UF_6 from the liquid argon cold trap, its temperature was raised to approximately 400 K and the UF_6 was cryopumped into a NaOH solution. The reaction of the UF_6 with the 1.9 molar NaOH solution formed an insoluble yellow precipitate of sodium metauranate (Na_2UO_4). This was also accompanied by a discharge of HF vapor. The Na_2UO_4 was filtered, washed, dried at 300 K, and weighed. A chemical assay analysis was used to determine the uranium content. An average value of 68.4 weight percent was obtained; from this the equivalent UF_6 elemental uranium was calculated.

Figures 31 and 32 are example electron photomicrographs and x-ray maps of the post-test sample residue (Na_2UO_4) removed from the UF_6 regeneration trap system. Positive identification was made using the scanning electron microprobe together with separate IR spectrophotometer absorption measurements including comparison against standard reference samples.

Figures 33 and 34 are examples of the type of information obtained using the SEM system on the sample residue removed from the exhaust trap after an rf uranium plasma test. Two magnifications were used to better illustrate the topographical variations present. Figure 34 shows the accompanying x-ray maps obtained; the predominance of uranium is shown by the white area.

Refer to APPENDIX C of this report and APPENDIX A of Ref. 11 for additional information on the reference standards used in the analysis. Prior analysis required the use of the ISS/SIMS system for positive identification of both the UF_4 and UO_2F_2. The availability of the PAS system permitted a rapid determination of these species including any associated contaminants. Considerably more reference samples and calibration tests would have to be conducted before complete positive identification together with quantitative mass analysis of each species present could be obtained.

The overall results indicate that adequate diagnostic techniques have been developed and applied to determine the composition of uranium compound residue from different components of the rf uranium plasma test hardware. Included has been an extended compilation of uranium compound reference standards for use in future post-test residue compound identification. The majority of these standards are for the U-O-F compounds.

REFERENCES

1. Latham, T. S.; F. R. Biancardi; and R. J. Rodgers: Applications of Plasma Core Reactors to Terrestrial Energy Systems. AIAA Paper 74-1074, AIAA/SAE 10th Propulsion Conference, San Diego, CA., 21-23 October 1974.

2. Rodgers, R. J.; et al.: Investigation of Applications for High-Power, Self-Critical Fissioning Uranium Plasma Reactors. NASA CR-145058, Sept. 1976.

3. Thom, K.; and F. C. Schwenk: Gaseous Fuel Reactor System for Aerospace Applications. AIAA Conference on the Future of Aerospace Power Systems, Paper No. 77-513, St. Louis, MO., Mar. 1977.

4. Kendall, J. S.; and R. J. Rodgers: Gaseous Fuel Reactors for Power Systems. Paper Presented at 12th Intersociety Energy Conversion Engineering Conference, Washington, D.C., 28 Aug.-2 Sept. 1977.

5. Rodgers, R. J.; et al.: Analyses of Low-Power and Plasma Core Cavity Reactor Experiments. United Technologies Research Center Report R75-911908-1, May 1975.

6. Thom, K.; et al.: Gaseous-Fuel Nuclear Reactor Research for Multimegawatt Power in Space. International Astronautics Federation XXVIIIth Congress, Prague, 25 Sept.-1 Oct. 1977.

7. Barton, D. M.; et al.: Plasma Core Reactor Experiments. Paper 3D-13, 1977, IEEE International Conference on Plasma Science, RPI, Troy, N.Y., May 1977.

8. Mensing, A. E.; and J. S. Kendall: Experimental Investigation of Containment of a Heavy Gas in a Jet-Driven Light-Gas Vortex. United Technologies Research Center Report D-910091-4, Mar. 1965. Also issued as NASA CR-68926.

9. Roman, W. C.; and J. F. Jaminet: Development of RF Plasma Simulations of In-Reactor Tests of Small Models of the Nuclear Light Bulb Fuel Region. United Technologies Research Center Report L-910900-12, Sept. 1972.

10. Roman, W. C.: Laboratory-Scale Uranium RF Plasma Confinement Experiments. United Technologies Research Center Report R76-912205, Sept. 1976. Also issued as NASA CR-145049, Sept. 1976.

REFERENCES (Continued)

11. Roman, W. C.: High Temperature UF_6 RF Plasma Experiments Applicable to Uranium Plasma Core Reactors. United Technologies Research center Report R78-912556, Dec. 1978 (to be issued as NASA CR).

12. Cameron, A. E.; and D. F. Eggers: Rev. Sci. Instr., 19, 605, 1948.

13. Wolff, M. M.; and W. E. Stevens: Rev. Sci. Instr., 24, 616, 1953.

14. Glenn, W. E.: University of California Radiation Laboratory Report UCRL-1511, Oct. 1951.

15. Wiley, W. C.; and I. H. McLaren: Rev. Sci. Instr., 26, 1150, 1955.

16. Zabielski, M. F.; H. T. Diem; and B. R. F. Kendall: Theoretical Analysis of a Cylindrical Time-of-Flight Mass Spectrometer With Radial Ion Paths. Int. J. Mass Spectrom. Ion Phys., 5, 1970, pp 349-360.

17. Zabielski, M. F.; R. Stein; and B. R. F. Kendall: Theoretical Analysis of a Time-of-Flight Mass Spectrometer With Spherical Electrodes and Radial Ion Paths. Int. J. Mass Spectrom. Ion Phys., 10, 1972/73.

18. Compton, R. N.: On the Formation of Positive and Negative Ions in Gaseous Uranium Hexafluoride. J. Chem. Phys., 66, 1977, pp 4478-4485.

19. Beattie, W. H.: Mass Spectral Intensities of Inorganic Fluorine - Containing Compounds. Applied Spectroscopy, Vol. 29, No. 4, 1975.

20. Nagatoro, Y.: Analysis of 235-U Isotope Ratio by a Mass Spectrometer for UF_6. (In Japanese) Shisuryo Bunseki, Vol. 23, 1975, pp 119-125.

21. Hassan, H. A.; and J. E. Deese: Thermodynamic Properties of UF_6 at High Temperatures. North Carolina State University, Raleigh, N.C. NASA Contractor's Report NASA CR-2373, Jan. 1974.

22. Hildenbrand, D. L.: Thermochemistry of the Gaseous Uranium Fluorides. Prepared for Los Alamos Scientific Laboratory. Stanford Research Institute Project NO. PYU 4822, June 1976.

23. Hildenbrand, D. L.: Thermochemistry of Gaseous UF_5 and UF_4. J. of Chemical Physics, Vol. 66, No. 11, June 1977.

24. Kistemaker, J.; M. J. P. C. Nieskens; and H. N. Stein: Thermodynamic Calculations on the System Uranium-Carbon-Fluorine. Part II FOM-Instituut Voor Atom-En Moleculaphysica, Amsterdam. FOM-RAPPORT NR 41.734, April 1977.

25. Dewitt, R.: Uranium Hexafluoride, A Survey of the Physico-Chemical Properties. Good Year Atomic Corp., Portsmouth, OH., REPT GAT-280, 1960.

26. Nagarajan, G.: Thermodynamic Properties of Some Metal Hexafluorides. Bulletin Des Societies Chimiques Belges, Vol. 71, Jan.-Feb. 1962, pp 77-81.

27. Galken, N. P.; Tumanov, Yu. N.; and Butylkin, Yu. P.: Thermodynamic Properties of Pentafluorides of 5F Elements. Russian J. of Physical Chemistry, Vol. 44, No. 12, 1970, pp 1726-1727.

28. Weinstock, B.: Rec. Chem. Prog. 23, 23 (1962).

29. Krohn, B. J.; W. B. Person; and J. Overend: J. of Chem. Phys. 65, 969 (1976).

30. Tumanov, Y. N.: Thermodynamic Stability of Uranium Hexafluoride. Russian J. of Inorganic Chemistry, Vol. 13, No. 6, 1968, p 782.

31. Godnev, I. N.; and Sverdlin, A. S.: Chaleurs de Formation Des Fluoreures D'Uranium Gazeux. CER-TR-R-1905 Commissariat A L'Energie Atomique, Paris 1968.

32. Godnev, I. N.; and A. S. Sverdlin: Izv. VYS. Ucheb Zaved Khim I Khim Tekhnol 9, 40 (1966).

33. Settle, J. L.; H. M. Feder; and W. N. Hubbard: Fluorine Bomb Calorimetry VI. The Enthalpy of Formation of Uranium Hexafluoride. J. of Phys. Chem. 67, 1892 (1963).

34. Stull, D. R.; and H. Prophet; et al.: JANAF Thermochemical Tables, 2nd Edition. NSRDS-NBS 37, National Bureau of Standards, Washington, D.C., June 1971.

35. Kendall, W. B.: Thermodynamic Properties of Uranium Gas. J. of Chem. and Eng. Data, Vol. 7, No. 4, Oct. 1962, p 540.

36. Hultgren, R. L.; R. L. Orr; P. D. Anderson; and K. K. Kelly: Selected Values of Thermodynamic Properties of Metals and Alloys. Wiley & Sons, N.Y., 1963.

37. Kazanskii, K. A.; and V. M. Novikov: Thermophysical and Electrophysical Properties of Uranium Hexafluoride at Temperatures of $(1\text{-}11)\cdot 10^3$ K and Pressures of 0.1-100 atm. Translated from Teplofizika Vysokikh Temperatur, Vol. 14, No. 3, pp 450-456, May-June 1976 by Plenum Publishing Corp., N.Y.

38. Adams, M. J.; and G. F. Kirkbright: Analyst, 102, 281, 1977.

39. Rosenewaig, A.; and A. Gersho: J. Appl. Physics, 47, 65, 1976.

40. Eaton, H.; and J. Stewart: A Microcomputer Assisted, Single Beam, Photoacoustic Spectrometer System for the Study of Solids. Chem. Dept. Rept. U-60, Univ. of Conn., Storrs, CT., Nov. 1977.

41. Adams, M. J.; B. C. Beadle; A. A. King; and G. F. Kirkbright: Analyst, 101, 533, 1976.

42. Rodden, C. J.: Analysis of Essential Nuclear Reactor Materials. U. S. Atomic Energy Commision Report, 1964, p 104.

LIST OF SYMBOLS

AMU	Atomic mass unit, kg
C	Constitutent concentration, ppm
C_P	Specific Heat, cal/mole-K
d	Time-of-Flight (T.O.F.) source significant dimension, cm
D	T.O.F. analyzer drift tube significant dimension, cm
e	Electron charge, C
f	RF operating frequency, MHz
ΔF	Heat of formation, kcal/mole
ΔG	Gibbs energy of formation, kcal/mole
H	Enthalpy, kcal/mole
I	Relative signal intensity, dimensionless
K_1, K_2	Equilibrium constants, dimensionless
M,m	Mass of molecules, charged particles, kg
$\dot{m}_{Ar}$	Argon flow rate, g/s
$\dot{m}_{F_2}$	Fluorine flow rate, g/s
$\dot{m}_{UF_6}$	Uranium hexafluoride flow rate, g/s
$\dot{m}_{UF_4}$	Uranium tetrafluoride flow rate, g/s
N	Number density, cm^{-3}
P	Pressure, atm, torr*, mm Hg, or Pa (1 atm = 101.3 kPa)
P_c	Chamber pressure, atm
P_{F_2}	Fluorine pressure, atm

*1 torr = 1 mm Hg = 133.3 Pa

LIST OF SYMBOLS (Concluded)

Q	Power, kW
S	Sensitivity factor, dimensionless
δ	Entropy, cal/mole-K
T	Temperature, K
$T_{\mathbb{Q}}$	Centerline temperature, K
t	Time, minutes (m) or seconds (s)
V	Accelerating potential or voltage, volts
W	Weight of residue material, mg
X	Mole fraction, dimensionless
λ	Wavelength, nm
η_c	Conversion efficiency, percent

APPENDIX A: SUPPORTING INFORMATION ON UTRC CUSTOM BUILT, RUGGEDIZED TIME-OF-FLIGHT (T.O.F.) MASS SPECTROMETER SYSTEM*

Introduction

A knowledge of the chemical fate of the uranium atom is crucial to gaseous UF_6 nuclear reactor design. However, it is not within the scope of this research effort or possible at this time to develop a kinetic model that can accurately describe the chemical processes from initial UF_6 injection into the plasma to exhaust product collection and reprocessing. The most important reasons for this are (1) uncertainties in and/or lack of fundamental data, (2) simultaneous homogeneous and heterogenous competing reactions, and (3) complex aerodynamic flow conditions and associated temperature gradients. In order to gain some understanding of the uranium atom fate, an analysis of reaction products was undertaken. This APPENDIX describes the system and method used to study the products that remain in the gas phase from room temperature up to the maximum temperature determined by probe operation.

Although the measurement of UF_6 is complicated by its high reactivity and the corrosiveness of its reaction products, a series of tests, which were reported in Ref. 11, showed that on-line mass spectrometry was a feasible measurement method and, in addition, possessed several distinct advantages over the alternate IR spectrometer technique. These cursory tests were conducted using a commercial T.O.F. mass spectrometer that could not, however, be exposed to significant amounts of UF_6 without serious damage to its ion optics and vacuum chamber. Because of this, consideration was given to adapting a UTRC mass spectrometer design specifically for UF_6 measurements.

Theory of Operation

Preceding a description of the various design considerations used for this mass spectrometer, some general information on the operation of a mass spectrometer will be given. Most mass spectrometers can be divided into three distinct components that are housed in a vacuum chamber (Fig. 35). The first of these components is the ion source. In the source, ions are produced from the gas of interest which has been introduced into this region by means of a gas sampling system. These ions are then accelerated into the analyzer, the second component. In the analyzer, the ions are physically separated according to their mass. Since most mass spectrometers compare electromagnetic effects with inertial effects, ions are actually separated according to

*Support and design of T.O.F. provided by M. F. Zabielski.

their mass-to-charge ratio. Thus, doubly charged ions will be indistinguishable from singly charged ions of half the mass. For convenience, however, the following text will hereafter refer to the "mass" of an ion, but it should be borne in mind that what is really meant is "mass-to-charge ratio". The third component is the detector. Its function is to provide a usable electrical signal for each group of mass-separated ions which impinge upon it. The magnitude of this electrical signal is related in a linear way to the partial pressure of the gas from which the ions were produced.

The basic theory of operation of the T.O.F. mass spectrometer is readily understood. If objects of different masses are given the same energy, the objects with smaller masses will have velocities greater than those with larger masses. Hence, if all the objects travel the same distance, and if the time required for each object to travel this distance is measured, then the mass of each object can be determined.

Specifically, in the T.O.F. system, gas molecules of interest are introduced into the source region and ionized by bombardment with low energy (70-100 eV) electrons, as schematically indicated in Fig. 36. Within this energy range, most molecules are usually singly ionized (i.e., only one electron is removed from the molecule). In the ionization process, in addition to the removal of an electron from the molecule, rupturing of molecular bonds can also occur. This bond rupture is normally called molecular fragmentation. The ionized molecules are then pulsed out of the source region by an electric field and enter a field free region, the analyzer. The ion source is designed so that most ions, regardless of their mass, acquire approximately the same energy. Because the drift region is field free, the ions simply coast with the lighter ions traveling faster than the heavier ones ($mv^2/2$ = constant). These differences in velocity result in the arrival of isobaric (equal mass) packets of ions at the detector at different times. The detector is normally an electron multiplier whose first stage converts the ion packets into electron packets. The electron packets are then amplified and fed into a display or data processing unit.

The concept of a T.O.F. mass spectrometer originated with A. E. Cameron and D. F. Eggers (Ref. 12) in 1948. The work of Wolff and Stephens (Ref. 13) and Glenn (Ref. 14) followed. However, the major advance in the ion optics of the T.O.F. instrument was made by W. C. Wiley and I. H. McLaren (Ref. 15). It is upon the basic concept of the Wiley and McLaren two-field source that modern T.O.F. instruments have been developed.

A detailed reproduction of the two-field theory is beyond the scope of this APPENDIX and would add little to the fundamental understanding of the T.O.F. mass spectrometer. However, a simplified single-field theory should prove informative. If it is assumed (1) that the source dimension, d, as

shown in Fig. 36, is considerably smaller than the drift tube dimension, D (i.e., $d \ll D$), (2) that the ions are produced in a plane parallel to the ion accelerating grid structure, (3) that the ion accelerating pulse is sufficiently long so that all ions of interest have left the source, then the following equations are valid. The time required for an ion to travel from the source to the detector is the sum of the times spent in the source and in the drift tube,

$$t_{total} = t_{source} + t_{drift} \tag{1}$$

The first assumption ($d \ll D$) implies $t_{source} \ll t_{drift}$, therefore:

$$t_{total} \cong t_{drift} \tag{2}$$

The second and third assumptions allow the following equation to be written:

$$m_i v_i^2/2 = n_i \, e \, V_p \tag{3}$$

where m_i is the mass of the ion of the i^{th} type, v_i is the velocity of that ion, V_p is the potential through which the ion falls, n_i is the number of electrons removed from the molecule, and e is the basic electronic charge. The velocity in the drift region can be written as

$$v_i = \frac{D}{t_{i\,drift}} \cong \frac{D}{t_{i\,total}} \cong \frac{D}{t_i} \tag{4}$$

which upon substitution into Eq. (3) yields:

$$t_i = K_i (m_i)^{1/2} \tag{5}$$

where

$$K_i = (D^2/2n_i e V_p)^{1/2} \tag{6}$$

Thus the flight time of an ion of a particular mass is proportional to the square root of its mass.

In the two-field instrument, the ion source has two accelerating regions. This field arrangement compensates for the fact that ions, in practice, are not produced in a plane, but over most of the volume of the source region. However, upon considering the equations of motion of this instrument, the

relation between time and mass is the same, except that an effective source potential, V_e, is substituted for V_p.

Design Considerations

For several years, UTRC has employed on-line mass spectrometry to study combustion, laser, and complex flow processes in nonlaboratory environments. Because commercially available spectrometers are not designed for these environments, UTRC has developed, under Corporate funding, a spectrometer specifically designed for nonlaboratory applications. This spectrometer consists of two separate sections: (1) a portable vacuum chamber for the spectrometer head and to which electronics associated with the ion source and detector are attached; and (2) a small master electronics control unit. These are shown in Figs. 8 and 9. This packaging scheme permits the spectrometer to be coupled to the gas source with shortest possible sampling lines and also allows instrument control from a remote location, if required.

The basic design of the spectrometer head was tailored for the analysis of low molecular weight ($m < 100$ atomic mass units (AMU)) combustion products. The design consisted of a mechanically simple, ruggedized structure with each major component constituting a module which could be readily replaced for cleaning or repair. For the UF_6 measurements of interest in this program, the ion optics were modified for high molecular weight analysis ($M \leq 425$ AMU). To obtain adequate resolving power along with an acceptable overall spectrometer size, a drift region of a nominal 50 cm was selected. The ion optics of the source were adapted using Corporate-developed ion optics programs similar to those previously reported (Refs. 16 and 17). The detection part of this spectrometer consisted of an ion gate and an electron multiplier. An ion gate, as opposed to an electron gate, was used because it provides: (1) a significantly simpler mechanical structure; (2) a more stable baseline; and (3) an opportunity to investigate metastables. This ion gate is used to convert the 50 MHz real-time output of the spectrometer into a signal suitable for a data acquisition system or recorder. The high mass transmission of this gate was improved by reducing the overall ion path length and by increasing the magnitude of the gating signal by a factor of four. Both of these design changes proved effective as will be shown in the following section on calibration. The detector chosen was a CuO/BeO 18-stage electron multiplier with replaceable dynodes which are relatively inexpensive. This type of detector was chosen because it seemed highly probable that UF_4 would seriously degrade the performance of the multiplier with exposure time to UF_6. This, indeed, was observed and was similar to that reported by Compton (Ref. 18).

To reduce the possibility of spectral interferences in the mass 300 region, a high speed vacuum station was used for the spectrometer head. The speed delivered to the head was approximately 400 ℓ/s. The terminal pressure in the head was approximately 2-4x10^{-8} torr (approximately 3-5x10^{-6} Pa*) while the typical operating pressure used in the experiments with sample injection was 4-10x10^{-6} torr (approximately 5-7x10^{-4} Pa). To minimize contamination of the spectrometer optics, chamber, and the diffusion pump, the ion source was cryopumped with a stainless steel cryo-finger cooled to liquid argon temperatures. The sample was injected perpendicular to the ion optical axis to maximize the efficiency of this pumping method. Because of the ion source design and the effectiveness of this pump, no servicing of the spectrometer ion source head was required, with the exception of the expected detector replacement, for all the tests made in this study.

The environment of this study was doubly harsh relative to typical combustion studies, because not only is the spectrometer exposed to corrosive gases, but also the spectrometer electronics and data acquisition system are exposed to a high radio-frequency (RF) environment (approximately 5.4 MHz). All the spectrometer electronics, which were constructed under Corporate funding, were provided with extra RF suppression with special attention to proper grounding techniques. Because of this, no electronic instabilities were observed even when the total RF power deposited into the plasma discharge was approximately 50 kW.

Similarly, the data acquisition system, which was a Northern Scientific NS575A signal averager, was also properly isolated and proved virtually immune to this RF environment. Through the use of this data system and proper tuning of the spectrometer detection electronics, the spectrometer was scanned from approximately 12 AMU to 425 AMU in approximately six seconds. Typically 16 to 32 spectra were averaged per data file which was then recorded on a digital tape system for computer processing. Because spectra of high quality could be obtained in a relatively short time, the amount of data obtained for a given experiment time was extremely large in comparison with that available from analog recording techniques. Since the display of the signal averager could be interrogated immediately after each run, trends in a test sequence could be established as the experiment progressed. Final data reduction, however, was performed using a computer. The major portions of the computer software used to process the spectra were the following: (1) a fast Fourier transform (FFT) routine to analyze the noise content of the spectra; (2) a Martin-Graham digital filter to smooth the data, if necessary; (3) a baseline subtraction routine; (4) a mass marker routine; (5) a peak area and height routine; and (6) a deconvolution routine for unfolding overlapping peaks when required.

*Pascals (alternate metric unit)

Fundamental and Calibration Data

The fragmentation pattern of molecules under bombardment by electrons in the ion source of the mass spectrometer is important for the reduction of spectra, especially in regions of spectral overlap. This fragmentation pattern for UF_6 on the UTRC modified T.O.F. mass spectrometer is given in TABLE III for an ionizing electron energy of 75 eV. The precision of the data (approximately 5 percent) for the lower abundances does not reflect a limitation of the spectrometer, but the limited statistics in the less intense peaks. These statistics could be improved by increasing the detection sensitivity; however, for this program, only the UF_5^+ peak, which is the dominant ion, was employed to estimate UF_6 concentrations. The precision of the more intense peaks is typically 1 to 2 percent. It should be noted that the UF_6 parent ion was easily detected, but is not an energetically favored ion. Also included in TABLE III are the T.O.F. fragmentation patterns reported by Beattie (Ref. 19) and the magnetic sector spectrometer pattern reported by Nagatoro (Ref. 20). In addition, fragmentation data for the UTRC spectrometer with the 20 ms data system filtering necessary for operation in the high RF background is also given.

In order to estimate molecular concentrations, account must be taken of ionization cross sections at specific electron energies and ion source pumping speeds. Figure 37 gives the sensitivity factors for two different data system filter time constants. The 20 μs filter data was converted from argon to nitrogen and compared with the commercial T.O.F. mass spectrometer data reported by Beattie (Ref. 19). This comparison showed that the UTRC spectrometer sensitivity for UF_6, relative to nitrogen, is approximately a factor of three greater than that of the commercial T.O.F. device*.

For all data included in this report, the inlet pressure was maintained at 20 torr (3×10^4 Pa) and the spectrometer pressure was between 1×10^{-6} torr (1×10^{-4} Pa) and 1×10^{-5} torr (1×10^{-3} Pa). The noise equivalent concentration of UF_6, as measured by the UF_5^+ ion after averaging 32 spectra in an RF environment, was approximately 50 ppm. This is approximately an order of magnitude better than the sensitivity of the commercial instrument used in the feasibility study reported previously in Ref. 11.

*Beattie reports a sensitivity which is the reciprocal of the convention used in this APPENDIX.

Summary

It has been demonstrated that 50 ppm measurements of UF_6, as determined by the UF_5^+ ion peak, can be made to better than ± 20 percent quantitative accuracy in a high RF background. With the use of a high speed data system and signal averaging, these measurements can be made in approximately three minutes. By proper modification of the ion optics and electronics, a significant improvement in the relative sensitivity of UF_6 to argon/nitrogen has been achieved. During all the measurements taken in this study, the instrument was serviced only once for the replacement of the CuO/BeO dynode electron multiplier. Such a replacement was anticipated and accomplished within one working day. The fragmentation pattern data, although this is not a laboratory instrument, compare favorably with previously reported data. The detection of impurities associated with the decomposition of reactor components and sampling handling has alsobeen demonstrated and an example is shown in the main body of this report.

These results suggest that this ruggedized T.O.F. mass spectrometer will prove useful in UF_6 conversion studies which are planned to be performed in future tests. In addition, the capability to perform additional fundamental studies, such as appearance potential measurements for all halide ions of uranium and UF_4 vapor pressure measurements has been demonstrated. Essentially no experimental data are available in the literature with this critical information. Finally, this measurement method may also prove suitable for composition measurements necessary in the study of nuclear pumped laser systems.

APPENDIX B: EVALUATION OF AVAILABLE THERMODYNAMIC PROPERTY DATA FOR UF_6, UF_5, AND UF_4*

The application of gaseous UF_6 at high pressures and temperatures to both gaseous core nuclear reactors and nuclear pumped laser systems has refocused interest in the thermodynamic property data for UF_6, UF_5, and UF_4. The property data are relatively well documented for gaseous UF_6 at low temperatures (<600 K). However, for UF_5 and UF_4, some available data are uncertain and thus only approximate thermochemical data are available. In the majority of the research, thermochemistry of UF_5 and UF_4 has been investigated by high temperature mass spectrometry. Refer to the list of references (21-37) given in the following discussion for a more detailed description of the previous investigations and instrumentation used.

The purpose of this APPENDIX is to provide a brief evaluation of the available thermodynamic property data for UF_6, UF_5, and UF_4 as applicable to the range of test conditions employed in the UF_6 rf plasma experiments reported herein and planned in future tests.

Hassan (Ref. 21) and Hildenbrand (Refs. 22 and 23) calculated thermodynamics functions of gaseous UF_6, UF_5, and UF_4 by standard statistical methods using spectroscopic and molecular constants from the following sources:

	Hassan	Hildenbrand
UF_6	Refs. 25,26	Ref. 28
UF_5	Ref. 27	Ref. 29
UF_4	Refs. 27,30	Ref. 30

As an example, a comparison of the thermodynamic properties at 1400 K calculated by Hassan and Hildenbrand are shown in the following TABLE:

*Assistance in analysis provided by Richard Roback.

	C_p cal/mole-K		$H_{1400}-H_{298}$ kcal/mole		δ cal/mole-K	
T=1400K	Hassan	Hildenbrand	Hassan	Hildenbrand	Hassan	Hildenbrand
UF_6	37.33	37.33	39.67	39.68	144.81	144.84
UF_5	31.33	31.44	32.92	33.44	130.51	136.10
UF_4	25.59	25.59	27.34	27.34	117.93	117.92

There is generally good comparison except for the enthalpy of UF_5. This difference, as shown in the last column of the TABLE, is not yet resolved.

Kistemaker (Ref. 24) utilizes Gibbs' free energy for UF_6 from Hassan (Ref. 21), along with the dependence of the free energy on temperature for UF_5. Kistemaker uses a linear relationship between $\Delta G^\circ_{293} = -374$ kcal/mole and $\Delta F^\circ_{1700} = -337$ kcal/mole which he calculates for UF_4.

Hildenbrand recommends that the entropy and free energy functions of UF4 and UF_5 he calculates be increased by 8.5 and 3.0 cal/mole-K, respectively, to be consistent with measured equilibrium data.

A summary of the heat of formation data and corresponding sources is shown in the following TABLE:

	$UF_6(G)$	$UF_5(G)$	$UF_4(G)$
Hassan	$-505^{(31)}$	$-440^{(31)}$	$-366^{(21)}$
Hildenbrand	$-510.8^{(33)}$	$-460.6^{(22,23)}$	$-377.8^{(22,23)}$
Kistemaker	$-505^{(32)}$	$-460^{(24)}$	$-386^{(24)}$

Hassan calculated the thermodynamic properties of UF_6 at relatively high temperatures (Ref. 21). This work was an extension of the work of Galken and Tumanov (Ref. 27). Hassan used the equilibrium constant approach assuming the following four reactions:

$$F_2 \rightleftarrows F \qquad (1)$$

$$UF_6 \rightleftarrows UF_4 + 2F \qquad (2)$$

$$UF_5 \rightleftarrows UF_4 + F \qquad (3)$$

$$UF_4 \rightleftarrows U + 4F \qquad (4)$$

The thermodynamic functions for F and F_2 were obtained from Ref. 24 while those for U were obtained from Ref. 25.

It appears that a discrepancy exists in the equilibrium constant reported by Hassan (Ref. 21, Table 15, p. 30) as pointed out by Kistemaker (Ref. 24). There is an indication that the heat of vaporization for uranium gas was omitted in the calculation for the free energy change for reaction (4). Kistemaker and Hildenbrand also utilize thermodynamic functions for uranium gas from Ref. 26.

Comparison of calculations made by Kistemaker (Ref. 24) with those reported by Hassan (Ref. 21) leads to the conclusion that UF_6 is much less stable if the Kistemaker thermodynamic data are used for UF_6, UF_5, and UF_4. Figure 38 is an example of the calculated thermal decomposition products of UF_6 using data from Hildenbrand, Kistemaker, and Hassan. The Kistemaker calculations show the start of UF_6 decomposition at approximately 1250 K while Hassan calculated the start at about 1700 K. Calculations performed at UTRC using Hildenbrand data indicated that UF_6 is slightly more unstable than that indicated by Kistemaker. Calculated equilibrium compositions of UF_6 reported by Hazanskii and Novikov (Ref. 37) generally agreed with the Hassan data.

This evaluation should aid in future calculations and analysis involving UF_6, UF_5, and UF_4 thermodynamic property data as applicable to UF_6 gaseous core nuclear reactors and nuclear pumped laser systems.

APPENDIX C: ADDITIONAL INFORMATION ON PHOTO-ACOUSTIC-SPECTROMETER (PAS) DIAGNOSTIC EQUIPMENT FOR POST-TEST ANALYSIS OF URANIUM COMPOUND RESIDUE

Several different complementary diagnostic techniques have been employed throughout the uranium plasma test program for post-test analysis of the location, quantity, and chemical composition of the residue obtained from the rf uranium plasma tests. The techniques employed have included (1) x-ray diffraction, (2) IR spectrophotometry, (3) scanning electron microprobe, (4) emission spectroscopy, (5) wet chemistry, and (6) ion mass spectrometry/secondary ion mass spectrometry (SIMS/ISS). References 10 and 11 contain details of each of the above systems.

In the present and prior experiments, uranyl fluoride, UO_2F_2, was identified by its infrared (IR) absorption band (10.6 μm). See Ref. 10 for example spectra and summary of key reference samples used in IR spectrophotometric analysis. The relatively expensive and time consuming SIMS/ISS procedures were successfully used to provide insight into the chemical composition of the various residues formed on the different surfaces of the test apparatus. However, the available x-ray/electron diffraction techniques could not be used to identify amorphous residue. For example, uranium tetrafluoride (UF_4) is not easily analyzed by any routine, nondestructive technique. Consequently, a new complementary technique was investigated to aid in characterizing amorphous uranium compound residues. Of particular importance was the establishment of a technqiue for positive identification and quantification of the amorphous, powdery UF_4 present in much of the exhaust system and other key components of the rf uranium plasma test apparatus. The UTRC Analytical Chemistry Laboratory* assisted in developing this technique and, in particular, tailoring it to nondestructive testing of the various uranium compounds found in the exhaust system of the rf uranium plasma experiment.

The basis of the PAS technique is the radiationless conversion of resonant, periodic, incident radiation into heat within the sample surface. The result is a periodic increase of the kinetic energy of the gas molecules in contact with the sample to produce pressure changes detectible as sound. References 38 and 39 describe the detailed theories of the signal generation process. In general, for a given incident wavelength, the magnitude of the sound is dependent on the optical absorption coefficient of the sample for that particular wavelength, the thermal diffusivity, and the sample thickness. By monitoring the magnitude of the sound versus the incident radiation wavelength, a photoacoustic spectrum is produced which is analogous to a conventional absorption or transmission spectrum.

*Assistance provided by H. Eaton.

Figure 21 is a schematic diagram of the single beam photoacoustic spectrometer overall system and detection cell. Reference 40 contains details of the apparatus. This system is schematically similar to that described in Ref. 41. As shown in Fig. 21a, the source was a 1 kW xenon lamp; the monochromator used a UV-VIS grating, 20-nm bandpass slits, f/3.5 efficiency, and a 20 nm/min drive assembly. Calibration was performed using the 633 nm line of a He-Nè laser. Figure 21b shows the PAS test cell. Reradiation passes through the quartz window and strikes the sample which was attached to the front surface of a 1-cm-dia solid optical grade quartz rod. The quartz rod was used to minimize the internal cell volume to approximately 0.5 cm^3. The sample size was normally 5 mg (sufficient to cover the end surface of the quartz spacer). A microphone was mounted inside the union and was insulated electronically with teflon material. The leads for the microphone were fed through an aluminum plate, as shown in Fig. 21b, to complete the seal of the PAS cell.

As shown in Fig. 21a, a lock-in amplifier was used for signal acquisition. A cadmium sulfide photoconductive cell was aimed directly at the source through the beam chopper (84 Hz) and provided the necessary reference signal. A microcomputer system was employed for data acquisition. Since both the output power of the xenon light source and the throughput efficiency of the monochromator vary with wavelength, it was necessary to correct the spectrum produced by the single beam instrument. The microcomputer system accomplished this by obtaining the signal ratio of the sample to a black-body absorber at each wavelength. The microcomputer system also accomplished the following: increased the signal to noise ratio by averaging several spectra; stored and updated the reference and sample spectra; produced the difference between two sample spectra; and permanently stored the data on magnetic tape for recall.

Figures 39 and 40 are examples of the uranium compound spectrum of UO_2F_2, UF_4, and UO_3 as obtained using the PAS system. A well-defined characteristic spectrum of UF_4 is noted with relative absorption peaks occurring at 438 nm, 478 nm, 536 nm, 623 nm, and 658 nm. This spectrum of the solid also agrees well with that obtained from the solution as reported in Ref. 42. The UF_4 spectrum shown in Fig. 39 is a good example of the type of resolution (approximately 15 nm) obtainable for a multibanded spectrum having comparatively large absorption coefficients. For UO_2F_2 the relative absorption peaks occur at 427 nm and 335 nm. For UO_3, the relative peaks occur at 447 nm and 348 nm. UF_4, UO_2F_2, and UO_3 exhibit unresolved absorption bands below 300 nm. Even though the PAS spectra are in many ways analogous to asborption spectra, it is difficult to assign absolute optical density values to individual peaks. Therefore, the technique is to use relative values obtained by comparison with internal standards. For example, binary mixtures of UF_4 and UO_2F_2 can be analyzed by normalization of the 643 nm peak of UF_4 followed by comparison of the magnitude of the 335 nm peak of UO_2F_2 with known calibrated mixtures of the two uranium compounds.

Figure 41 shows results of an analysis of binary and trinary mixtures of UF_4, UO_2F_2, and UO_3. The relative PAS signal intensity is shown as a function of the UF_4 weight percent concentration. A relatively linear relationship was found for weight composition of UO_2F_2 (between 1-90 percent) versus relative photoacoustic signal. Both UF_4 and UO_2F_2 are stable in the presence of oxygen at room temperature and are formed under conditions where oxygen is only a contaminant; whereas, UO_3 represents an interference to the analysis. Based on this, the UO_3 concentration would be expected to be relatively low. In comparison, UO_2 and U_3O_8 have spectra similar to carbon black (exhibit strong absorption throughout the UV and visible region) and would contribute to the background rather than acting as interferences. UO_2 and U_3O_8 would not normally be expected to form except by combustion in the presence of large amounts of oxygen.

The analysis of the UO_2F_2 in a UF_4 matrix using the normalization technqiue as an internal standard is considered significant and shows for the first time that the PAS technique can be used with complex mixtures where there exists an interfering contribution to the analyte absorption peak. The limit of sample detection and the linearity of the signal strength with component concentration are sample dependent due primarily to the magnitude of the absorption coefficient and the background contribution from the more abundant component present, respectively. The overall results indicate that the limit of detection (for a 5 mg sample size) is less than 50 μg for UO_2F_2 and less than 500 μg for UF_4.

In addition to identification of the stable uranium compounds, the study of the effects of the most likely contaminants, oxygen, and water vapor is also important because these contaminants within the uranium rf plasma test configuration can react with the UF_6 to produce side reactions and thus lower the overall regeneration efficiency of the system. The UO_2F_2 would normally be formed as a result of contamination since the UF_6 was relatively pure as received, filtered prior to use, and should contain essentially no water vapor or oxygen. From thermodynamic considerations, the UO_2F_2 can be formed from UF_6 as a result of hydrolysis (e.g., $UF_{6_g} + 2H_2O_g \xrightarrow[K_1]{} UO_2F_{2_g} + 4HF_g$.

Similarly, UF_4 can be produced by the reaction of UF_6 with water vapor (e.g., $UF_{6_g} + H_2O_g \xrightarrow[K_2]{} UF_{4_g} + 2HF_g + \frac{1}{2}O_{2_g}$) Approximate equilibrium constants K_1 and K_2 are given by $K_1 = (UO_2F_2)(HF)^4/(UF_6)(H_2O)^2 \approx 4 \times 10^{12}$ and $K_2 = (UF_4)(HF)^2(O_2)^{\frac{1}{2}}/(UF_6)(H_2O) \approx 1.8 \times 10^{11}$, respectively, as calculated from the free energy functions. By monitoring the ratio of UO_2F_2 to UF_4 in the deposit, the effect of common contaminants such as water vapor and oxygen may be evaluated using thermodynamic equilibrium calculations. This new technique may prove valuable in future UF_6 plasma experiments and can be used to supplement the other techniques currently in use.

TABLE I

EXAMPLE OF UF_6 CONCENTRATIONS AS MEASURED AT DIFFERENT EXHAUST LOCATIONS OF RF UF_6 PLASMA FACILITY USING ON-LINE T.O.F. SYSTEM

See Fig. 18 for Schematic of Test Configuration
See Fig. 19 for Photograph of Overall Configuration
See Fig. 30 for Example of Mass Spectral Intensity Output

f_o (MHz)	Q (kW)	P_c (atm)	$\dot{m}_{Ax}$ (g/s)	$\dot{m}_{UF_6}$ (g/s)	$\dot{m}_{UF_6}$ (g/s)	t (min)	Sampling Probe Location See Fig.18 for Location Code	Concentration (ppm)
5.4322	44	2.4	3.02	1.1	0.031	4.8	#1	≤ 50
							#2	465
							#3	<50

TABLE II

See Fig. 18 for Schematic of Test Configuration
See TABLE I for Corresponding Test Conditions - Total Amount of UF_6 Injected: 8.93 g
See Figs. 31 and 33 for Example of Post-Test Residue Removed and Analyzed
See Fig. 26 for Example of Post Test UF_6 Regeneration Results Using Batch-type Fluorine System
See Description of Principal Equipment Section for List of Complementary Diagnostic Equipment Employed

Component	Weight of Residue W(mg)	Constituents	Coating Pattern
UF_6 Injector	8.04	UF_4, UO_2F_2, UO_3	No coating on endface, whitish grey coating near tip region, mint green coating near endwall interface.
Right End-Wall Assembly	5.32	UF_4, UO_2F_2, UO_2	Annular rings from center toward appx. mid radius of endwall, mint green at inner region progressing toward dark grey at outer region.
Fused-Silica Tube	12.71	UO_2F_2, UF_4, UO_2	End regions clean, whitish pale green mist over central region progressing to slate grey at edges.
Left Endwall Assembly	3.2	UF_4, UO_2F_2	Annular coating similar to right endwall, progressing from pale green to brownish green at near mid radius location.
Axial Bypass Duct	105.37	UF_4, UO_2F_2	Light mint green coating, relatively uniform over entire inside surface near endwall assembly, cleaner region downstream.
Interstage Exhaust Duct	3.42	UF_4, UO_2F_2	Light mint green uniform coating - somewhat more whitish at inlet region - indication of swirl pattern noted.
High Pressure Water-Cooled Exhaust Duct	293.81	UF_4, UO_2F_2	Light mint green uniform coating - trace of paler green at downstream end, swirl pattern also noted
Low Pressure Water-Cooled Exhaust Duct	6426.51	UF_4, UO_2F_2	Pale green coating at inlet region - darker green coating toward exit portion - circumferentially uniform coating.
Cryogenic Trap	317.40	UF_6 (Qnt. transferred to liquid N_2 conversion trap (Na_2UO_4) UF_4, UO_2F_2, UO_3	
	1225.28	Residual Left in Trap after cryopumping out UP_6	Post-test sectioning of cryogenic trap revealed relatively uniform pale green coating.
Exhaust Lines Downstream of Cryogenic Trap	0	-	Clean lines - no observable or measurable coating.

TABLE III: UF_6 FRAGMENTATION PATTERN

Source of Data		UTRC (20μs filter Time Constant)	Beattie	Nagataro	UTRC (20ms filter Time Constant)
Instrument Type		Ruggedized T.O.F.	Commercial T.O.F.	Magnetic Sector	Ruggedized T.O.F.
Electron Energy (eV)		75	70	75	75
Mass Number	Ion	Abundance	Abundance	Abundance	Abundance
119	U^{++}	0.0534	0.032	*	*
128.5	UF^{++}	0.0550	0.063	*	*
138	UF_3^{++}	0.0534	0.057	*	*
147.5	UF_3^{++}	0.0568	0.052	*	*
157	UF_4^{++}	0.0542	0.046	*	*
238	U^{+}	0.0593	0.085	0.054	0.048
257	UF^{+}	0.1097	0.185	0.109	0.081
276	UF_2^{+}	0.1964	0.332	0.203	0.169
295	UF_3^{+}	0.1865	0.283	0.193	0.161
314	UF_4^{+}	0.2425	0.262	0.277	0.226
333	UF_5^{+}	1.0000	1.000	1.000	1.000
352	UF_6^{+}	0.0160	0.004	*	*

*Not given.

SCHEMATIC OF COMPONENTS USED IN UF_4/F_2 BATCH UF_6 REGENERATION TESTS

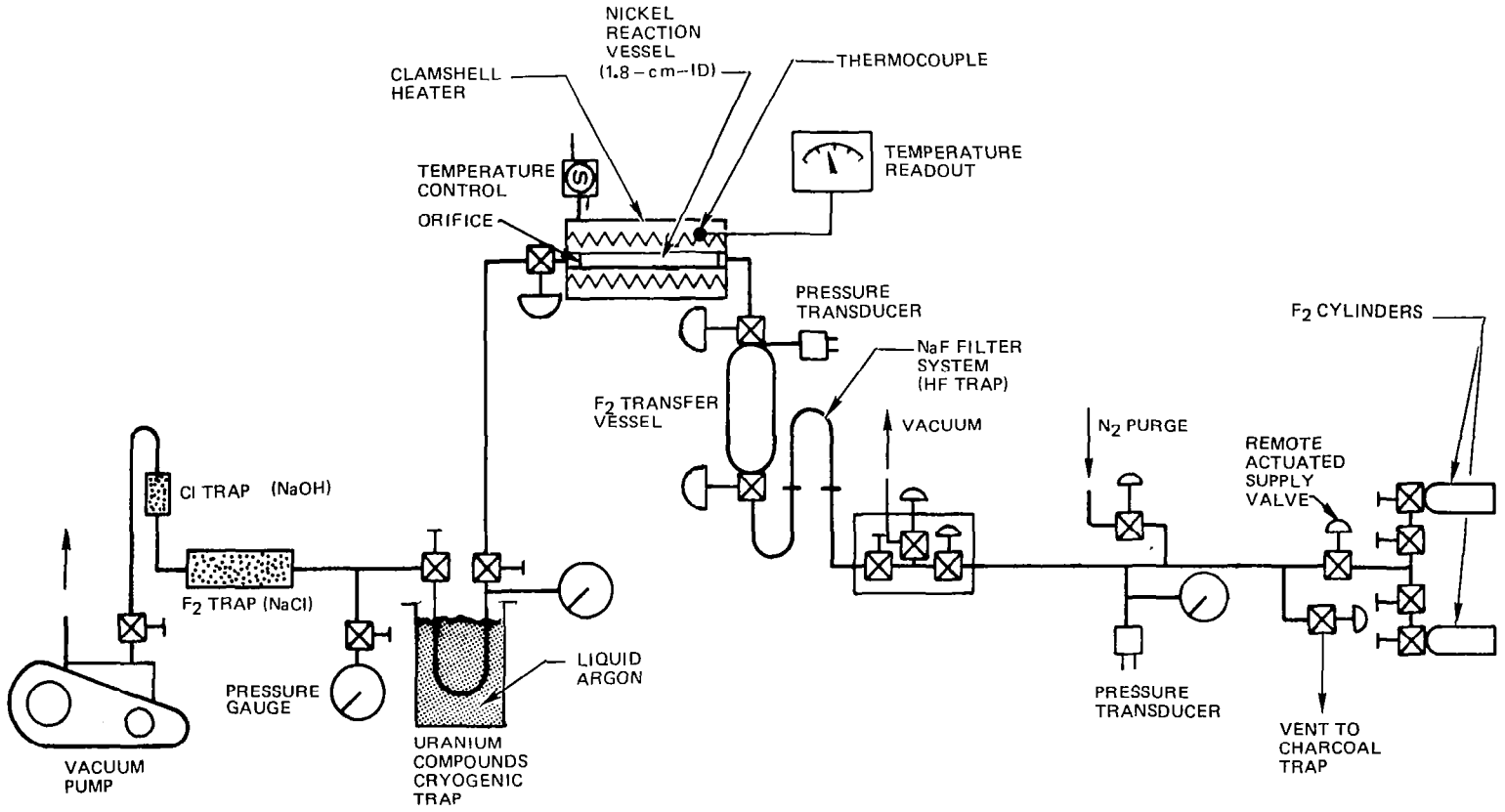

FIG. 1

PHOTOGRAPH OF FLUORINE TEST FACILITY USED IN UF_4/F_2 BATCH UF_6 REGENERATION TESTS

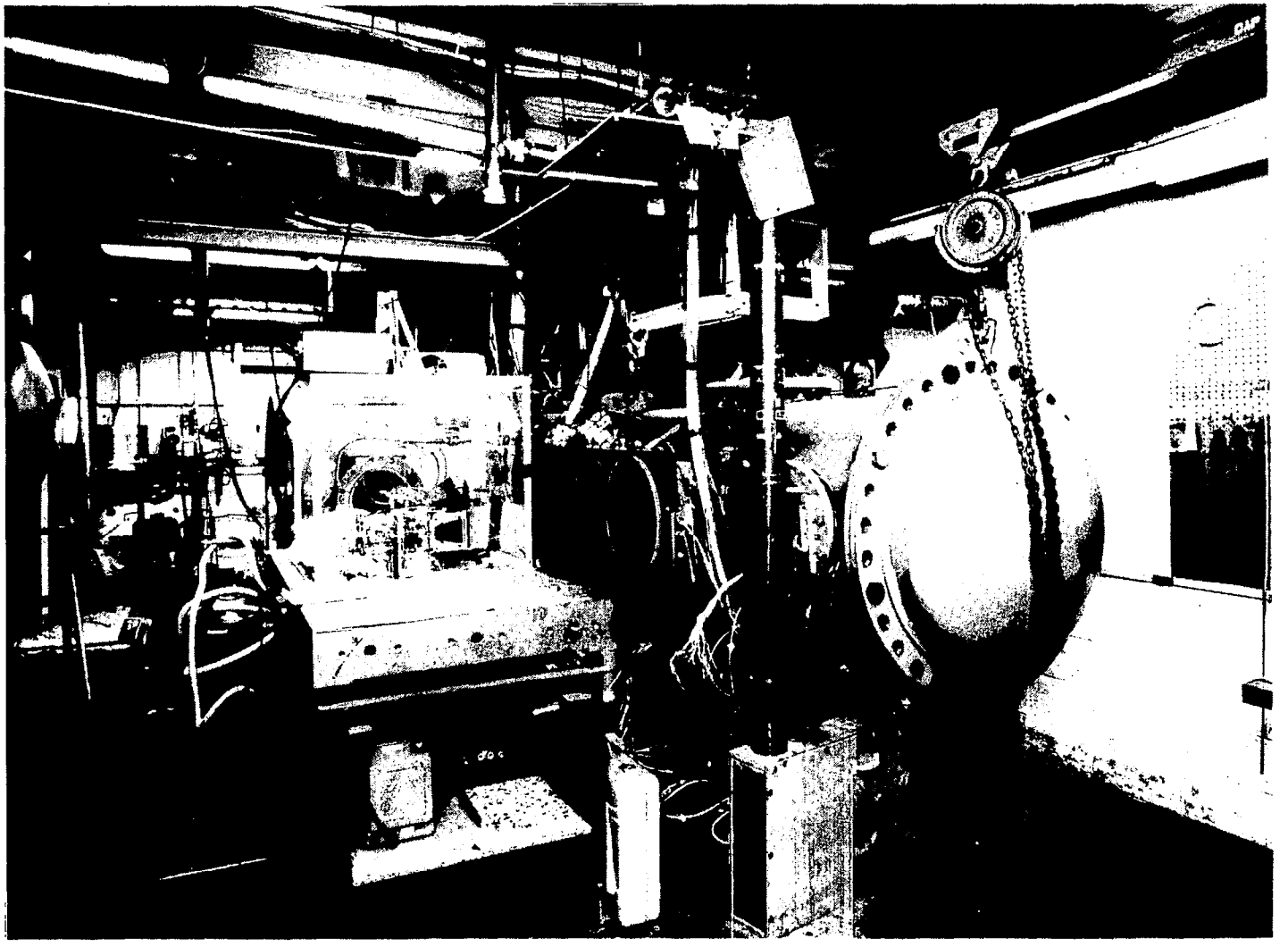

FIG. 2

FIG. 3

PHOTOGRAPH OF REMOTE MASTER CONTROL CONSOLE USED IN UF_4/F_2 BATCH UF_6 REGENERATION TESTS

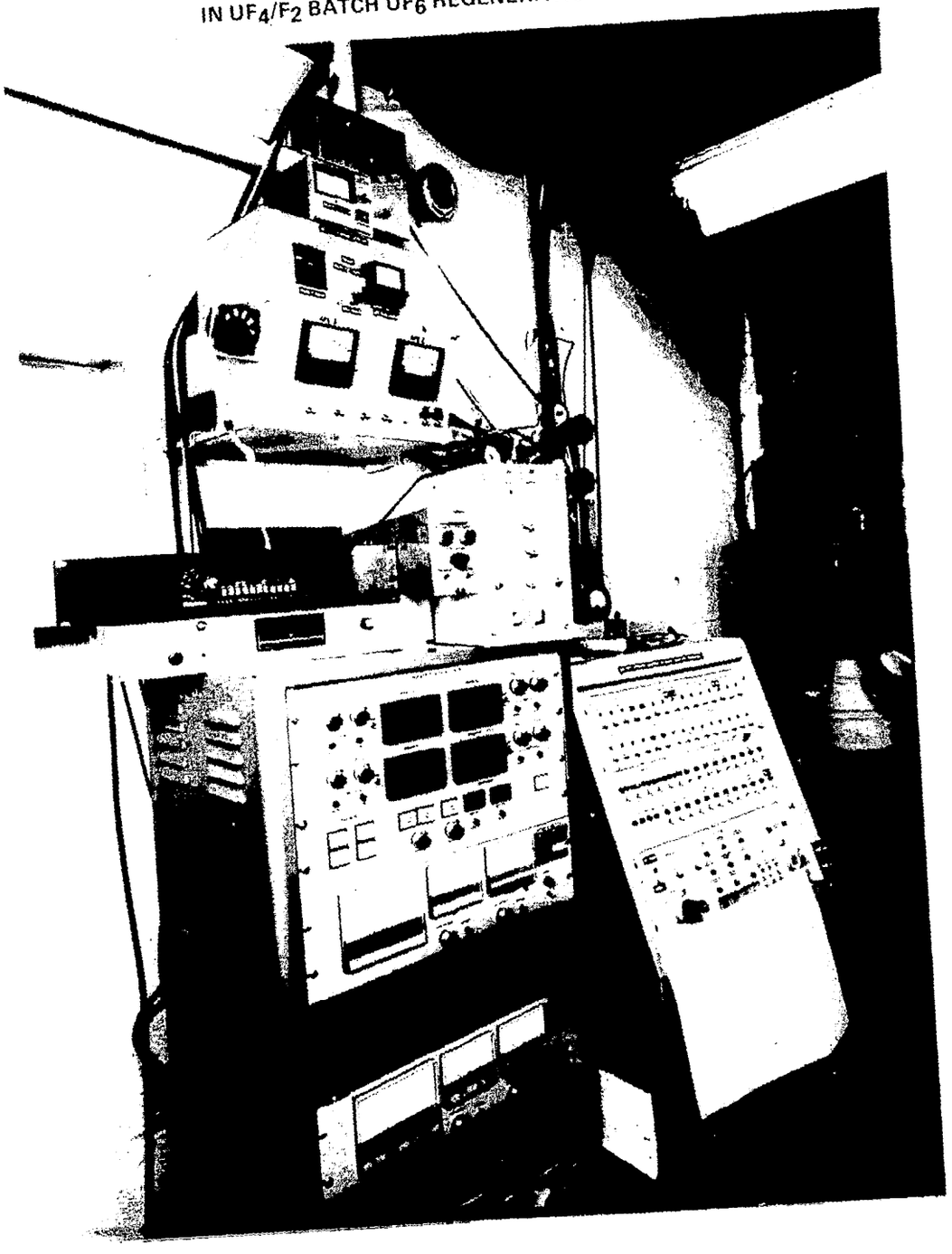

PHOTOGRAPH OF TEST COMPONENTS USED IN UF_4/F_2 BATCH UF_6 REGENERATION TESTS

(FRONT DOME REMOVED)

FIG 4

SCHEMATIC OF COMPONENTS USED IN FLOWING UF_4/F_2 TO UF_6 REGENERATION TESTS

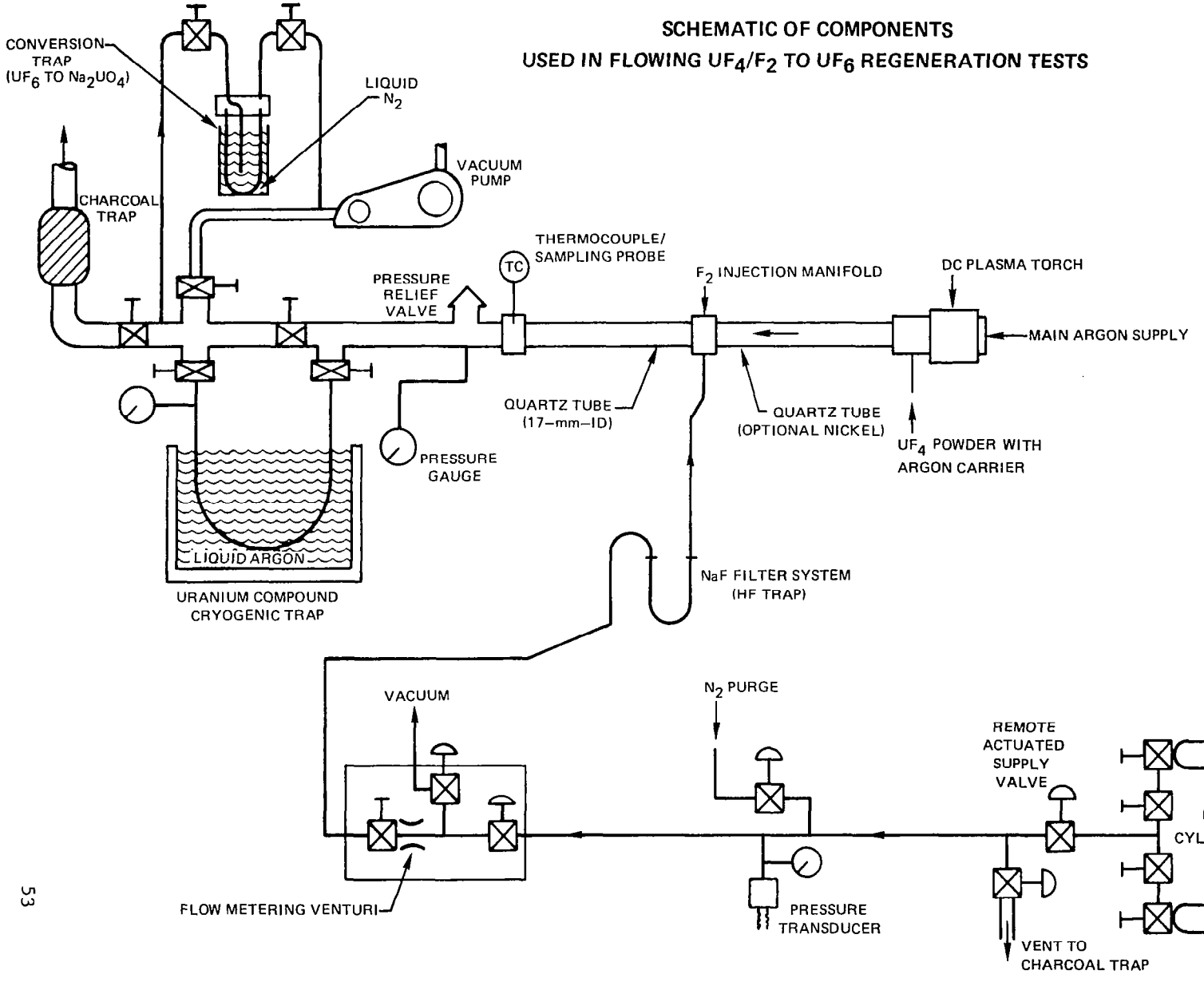

FIG. 5

PHOTOGRAPH OF FLUORINE TEST FACILITY USED IN FLOWING UF_4/F_2 TO UF_6 REGENERATION TESTS

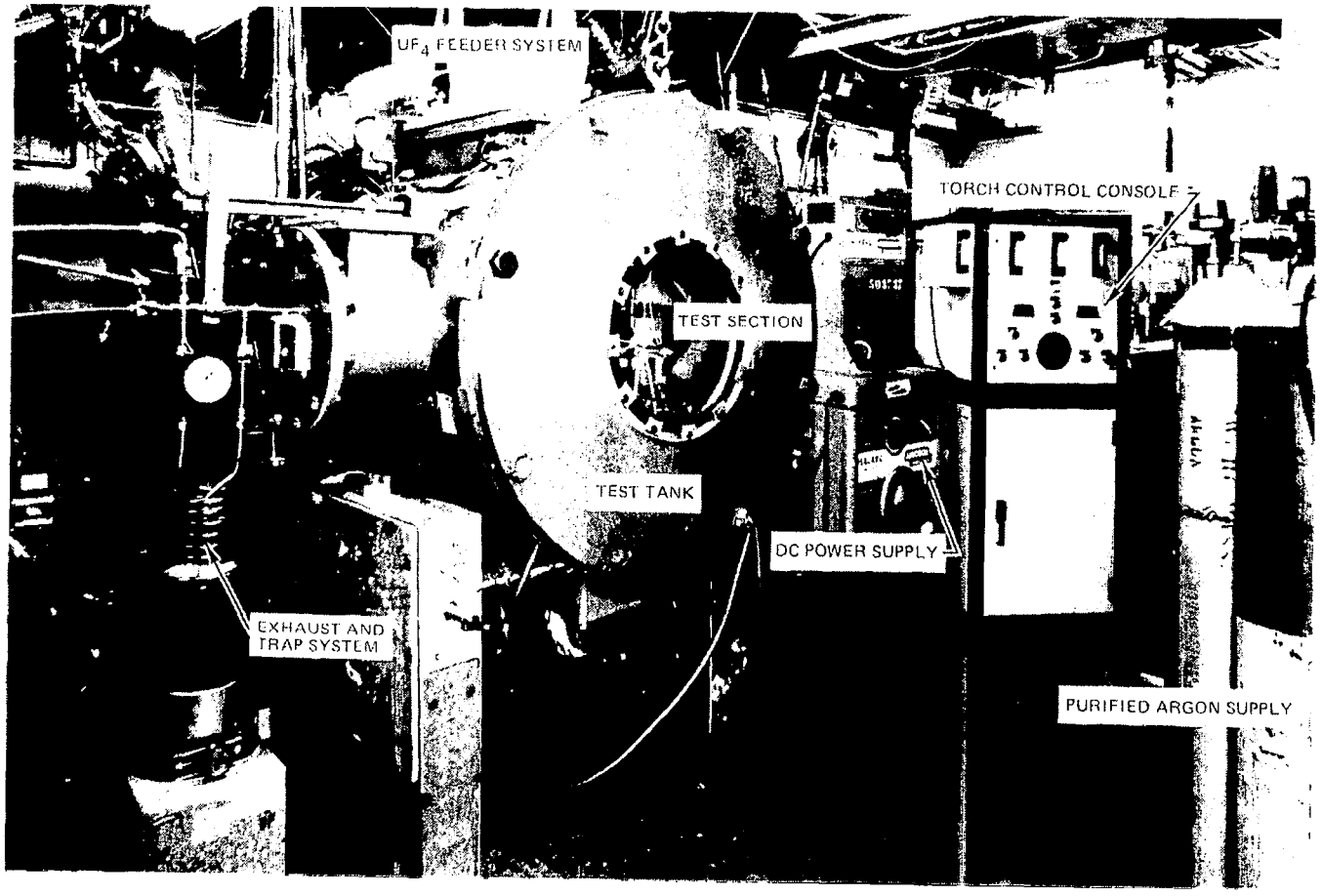

FIG. 6

FIG. 7

PHOTOGRAPH OF TEST COMPONENTS USED IN FLOWING UF_4/F_2 TO UF_6 REGENERATION TESTS

(FRONT COVER REMOVED)

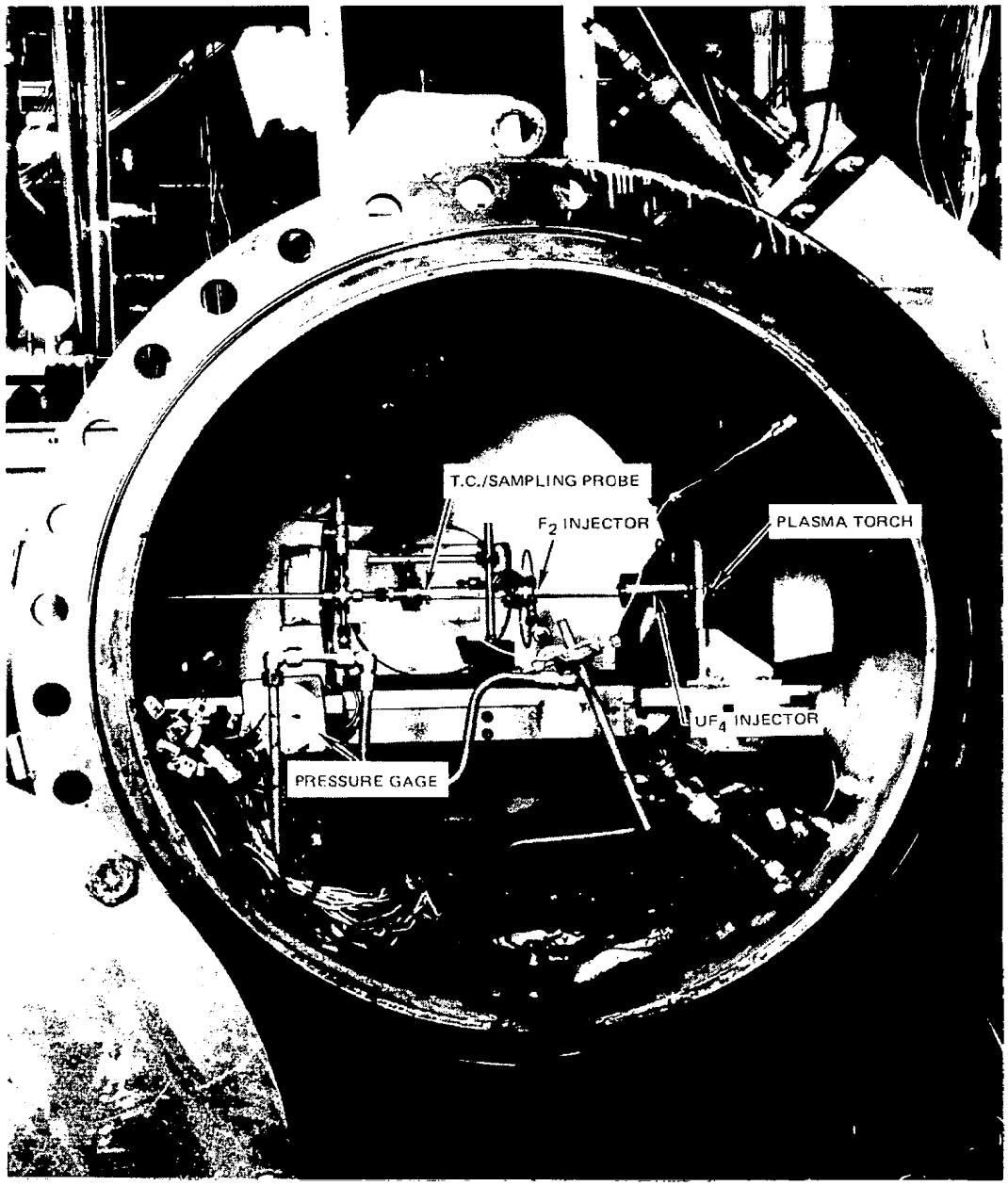

SCHEMATIC OF FLUORINE SUPPLY AND CONTROL SYSTEM FOR USE IN BATCH UF_6 REGENERATION TESTS WITH 1.2 MW RF URANIUM PLASMA TEST FACILITY

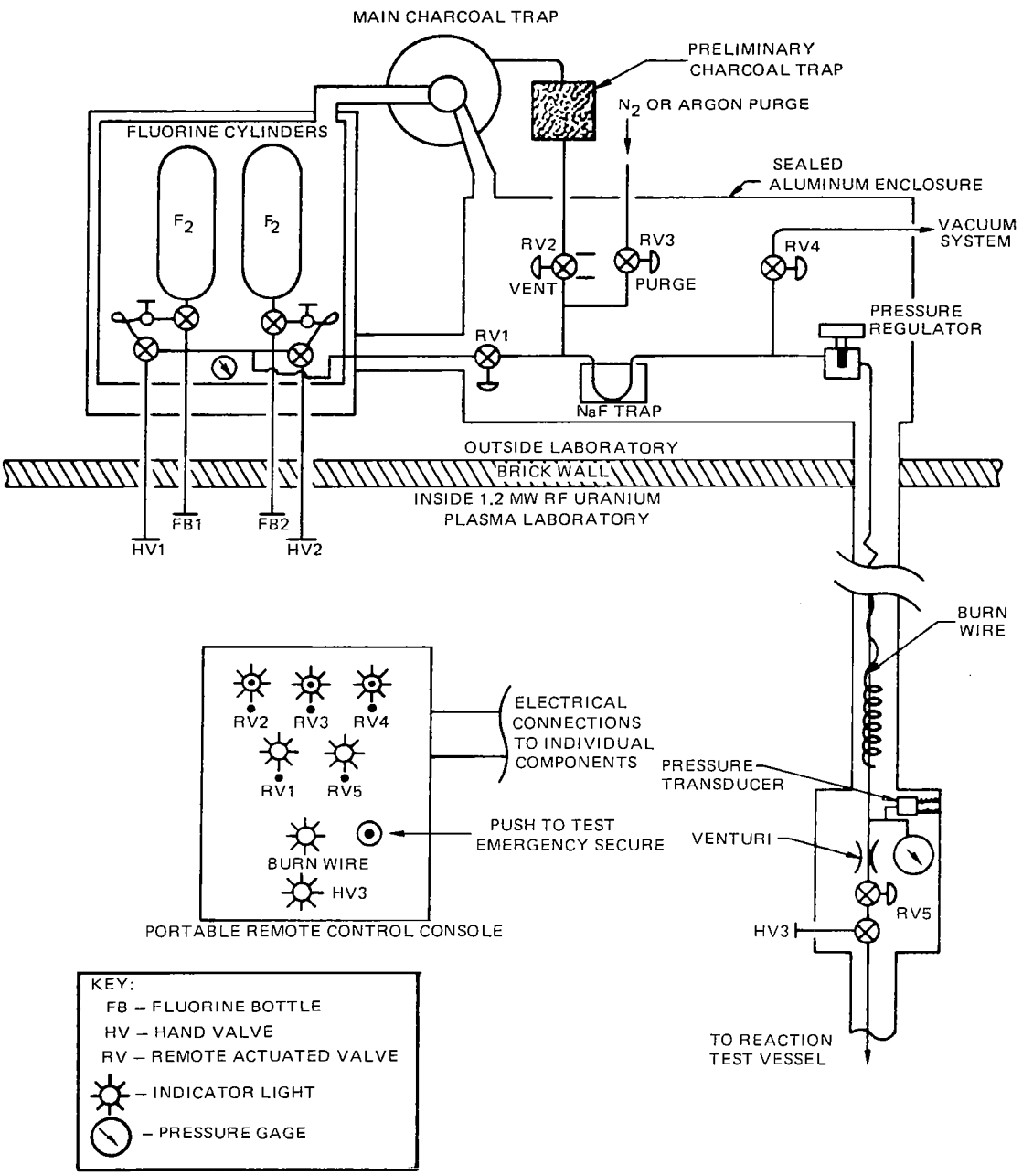

PHOTOGRAPH OF FLUORINE SUPPLY AND TRAP SYSTEM USED IN BATCH UF_6 REGENERATION TESTS

(EQUIPMENT LOCATED OUTSIDE LABORATORY)

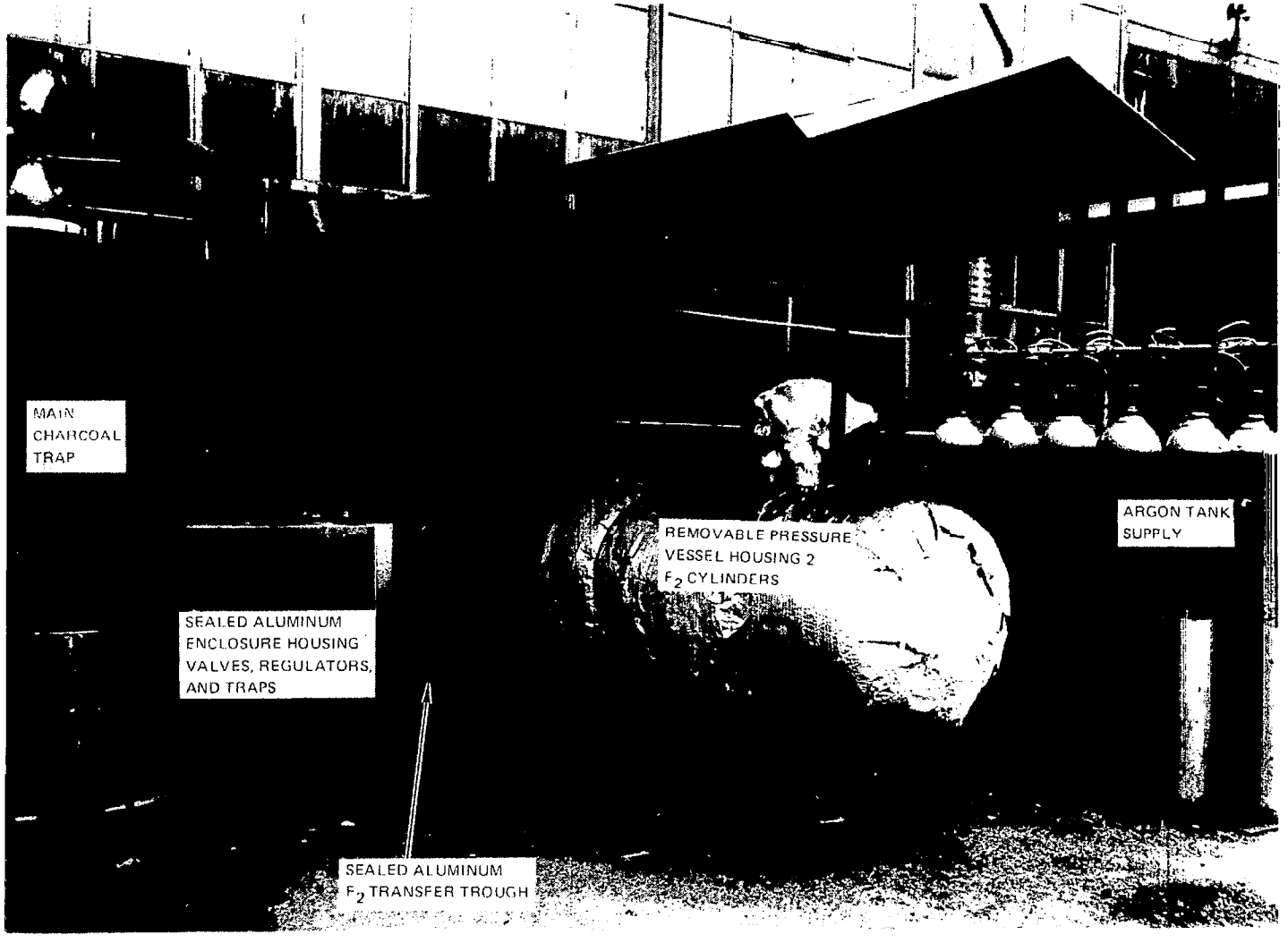

FIG. 9

PHOTOGRAPH OF F_2/UF_6 BATCH REGENERATION TEST TANK

(FRONT COVER PLATE REMOVED)

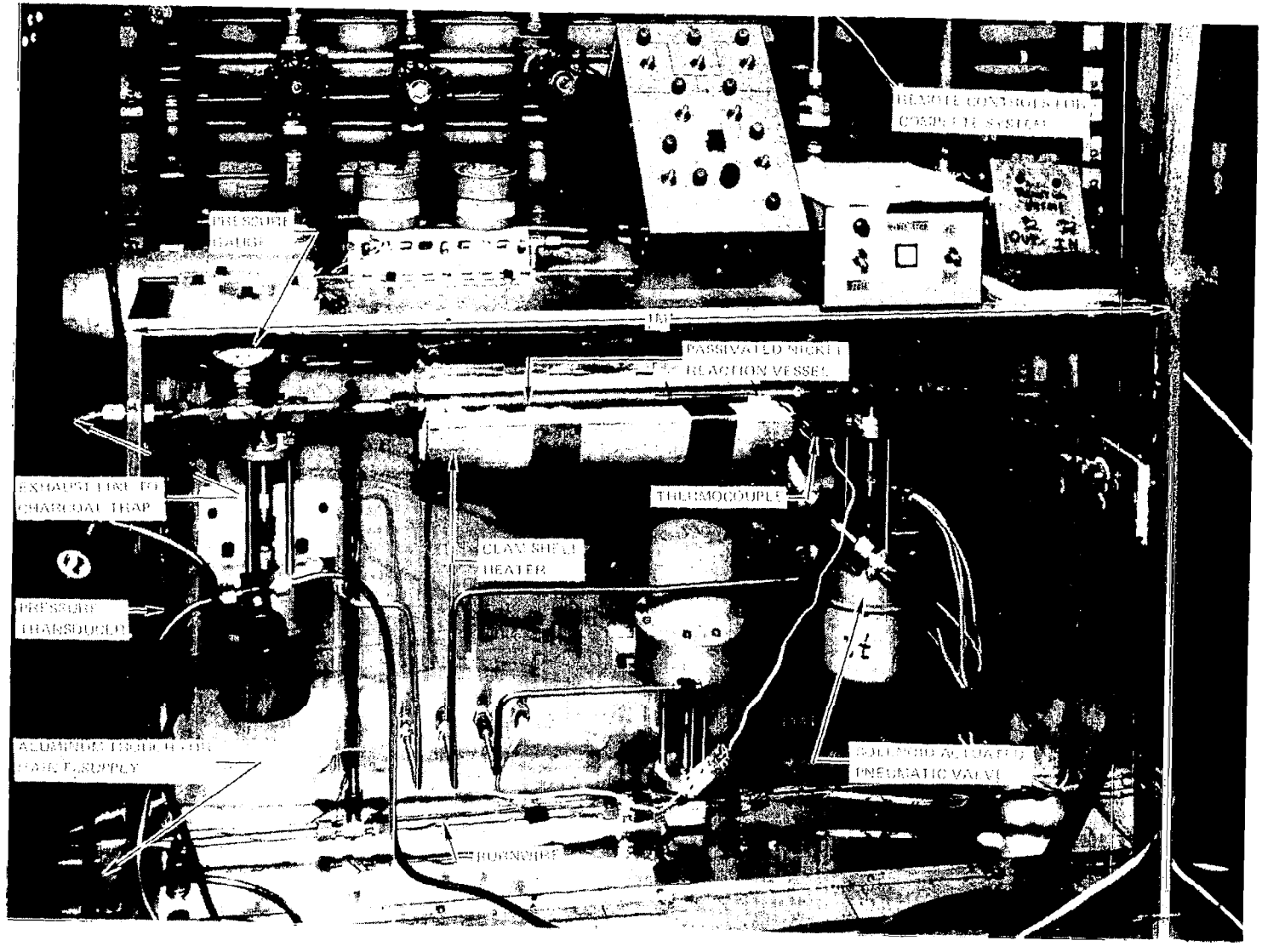

FIG. 10

PHOTOGRAPH OF FLUORINE LEAK DETECTION/ALARM SYSTEM USED IN F_2/UF_6 BATCH REGENERATION TESTS

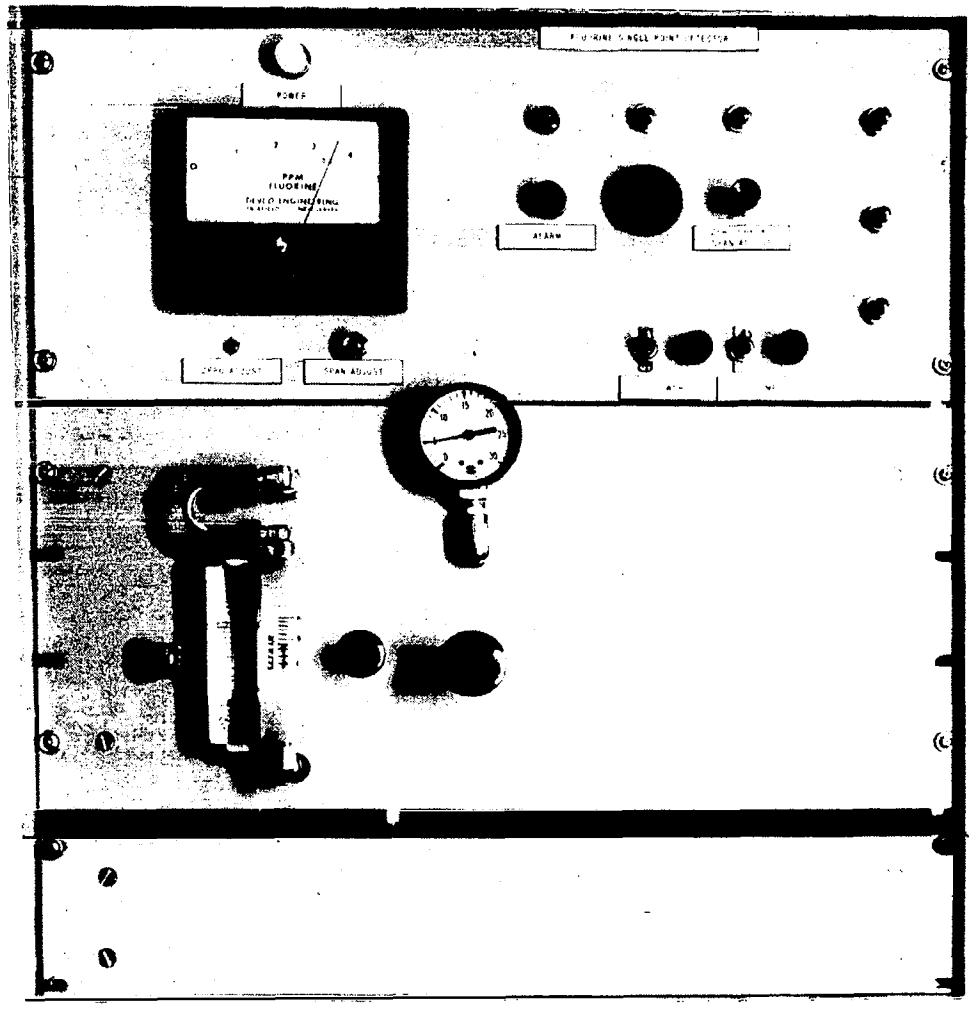

SKETCH OF BASIC TEST CHAMBER CONFIGURATION USED IN UF_6 RF PLASMA TESTS

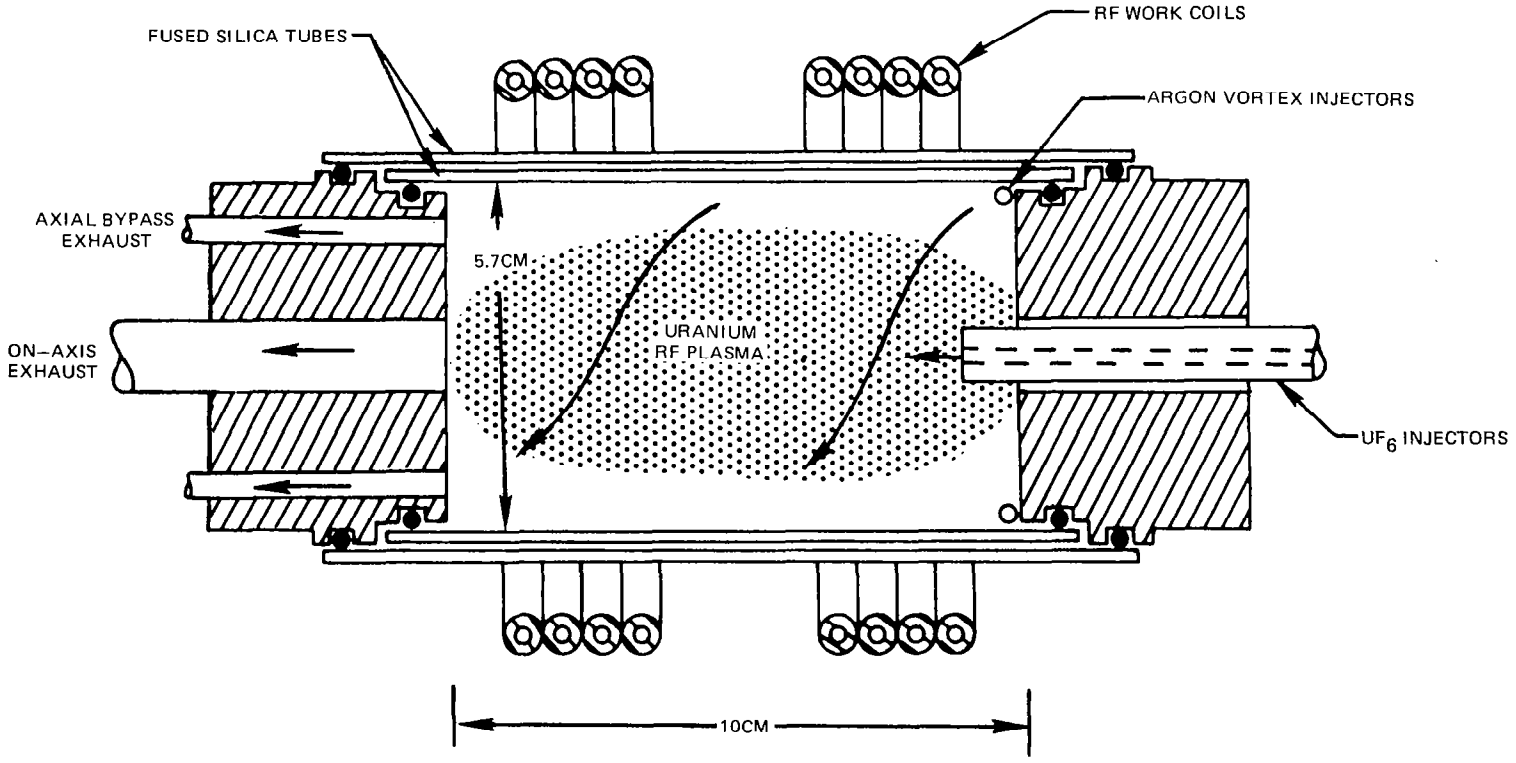

(NOT TO SCALE)

FIG. 12

FIG. 13

PHOTOGRAPH OF UF_6 TRANSFER SYSTEM USED IN 1.2MW RF URANIUM PLASMA TESTS

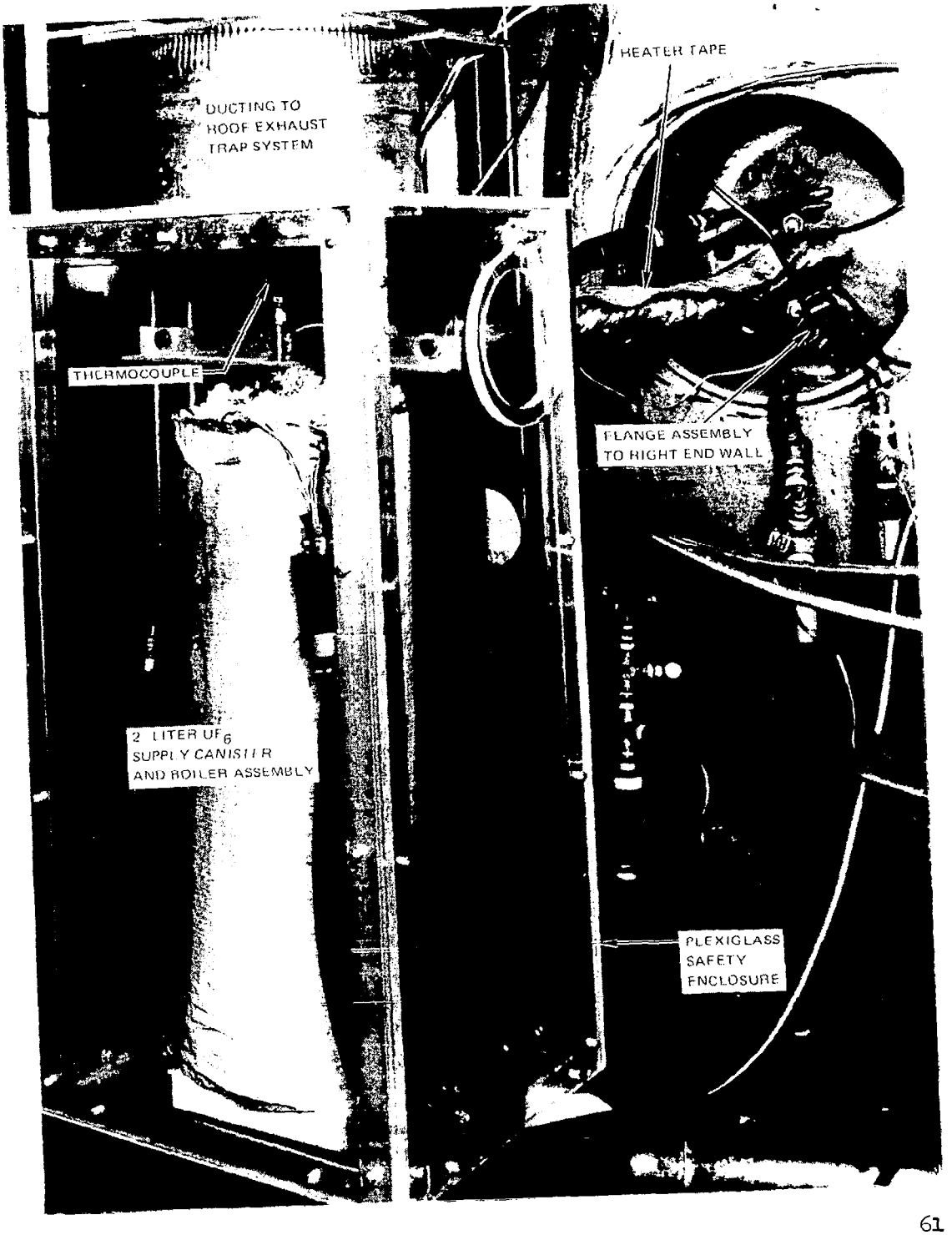

FIG. 14

PHOTOGRAPH OF 1.2 MW RF URANIUM PLASMA TEST FACILITY AND ASSOCIATED DIAGNOSTIC EQUIPMENT

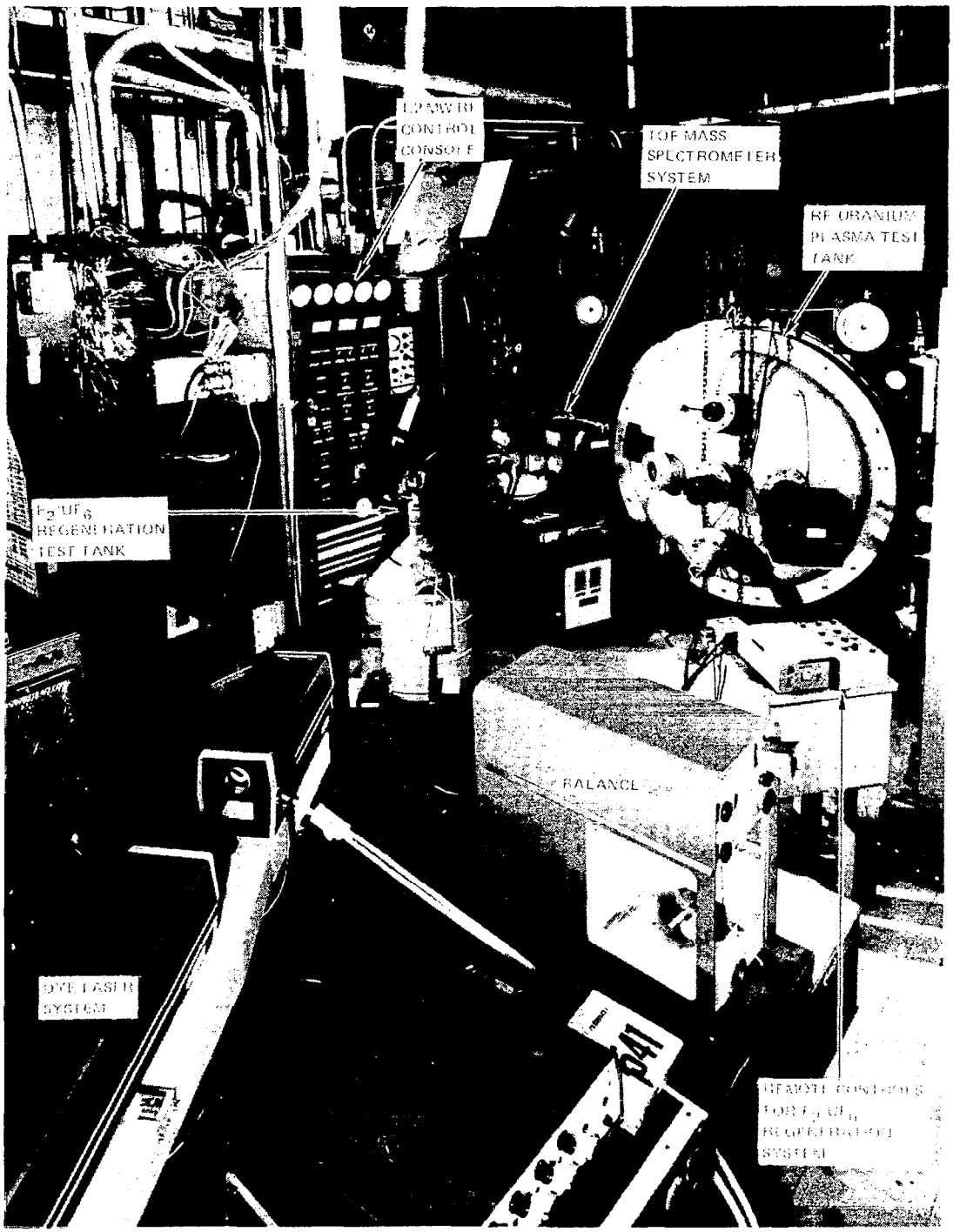

FIG. 15

PHOTOGRAPH OF RUGGEDIZED TOF MASS SPECTROMETER SYSTEM USED IN ARGON/UF_6 PLASMA CONFINEMENT AND EXHAUST GAS SEPARATOR TESTS

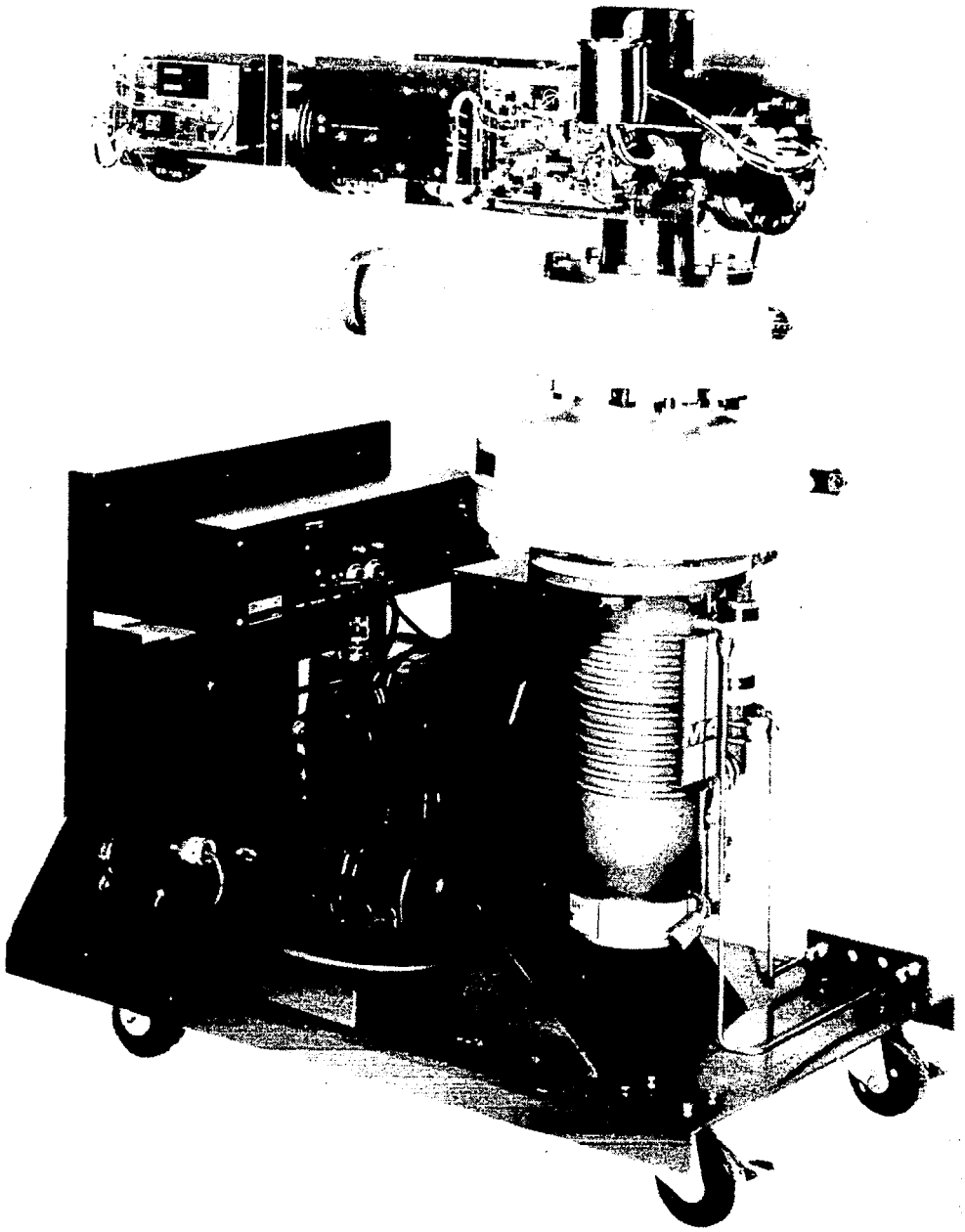

PHOTOGRAPH OF TOF MASS SPECTROMETER MASTER CONTROL CONSOLE USED IN ARGON/UF_6 PLASMA AND EXHAUST GAS SEPARATOR TESTS

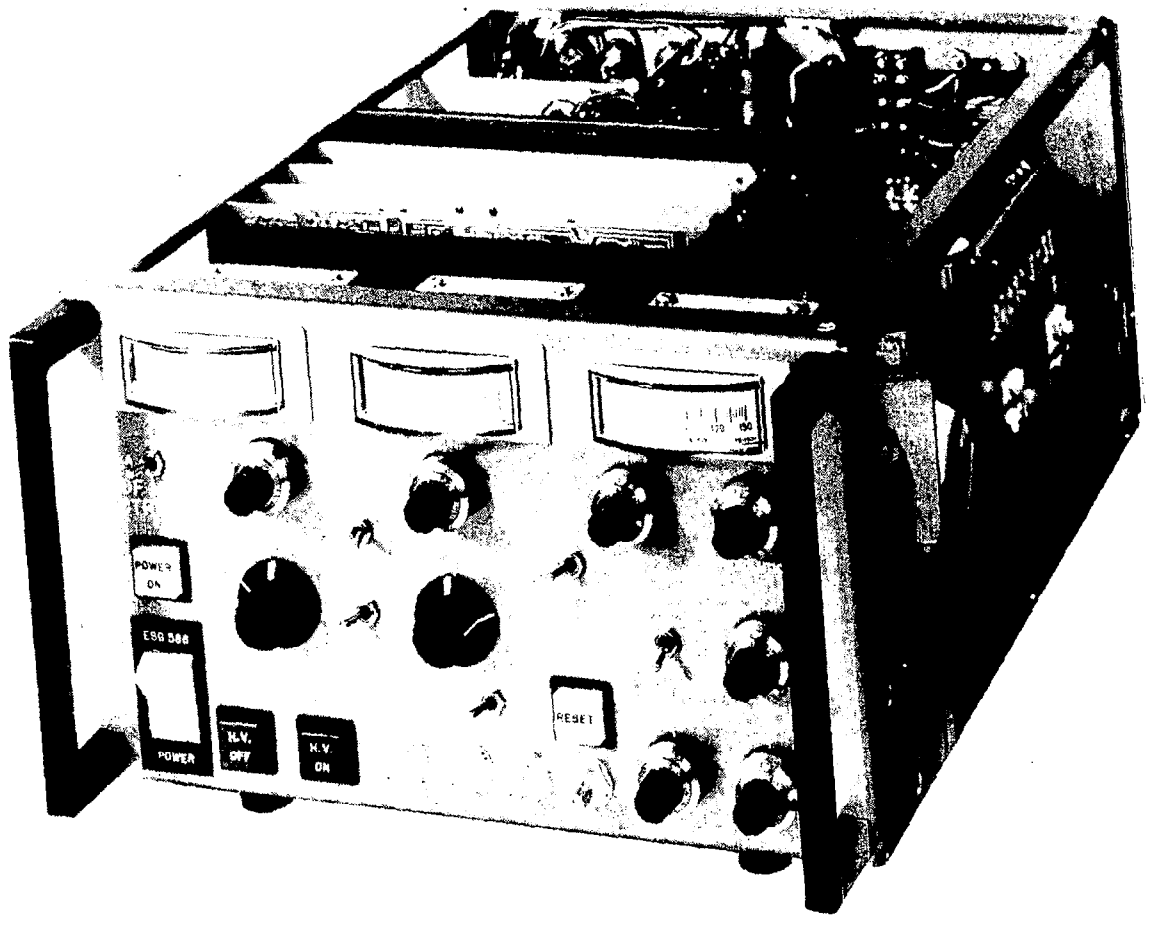

FIG 16

FIG. 17

PHOTOGRAPH OF DATA SYSTEM EMPLOYED WITH RUGGEDIZED TOF MASS SPECTROMETER SYSTEM IN RF URANIUM PLASMA EXHAUST GAS ANALYSIS TESTS

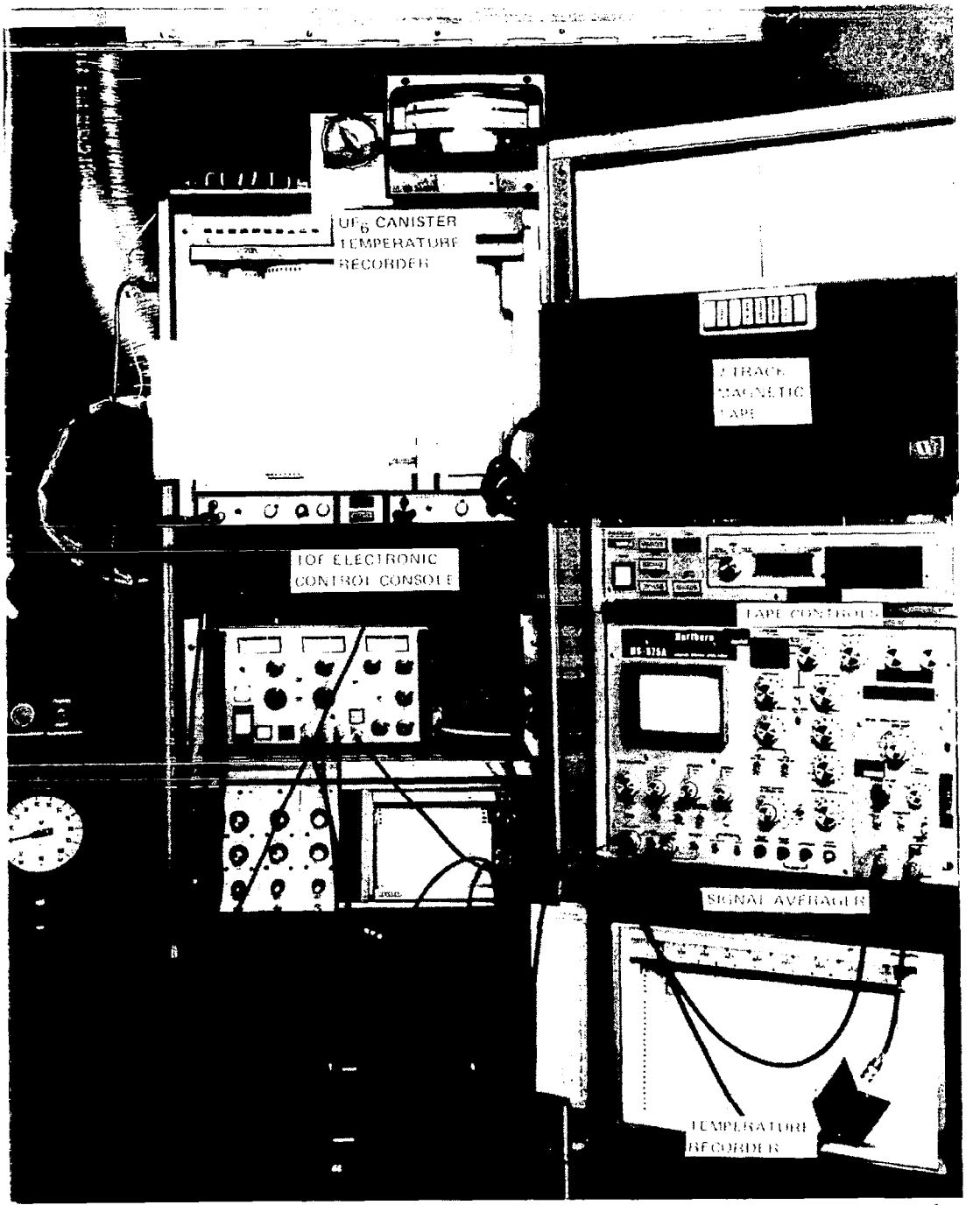

SCHEMATIC OF TEST CONFIGURATION USED IN RF URANIUM PLASMA TESTS EMPLOYING EXHAUST GAS SAMPLING AND POST TEST BATCH UF_6 REGENERATION

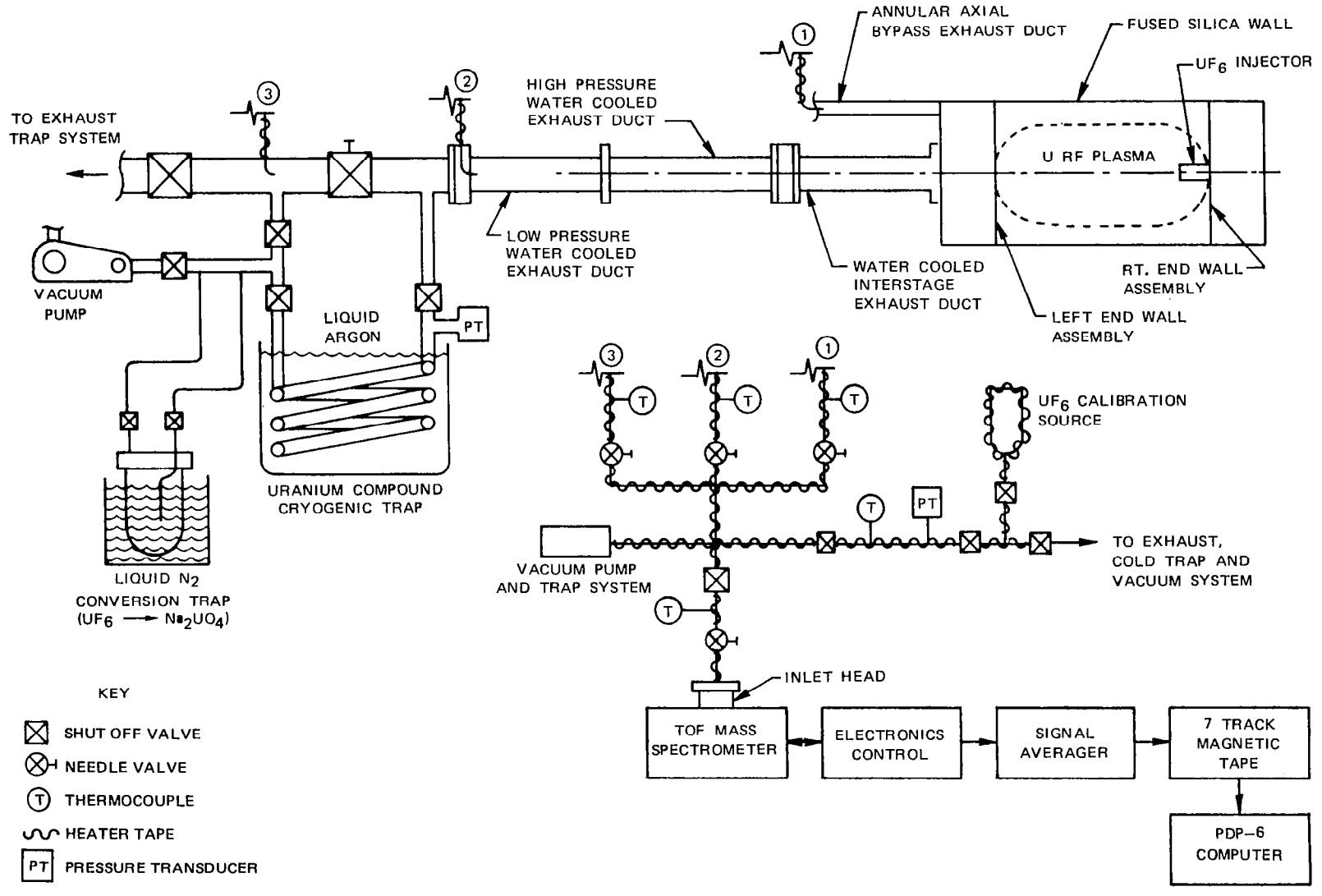

FIG. 18

FIG. 19

PHOTOGRAPH OF RUGGEDIZED TOF MASS SPECTROMETER USED IN RF URANIUM PLASMA EXHAUST GAS ANALYSIS TESTS

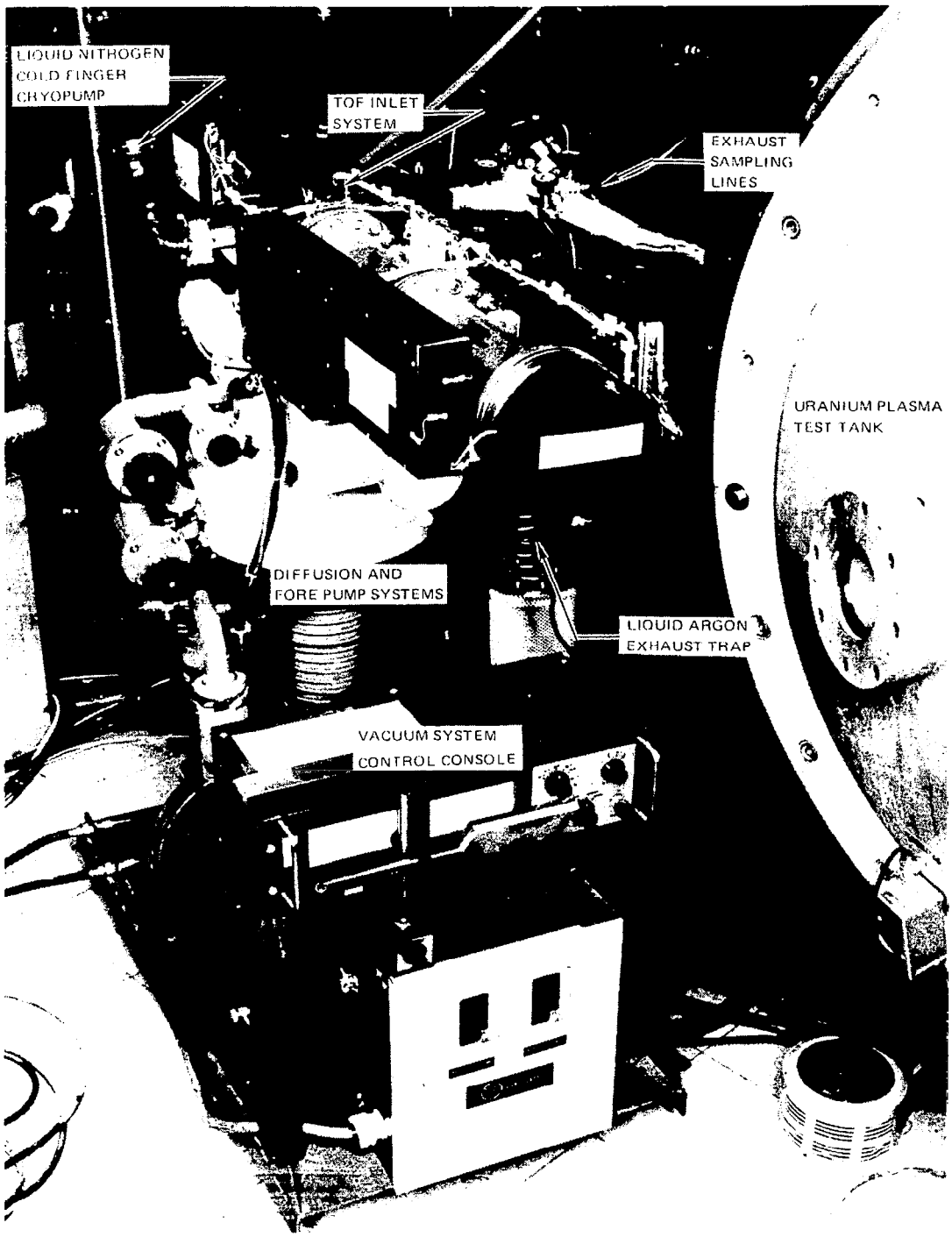

PHOTOGRAPH OF IR SPECTROPHOTOMETER USED IN ANALYSIS OF RESIDUES OBTAIN FROM RF URANIUM PLASMA TESTS

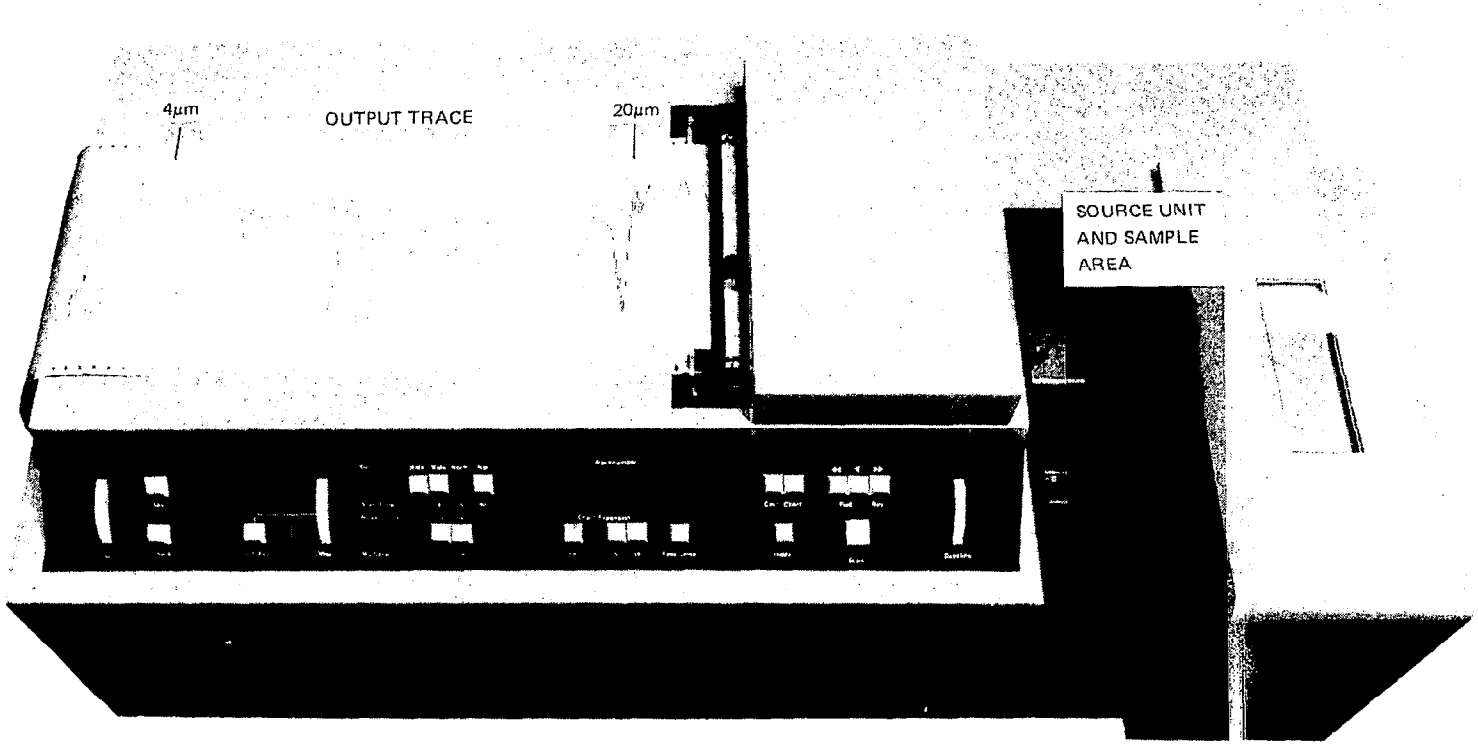

FIG. 20

SCHEMATIC DIAGRAM OF PHOTOACOUSTIC SPECTROMETER SYSTEM AND DETECTION CELL

(STANDARD SAMPLE SIZE –5MG)

A) OVERALL SYSTEM

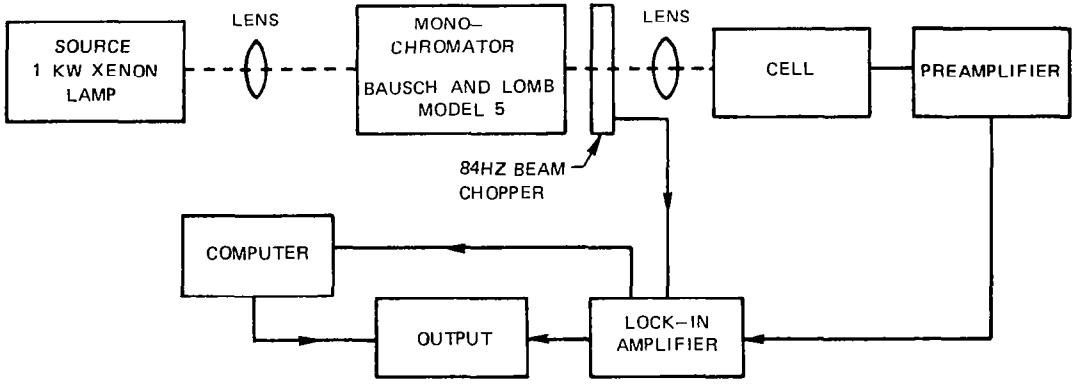

B) TEST CELL

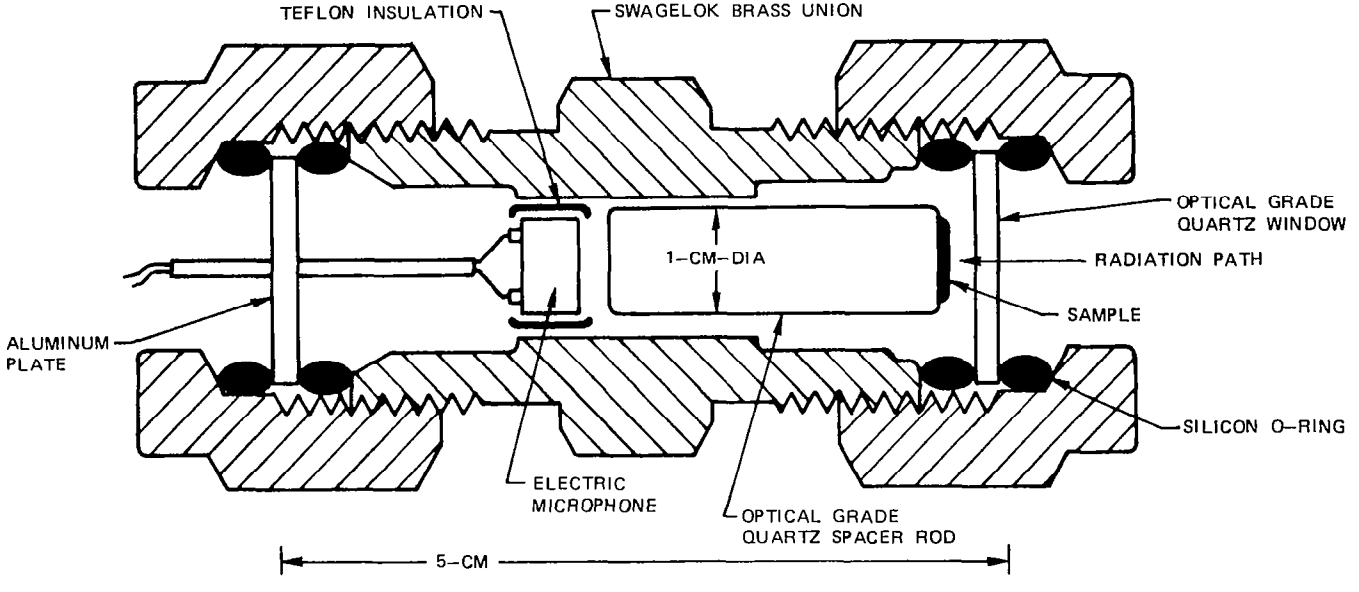

FIG. 21

FIG. 22

PHOTOGRAPH OF NICKEL BOAT ASSEMBLIES USED IN BATCH TYPE UF_4/F_2 TO UF_6 REGENERATION TESTS

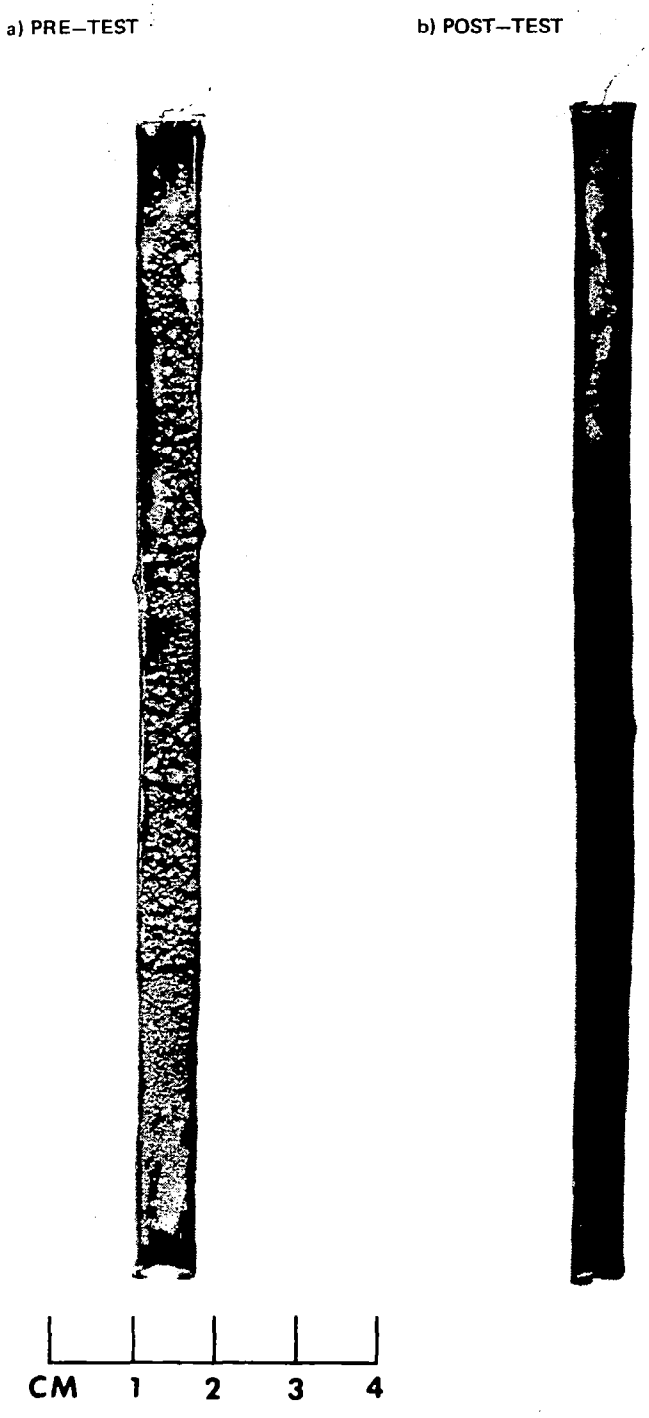

EXAMPLE OF MEASURED UF_4 CONVERSION DATA FROM BATCH UF_6 REGENERATION TESTS

KEY		
SYMBOL	F_2 PRESSURE (ATM)	RESIDENCE TIME (MIN)
□	1	1
⬡	1	5
△	3	1
◇	3	5

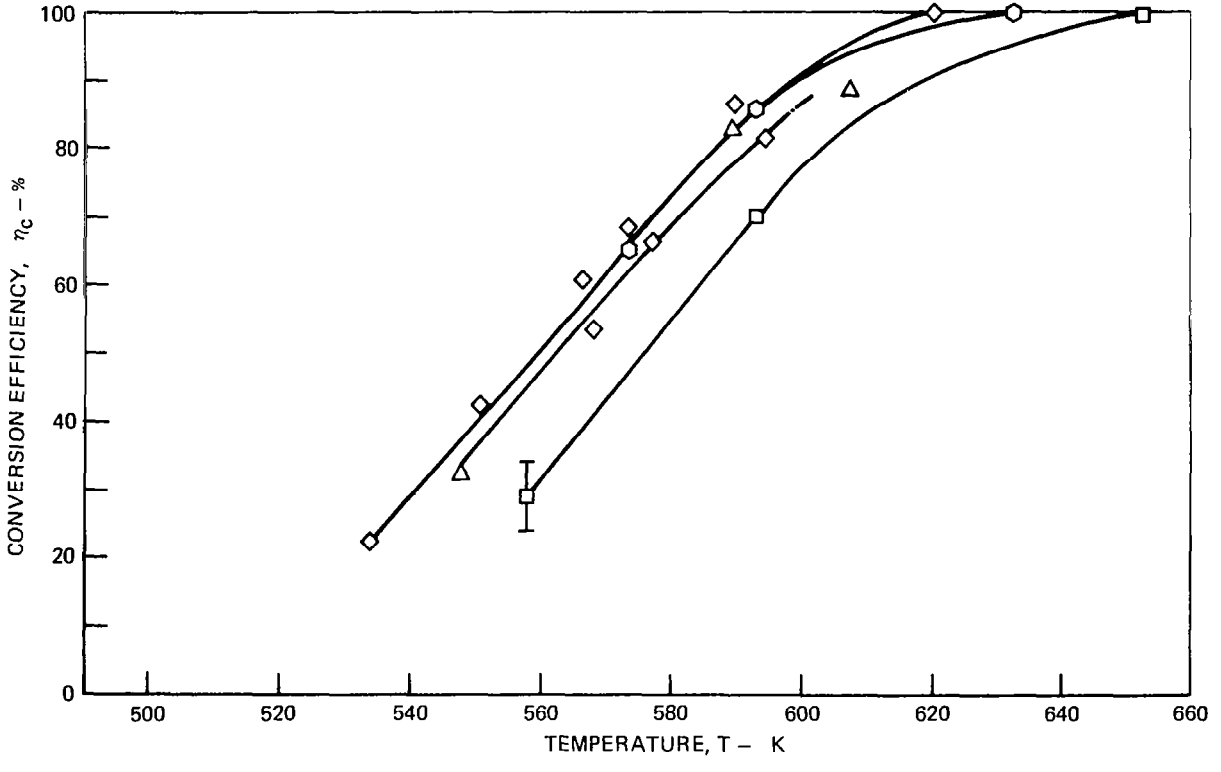

FIG. 23

FIG. 24

PHOTOGRAPH OF PASSIVATED NICKEL BOAT AND METALLIC TEST SAMPLES AFTER HOT UF_6 CORROSION TEST

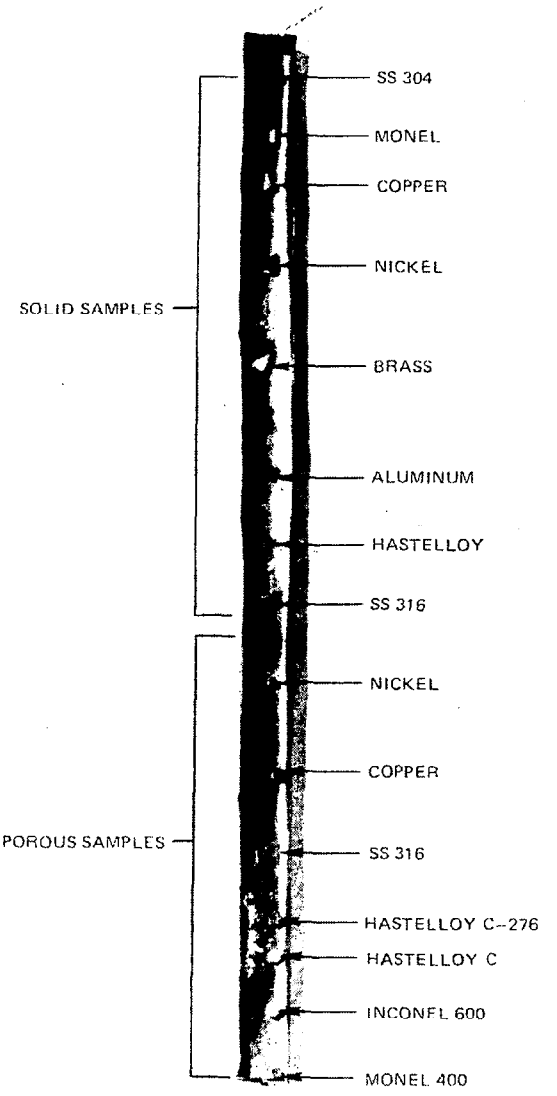

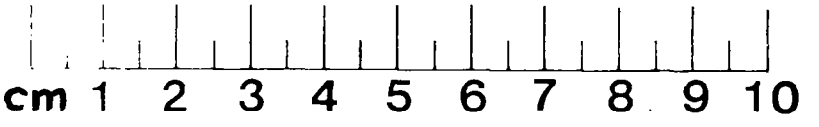

EXAMPLE OF MEASURED UF_4 CONVERSION DATA OBTAINED FROM FLOWING UF_6 REGENERATION TESTS

KEY	
SYMBOL	CONFIGURATION
○	STANDARD REFERENCE/LOW $\dot{m}_{UF_4}$
△	MODIFIED NICKEL INLET/HIGH $\dot{m}_{UF_4}$
□	POROUS WALL F_2 INJECTOR/HIGH $\dot{m}_{UF_4}$

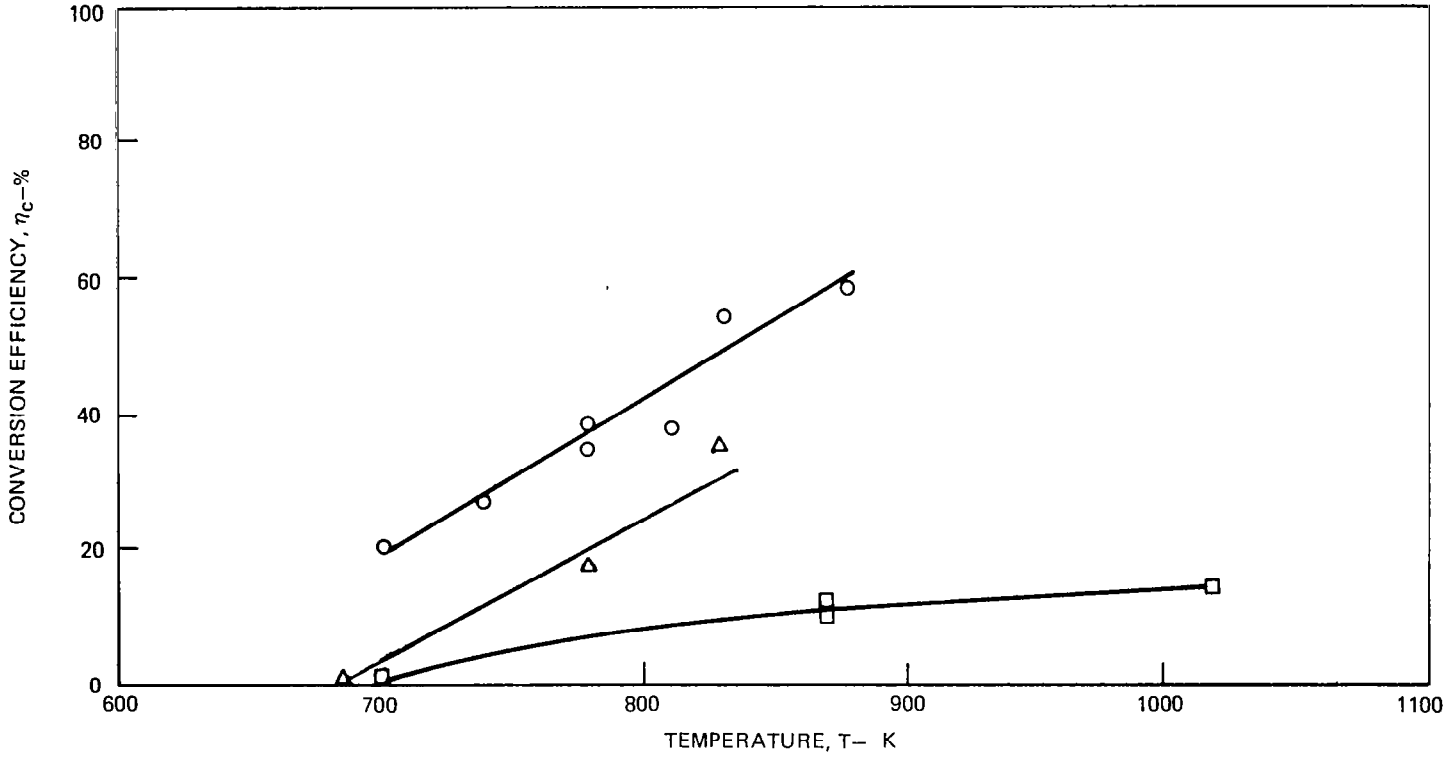

FIG. 25

EXAMPLE OF URANIUM COMPOUND RESIDUE CONVERSION DATA OBTAINED FROM RF URANIUM PLASMA EXHAUST SEPARATOR TESTS

ALL SAMPLES ≈ 50 mg TOTAL WEIGHT
F_2 PRESSURE–1 ATM

KEY		
SYMBOL	SAMPLE	RESIDENCE TIME (MIN.)
□	LAB. PURE UF_4 REF. STANDARD	5
○	POST TEST EXHAUST TRAP RESIDUE	5
△	POST TEST EXHAUST TRAP RESIDUE	1
◇	POST TEST EXHAUST TRAP RESIDUE	0.2
▲	LAB. PURE 50% UF_4 /50% UO_2F_2	1
■	LAB PURE 90% UF_4/10% UO_2F_2	1
◆	LAB PURE 80% UF_4/10% UO_2F_2/10%UO_3	1

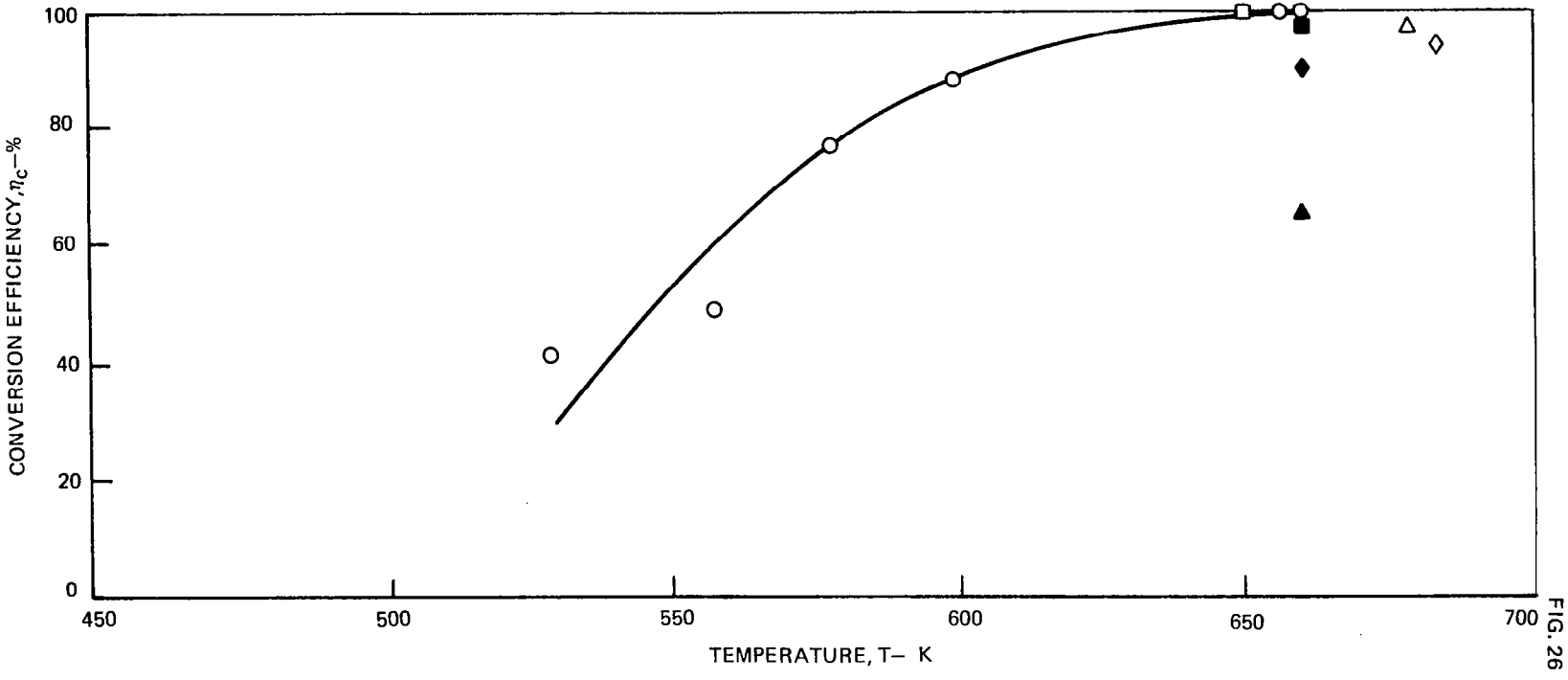

FIG. 26

EXAMPLE OF PORTION OF UF_6 MASS SPECTRUM (m/e = 238–352) OBTAINED USING TOF MASS SPECTROMETER AND DATA PROCESSING SYSTEM

(DATA POINT NUMBER EQUIVALENT TO ADDRESS NUMBER IN MULTICHANNEL SCALER)

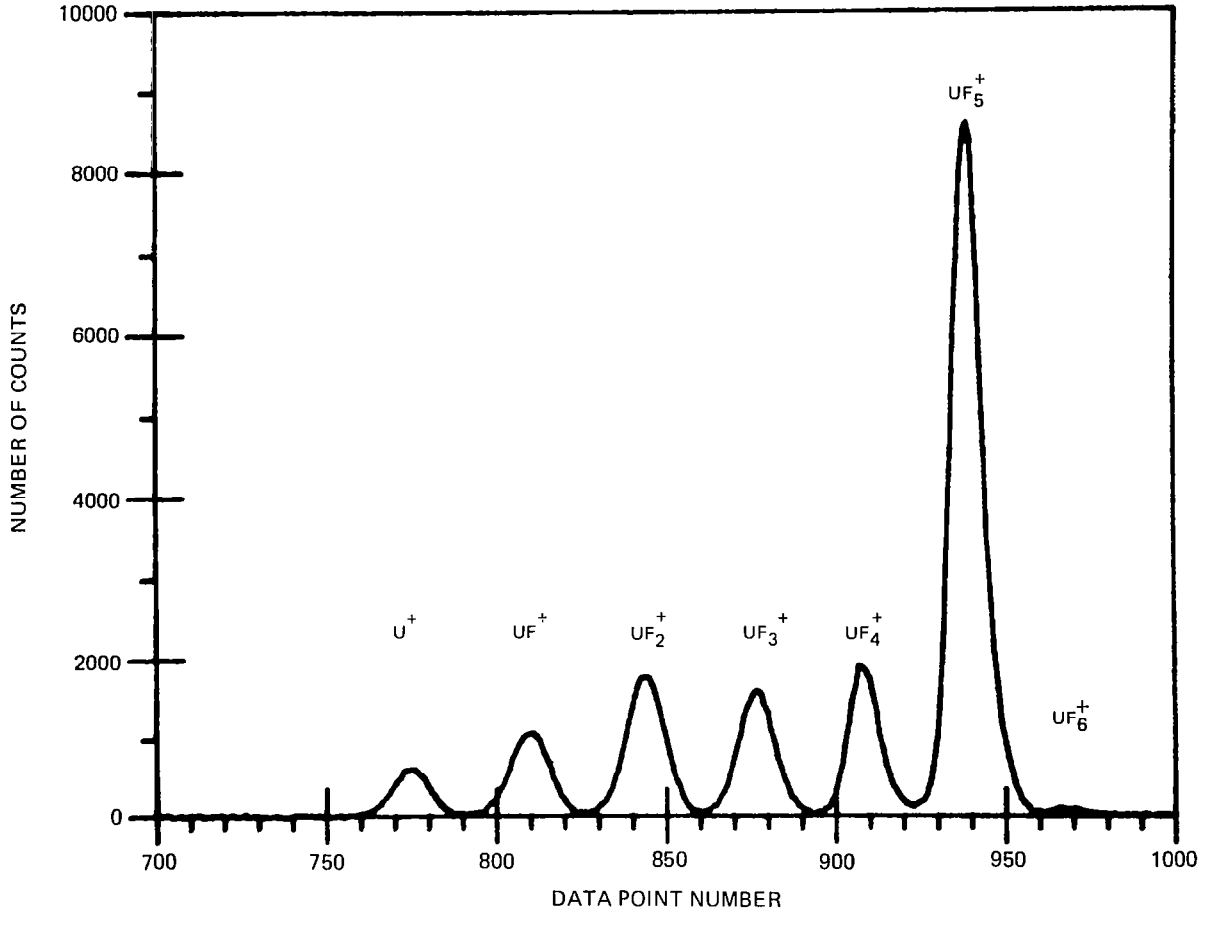

FIG. 27

EXAMPLE OF PORTION OF UF_6 MASS SPECTRUM (m/e = 119–157) OBTAINED USING TOF MASS SPECTROMETER AND DATA PROCESSING SYSTEM

(DATA POINT NUMBER EQUIVALENT TO ADDRESS NUMBER IN MULTICHANNEL SCALER)

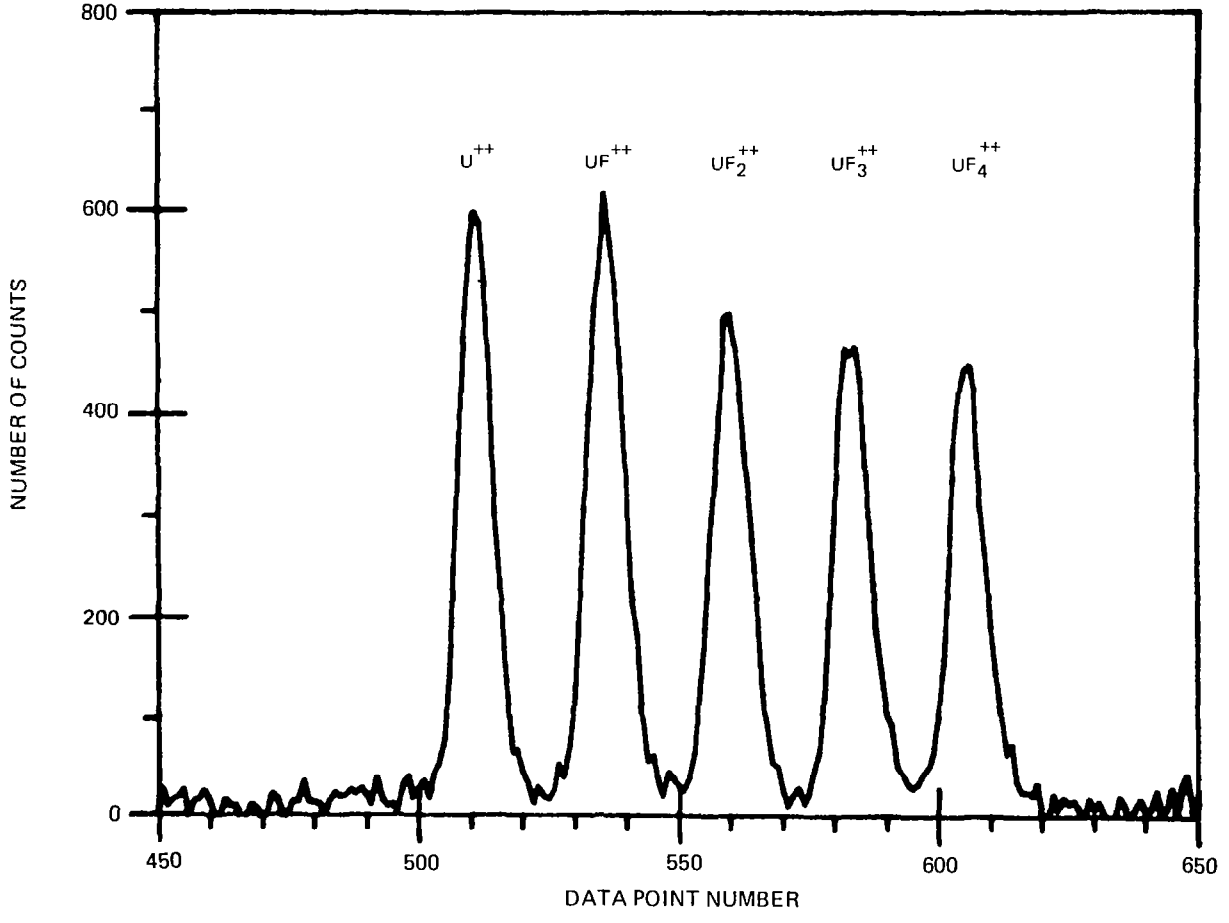

FIG. 28

EXAMPLE OF Ar/UF_6 MASS SPECTRUM FROM MASS 28–400 OBTAINED USING TOF MASS SPECTROMETER AND DATA PROCESSING SYSTEM

LOW VERTICAL SENSITIVITY

DATA POINT NUMBER EQUIVALENT TO ADDRESS NUMBER IN MULTICHANNEL SCALER

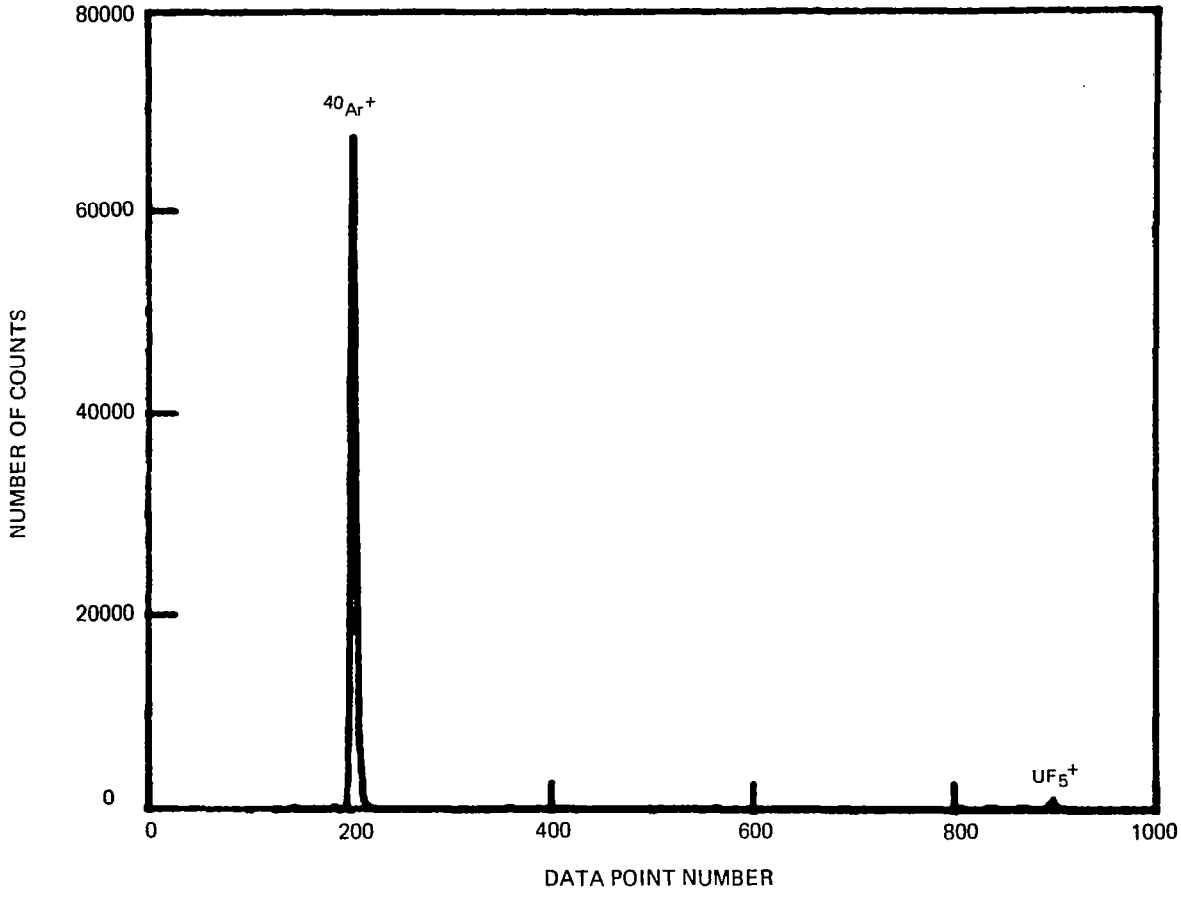

FIG. 29

EXAMPLE OF Ar/UF_6 MASS SPECTRUM FROM MASS 28–400 OBTAINED USING TOF MASS SPECTROMETER AND DATA PROCESSING SYSTEM

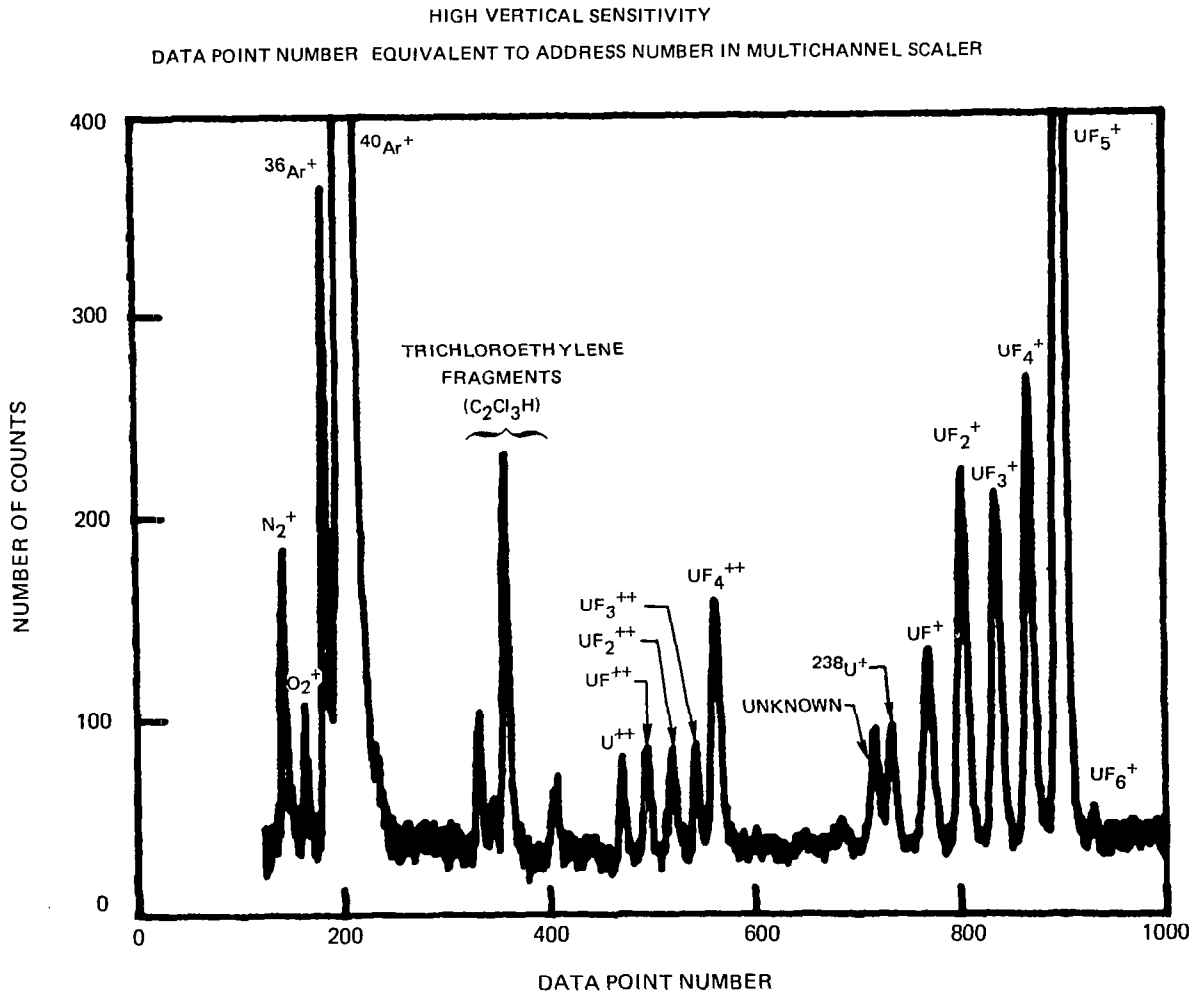

FIG. 30

ELECTRON PHOTOMICROGRAPHS OF POST TEST SAMPLE RESIDUE REMOVED FROM UF_6 REGENERATION TRAP SYSTEM

(Na_2UO_4)

a)

MAG: 300X

b)

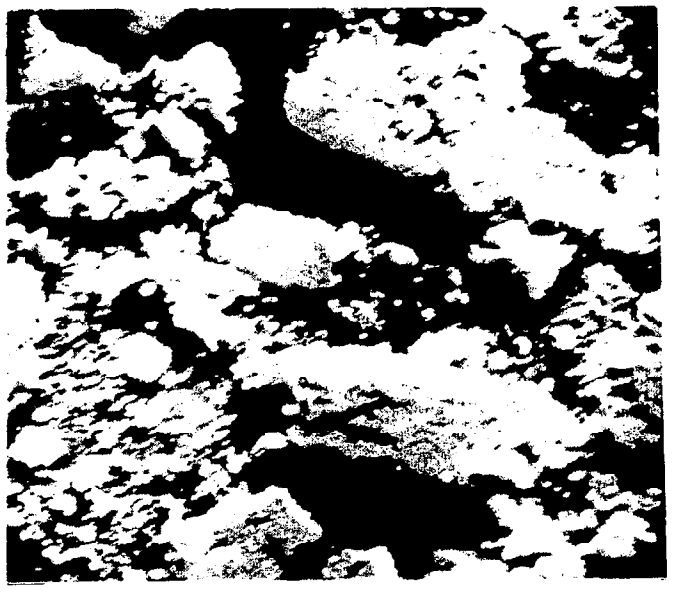

MAG: 1200X

FIG. 31

PHOTOGRAPHS OF X-RAY MAPS OF POST TEST SAMPLE RESIDUE REMOVED FROM UF_6 REGENERATION TRAP SYSTEM

(Na_2UO_4)

a) X-RAY SHOWING URANIUM (WHITE AREA)

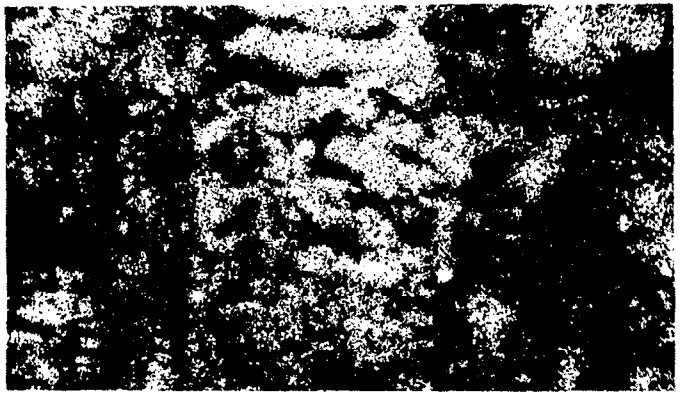

MAG: 300X

b) X-RAY SHOWING OXYGEN

MAG: 300X

c) X-RAY SHOWING SODIUM

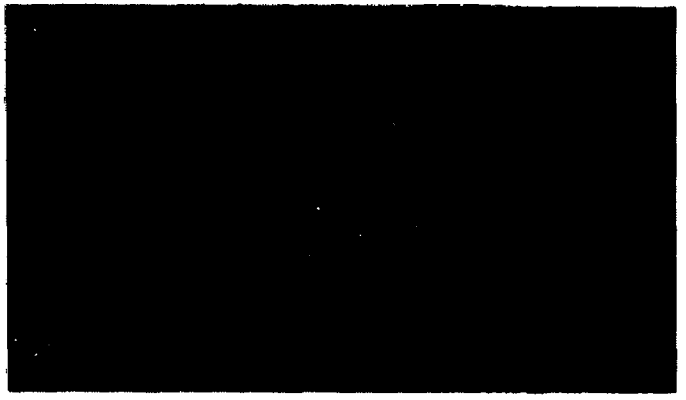

MAG: 300X

FIG. 32

ELECTRON PHOTOMICROGRAPHS OF SAMPLE RESIDUE REMOVED FROM EXHAUST TRAP AFTER RF URANIUM PLASMA TEST

(UF_4, UO_2F_2, UO_3)

a)

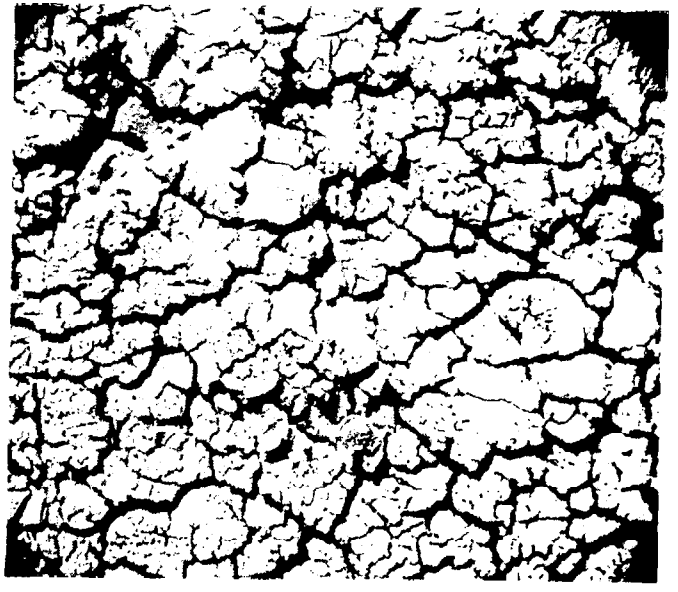

MAG: 300X

b)

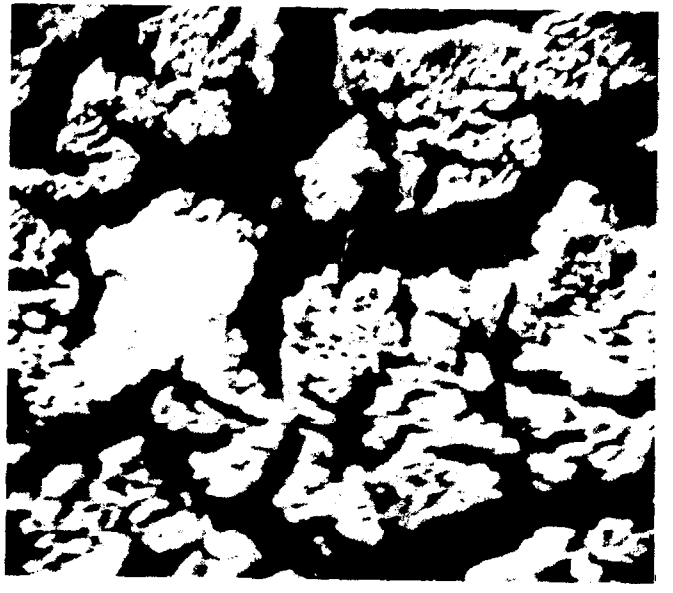

MAG: 1200X

FIG. 33

PHOTOGRAPHS OF X-RAY MAPS OF SAMPLE RESIDUE REMOVED FROM EXHAUST TRAP AFTER RF URANIUM PLASMA TEST

(UF_4, UO_2F_2, UO_3)

a) X-RAY MAP

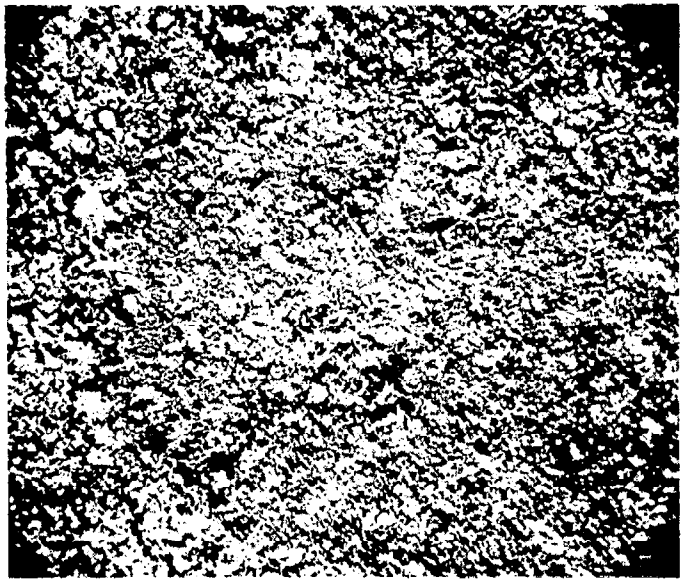

MAG: 300X

b) X-RAY SHOWING URANIUM (WHITE AREA)

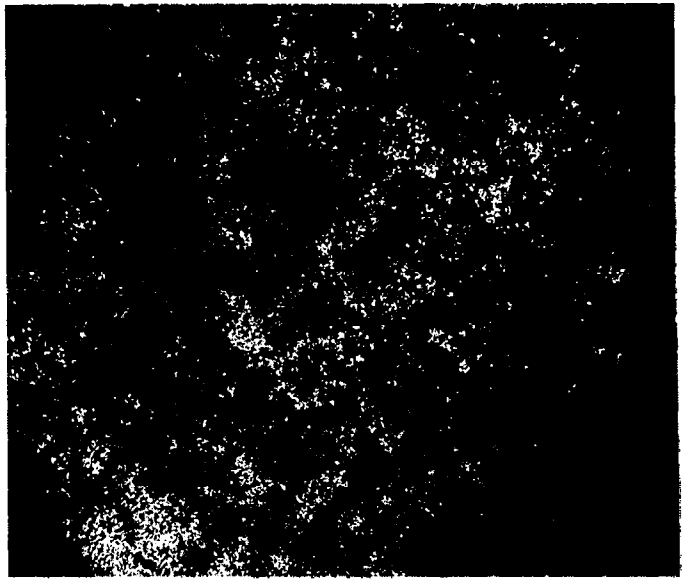

MAG: 300X

FIG. 34

BLOCK DIAGRAM OF A MASS SPECTROMETER

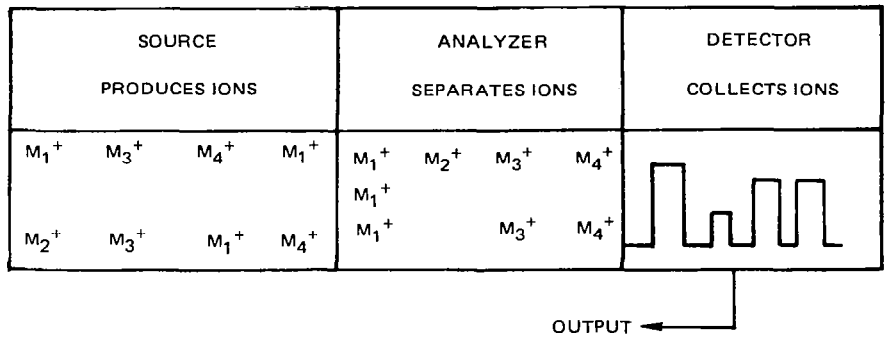

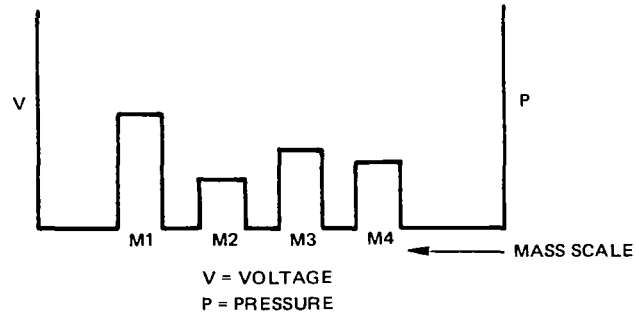

V = VOLTAGE
P = PRESSURE

SCHEMATIC REPRESENTATION OF A TIME–OF–FLIGHT (TOF) MASS SPECTROMETER

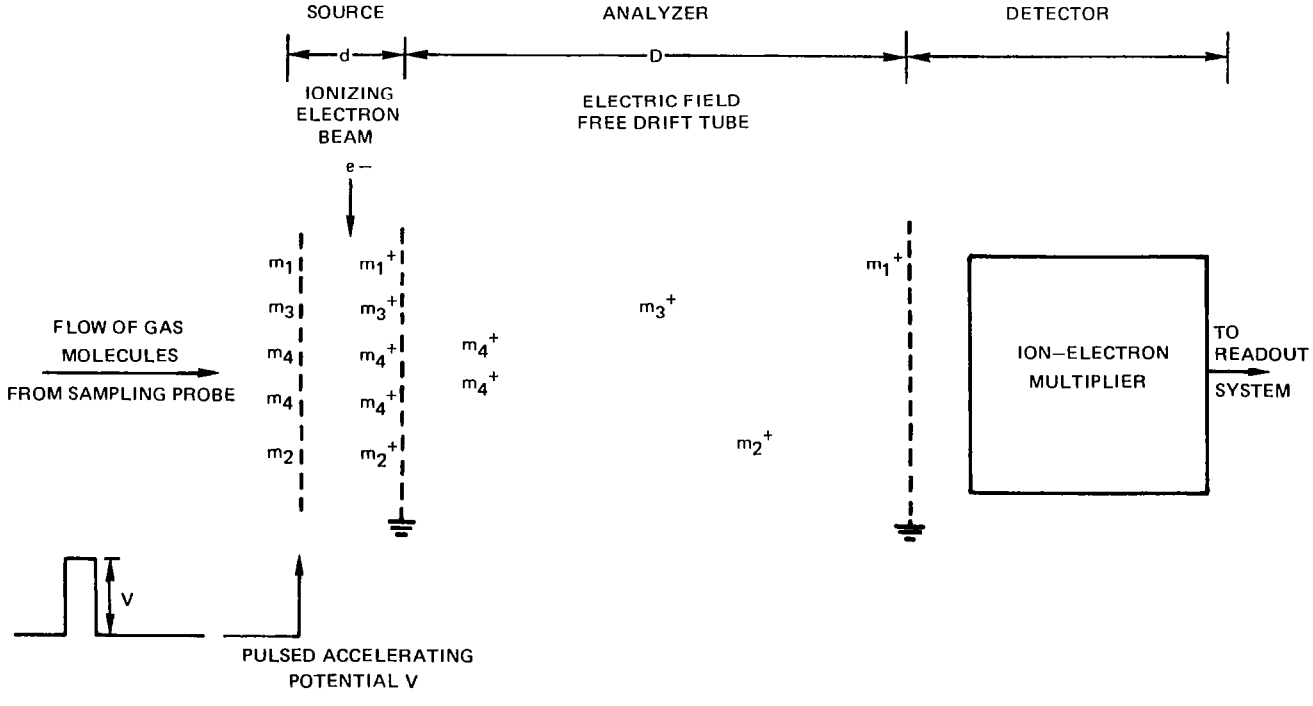

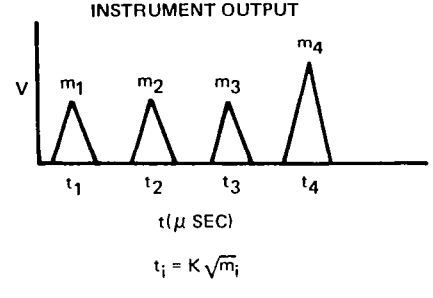

$t_i = K\sqrt{m_i}$

FIG. 36

FIG. 37

EXAMPLE OF SENSITIVITY FACTORS OF UF_6 RELATIVE TO Ar FOR SPECIFIED DATA SYSTEM TIME CONSTANTS

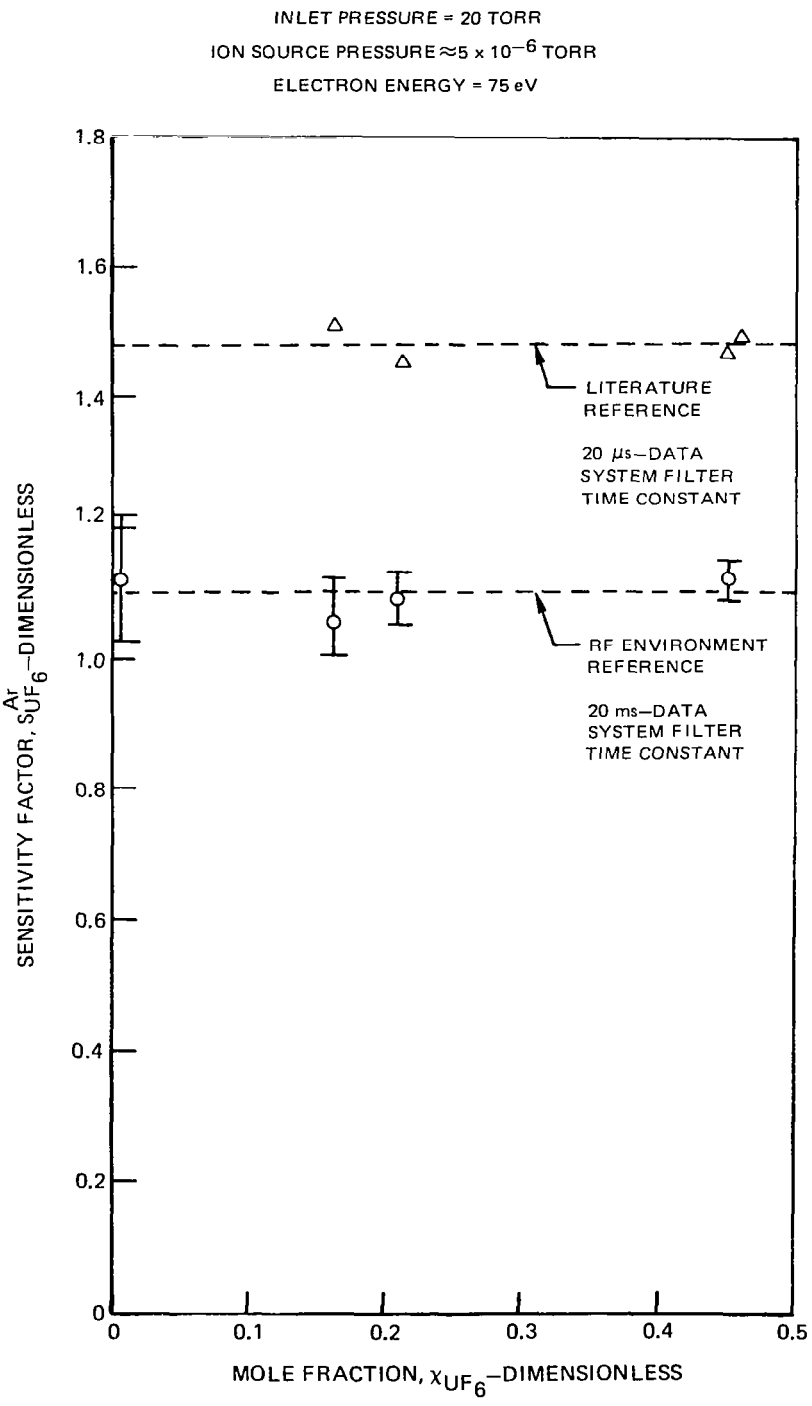

EXAMPLE OF CALCULATED THERMAL DECOMPOSITION PRODUCTS OF UF_6

TOTAL PRESSURE = 1.5 ATM

$\dot{m}_{Ar}$ = 1.91 GM/SEC

$\dot{m}_{UF_6}$ = 0.08 GM/SEC

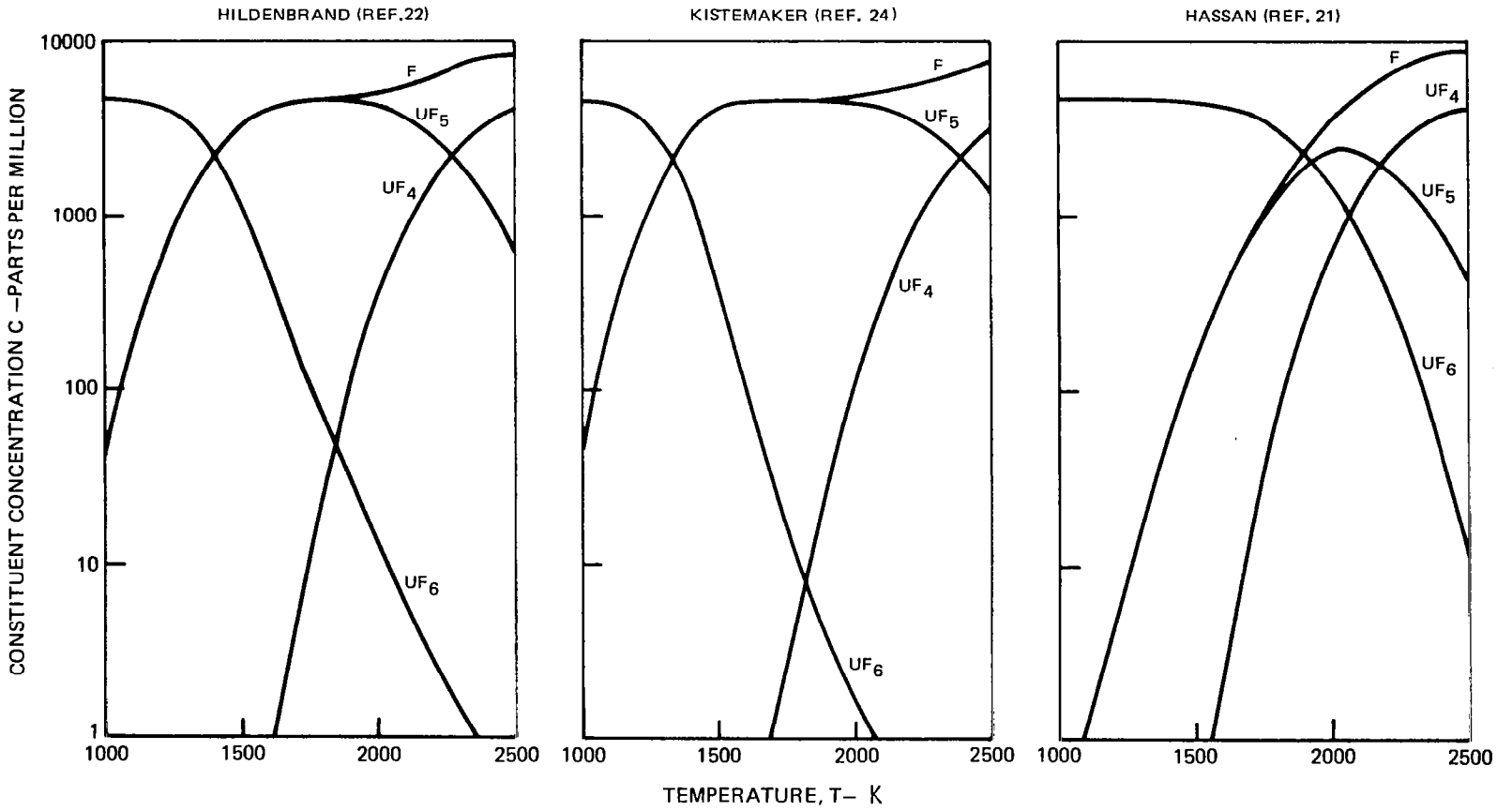

FIG. 38

FIG. 39

EXAMPLE OF URANIUM COMPOUND SPECTRUM OF UF_4 AND UO_2F_2 OBTAINED USING PHOTOACOUSTIC SPECTROMETER SYSTEM

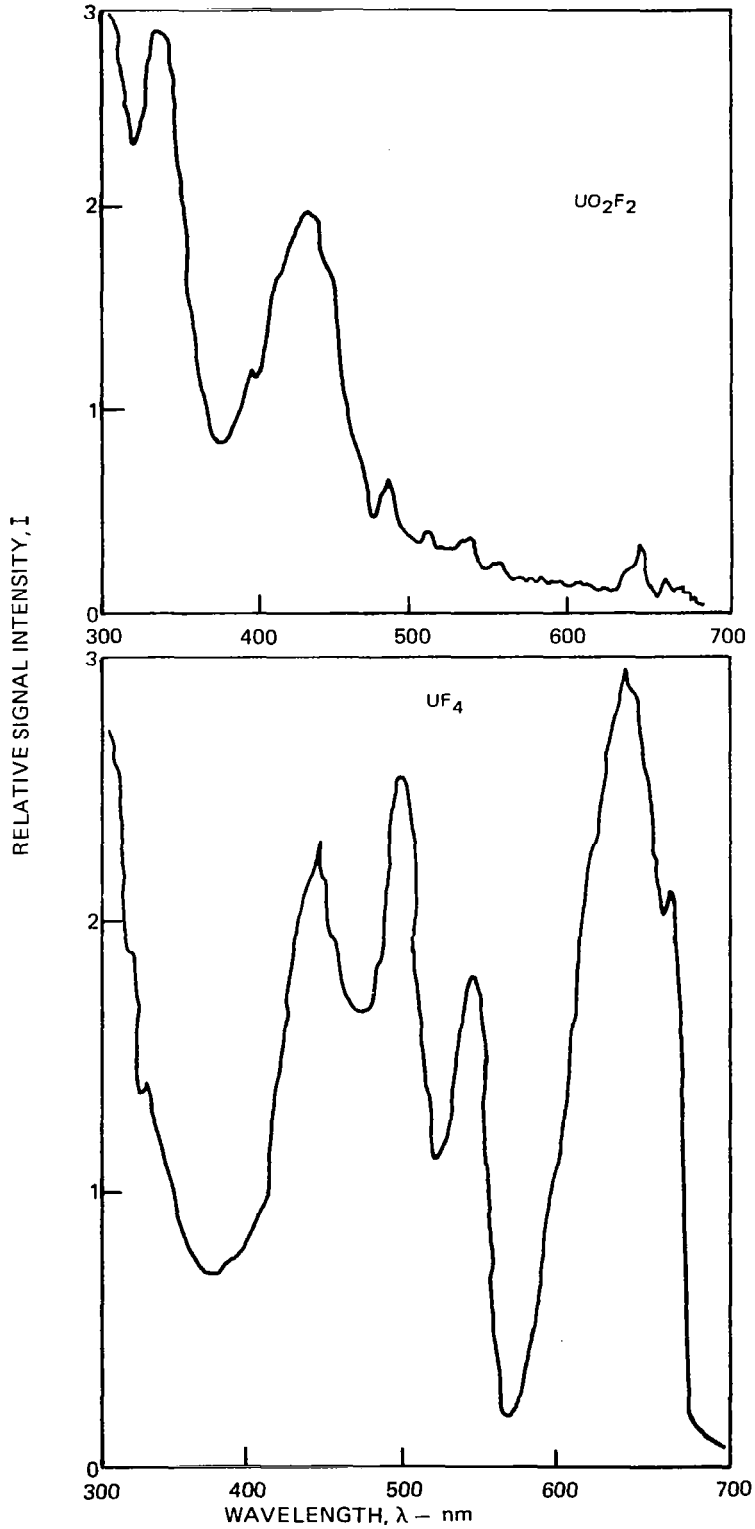

FIG. 40

EXAMPLE OF URANIUM COMPOUND SPECTRUM OF UO_3 OBTAINED USING PHOTOACOUSTIC SPECTROMETER SYSTEM

FIG. 41

EXAMPLE OF RELATIVE INTENSITY OF PHOTOACOUSTIC SPECTROMETER (PAS) SIGNAL VERSES WEIGHT PERCENT UF_4

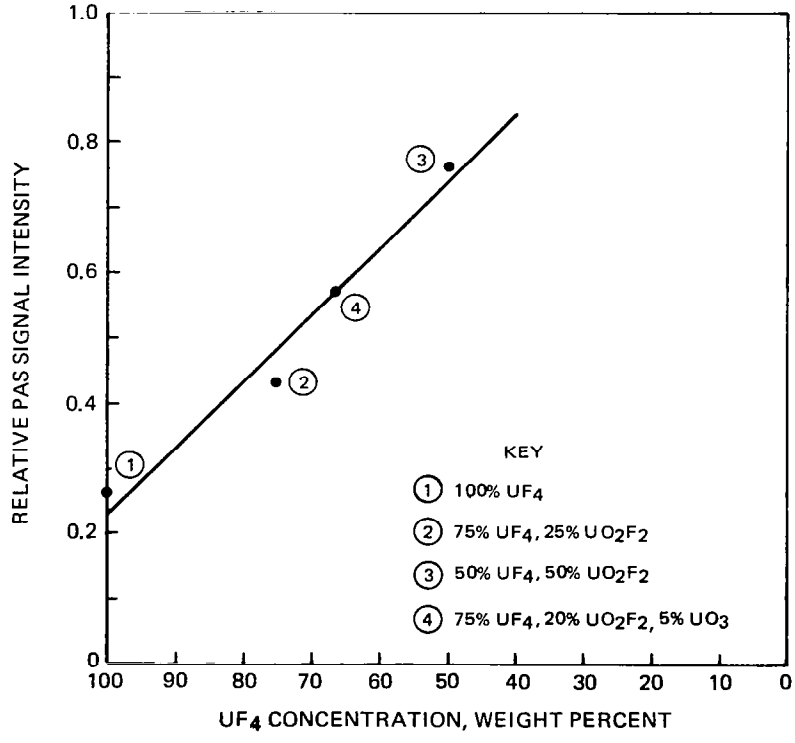

1. Report No.	2. Government Accession No.	3. Recipient's Catalog No.
NASA CR-3258		

4. Title and Subtitle	5. Report Date
Argon/UF_6 Plasma Experiments: UF_6 Regeneration and Product Analysis	March 1980
	6. Performing Organization Code 6460
7. Author(s)	8. Performing Organization Report No.
Ward C. Roman	
	10. Work Unit No.
9. Performing Organization Name and Address	
United Technologies Research Center East Hartford, CT 06108	11. Contract or Grant No. NAS1-14329
	13. Type of Report and Period Covered
12. Sponsoring Agency Name and Address	Contractor Report
National Aeronautics and Space Administration Washington, DC 20546	14. Army Project No.

15. Supplementary Notes

Langley Technical Monitor: Frank Hohl
Topical Report

16. Abstract

An experimental and analytical investigation was conducted to aid in developing some of the technology necessary for designing a self-critical fissioning uranium plasma core reactor (PCR). This technology is also applicable to gaseous uranium hexafluoride (UF_6) nuclear-pumped laser systems.

The principal equipment used included the United Technologies Research Center (UTRC) 1.2 MW RF induction heater, a d.c. plasma torch, uranium tetrafluoride (UF_4) feeder system, and batch-type fluorine/UF_6 regeneration systems.

This follow-on research included the following overall objectives: (1) continue to develop and test materials and handling techniques suitable for use with high-temperature, high-pressure, gaseous UF_6; (2) continue development of complementary diagnostic instrumentation and measurement techniques to characterize the effluent exhaust gases and residue deposited on the test chamber and exhaust system components. Specific objectives include: (1) development of a batch-type UF_6 regeneration system employing pure high-temperature fluorine; (2) development of a ruggedized time-of-flight (T.O.F.) mass spectrometer and associated data acquisition system capable of making on-line concentration measurements of the volatile effluent exhaust gas species in a high RF environment and corrosive environment of UF_6 and related halide compounds.

17. Key Words (Suggested by Author(s))	18. Distribution Statement
Gas Core Reactor Uranium Hexafluoride Regeneration	Unclassified-Unlimited Subject Category 73

19. Security Classif. (of this report)	20. Security Classif. (of this page)	21. No. of Pages	22. Price*
Unclassified	Unclassified	91	$6.00

*For sale by the National Technical Information Service, Springfield, Virginia 22161

NASA-Langley, 1980